Titre: Title:	Performance assessment of tendon support systems submitted to dynamic loading
Auteur: Author:	David Gaudreau
Date:	2004
Type:	Mémoire ou thèse / Dissertation or Thesis
Référence: Citation:	Gaudreau, D. (2004). Performance assessment of tendon support systems submitted to dynamic loading [Master's thesis, École Polytechnique de Montréal]. PolyPublie. https://publications.polymtl.ca/7483/

UNIVERSITÉ DE MONTRÉAL

PERFORMANCE ASSESSMENT OF TENDON SUPPORT SYSTEMS SUBMITTED TO DYNAMIC LOADING

DAVID GAUDREAU
DÉPARTEMENT DES GÉNIES CIVIL, GÉOLOGIQUE ET DES MINES
ÉCOLE POLYTECHNIQUE DE MONTRÉAL

MÉMOIRE PRÉSENTÉ EN VUE DE L'OBTENTION
DU DIPLÔME DE MAÎTRISE ÈS SCIENCES APPLIQUÉES
(GENIE MINÉRAL)
MARS 2004

Your file Votre référence
ISBN: 0-612-97950-4
Our file Notre référence
ISBN: 0-612-97950-4

UNIVERSITÉ DE MONTRÉAL

ÉCOLE POLYTECHNIQUE DE MONTRÉAL

Ce mémoire intitulé:

PERFORMANCE ASSESSMENT OF TENDON SUPPORT SYSTEMS SUBMITTED TO DYNAMIC LOADING

présenté par: GAUDREAU David

en vue de l'obtention du diplôme de: Maîtrise ès sciences appliquées

a été dûment accepté par le jury d'examen constitué de:

M. CORTHÉSY, Robert, Ph.D., président

M. AUBERTIN Michel, Ph.D., membre et directeur de recherche

M. SIMON Richard, Ph.D., membre et codirecteur de recherche

M. MITRI Hani, Ph.D., membre

Pour Manon

ACKNOWLEDGEMENTS

I would like to thank Noranda Inc. for supporting this effort and for permission to publish these results. Special thanks to Luc Vandamme, Michel Ménard and Glen Crowther.

To Michel Aubertin and Richard Simon, thank you for your support.

Thanks to Manon, Samuel and Charles-Antoine, my loved ones.

ABSTRACT

Deep mines and some underground operations with a high extraction ratio can generate high ground stresses. High stresses in a mining area can cause the failure of rock masses around openings and convergence of rock towards the exposed surfaces of excavations. Under a combination of circumstances such as the presence of brittle rock and high stresses, it is possible for the rock mass to fail violently thus causing a rockburst.

Reinforcement and tunnel support means such as the use of rock bolts, reaction plates and mesh are well suited for gravity driven situations when the support systems are subjected to static and quasi-static loading. The performance of the systems can be at any time verified, through pull out testing of the tendon support elements and the meshing units for example. Bolting patterns and support system design can be inspired from a number of published references to meet specific performance requirements.

The design of support strategies for dynamic loading has been for now less obvious. Published guidelines suggest adopting a tendon burden as well as an arbitrary ejection velocity. These factors can be used to calculate the energy absorption capacity requirements of a support system so that it can be compared to the work energy during a pull out test in quasi-static loading mode. This method was proposed due to the lack available impact testing results on tendon support systems.

In the context of this thesis, the energy absorption capacity of a prototype tendon support system was tested using an impact-testing rig on Noranda Inc.'s Technology Centre premises. The verification tests done on the Modified Cone Bolt (MCB) prototype support system in quasi-static and impact loading modes was also used to propose a displacement evaluation method for tendons submitted to impact loading. It relies on parameters that can be extracted from pull out tests, which can be easily performed

underground. Velocity damping is introduced in the reaction of the tendon as well as other means of energy dissipation through the use of a critically damped harmonic motion system. It was found that results from the proposed calculation method were consistent with laboratory investigations. The input parameters for the calculation method are the plastic stiffness of the support system and its yield point, as obtained from pull out testing. By choosing the tendon burden and ejection velocity, one can calculate the displacement of the tendon as well as its axial load through time. Because the complete load-displacement characteristic curve is available with the calculations, one can estimate the work energy dissipation during the impact loading of the tendon support system for a given tendon burden and ejection velocity. This could help for case analysis in areas damaged by seismicity, as well as for the determination of bolt spacing given a probable depth of failure and an arbitrary velocity of ejection range.

MCB prototype quasi-static pull tests in the field revealed a plastic stiffness range of 630-775 kN/m. If the proposed calculation method is applied to the MCB prototype, its maximum estimated energy absorption capacity is 32-40 kJ at an ejection velocity of 5.4 m/s. At 3.0 m/s ejection velocity, the capacity increases to a 45-50 kJ range. The impact test rig used to test the prototypes was limited to a 15 kJ capacity, none of the tendons could be broken with a single impact using a drop weight of 1000 kg at a height corresponding to an impact velocity of 5.4 m/s. The proposed displacement evaluation method could provide a means of calculating the maximum capacity range of tendons for rockburst support design.

RÉSUMÉ

Les mines profondes et celles ayant une forte quantité de réserves minées par rapport aux réserves en place sont susceptibles de générer de fortes contraintes. L'accroissement de contraintes dans une zone minière peut causer la rupture des massifs rocheux autour des ouvertures et une convergence du roc vers les faces exposées des excavations. Sous une combinaison de circonstances telles la présence de roche fragile et de fortes contraintes, il devient possible pour le massif rocheux de se briser violemment et de causer un coup de terrain.

Les méthodes de renforcement et de support de tunnels, comme l'utilisation de boulons d'ancrage, de plaques de réaction et de maillage d'acier sont bien adaptés pour des conditions de chargement gravitaire lorsque les systèmes de support sont soumis à des charges statiques et quasi-statiques. La performance des systèmes peut à tout moment être vérifiée, à l'aide de tests d'arrachement des éléments de support par tendons et les unités de maillage par exemple. Les patrons de boulonnage et la conception du système de support peut être inspirés d'un bon nombre de publications pour atteindre des objectifs de performance spécifiques.

La conception d'une stratégie de support en mode de chargement dynamique est pour le moment moins facile. Les lignes directrices publiées suggèrent d'attribuer un fardeau à chaque tendon ainsi qu'une vitesse d'éjection arbitraire. Ces facteurs peuvent être utilisés pour calculer la capacité d'absorption d'énergie nécessaire d'un système de support et de le comparer à celui du travail épuisé lors d'un test d'arrachement en mode de chargement quasi-statique. Cette méthode a été proposée dû au manque de données disponibles, particulièrement en tests d'arrachement en mode dynamique sur des systèmes de support par tendons.

Dans le contexte de ce mémoire, la capacité d'absorption d'énergie du système de support prototype Modified Cone Bolt (MCB) a été testée en utilisant un bâti de tests d'impact situé sur le site du Centre de Technologie Noranda Inc. Les tests de vérification du prototype MCB en chargement quasi-statique et en mode d'impact furent ensuite analysés pour proposer un modèle de déplacement du tendon en chargement rapide. Ce modèle repose sur des paramètres qui peuvent être mesurés à partir de tests d'arrachement, relativement faciles à exécuter sous-terre. L'amortissement de la vitesse est introduit dans le modèle d'interprétation du mouvement aussi bien que d'autres sources de dissipation d'énergie via l'utilisation d'un système de mouvement harmonique simple amorti. Il a été découvert que les résultats de la méthode de calcul proposée correspondent bien aux données expérimentales. Les paramètres d'entrée du modèle sont la rigidité plastique du système de support ainsi que sa limite d'élasticité, tel qu'obtenu à partir de tests d'arrachement. En choisissant le fardeau du tendon et la vitesse d'éjection, il est possible de calculer le déplacement du tendon dans le temps ainsi que sa charge axiale. Puisque la courbe complète charge-déplacement peut être évaluée à l'aide des calculs, on peut estimer la quantité d'énergie dissipée durant l'impact du système de boulonnage pour un fardeau et une vitesse d'éjection donnés.

Les essais d'arrachement du système prototype MCB en chargement quasi-statique ont révélé une rigidité plastique de l'ordre de 630-775 kN/m. Si la méthode de calcul proposée pour l'évaluation du déplacement du tendon en chargement dynamique est utilisé pour le prototype MCB, sa capacité maximale d'absorbtion d'énergie est de 32-40 kJ à une vitesse d'éjection de 5.4 m/s. À une vitesse d'éjection du fardeau de 3.0 m/s, la capacité du tendon augmente à une valeur de 45-50 kJ. Le bâti de tests d'impact utilisé pour les essais dynamiques était limité à une capacité de 15 kJ, aucun des tendons MCB n'a pu être brisé avec un seul impact utilisant une masse de 1000 kg et une hauteur de charge correspondant à une vitesse d'impact de 5.4 m/s. Le modèle proposé pourrait fournir un moyen de calculer la capacité maximale en absorbtion d'énergie de tendons pour la conception de systèmes de support pour les coups de terrain.

CONDENSÉ

Les mines profondes et celles ayant un fort ratio d'extraction sont susceptibles de générer de fortes contraintes. L'accroissement de contraintes dans une zone minière peut causer la rupture des massifs rocheux autour des ouvertures et une convergence du roc vers les faces exposées des excavations. Sous une combinaison de circonstances telles la présence de roche compétente et fragile et de fortes contraintes, il devient possible pour le massif rocheux de se briser violemment et de causer un coup de terrain. Un exemple de dommages est présenté à la figure 1. La largeur de la galerie illustrée est d'environ 7 mètres et sa hauteur 5.5 mètres. Le matériel au plancher a été projeté à partir des murs.

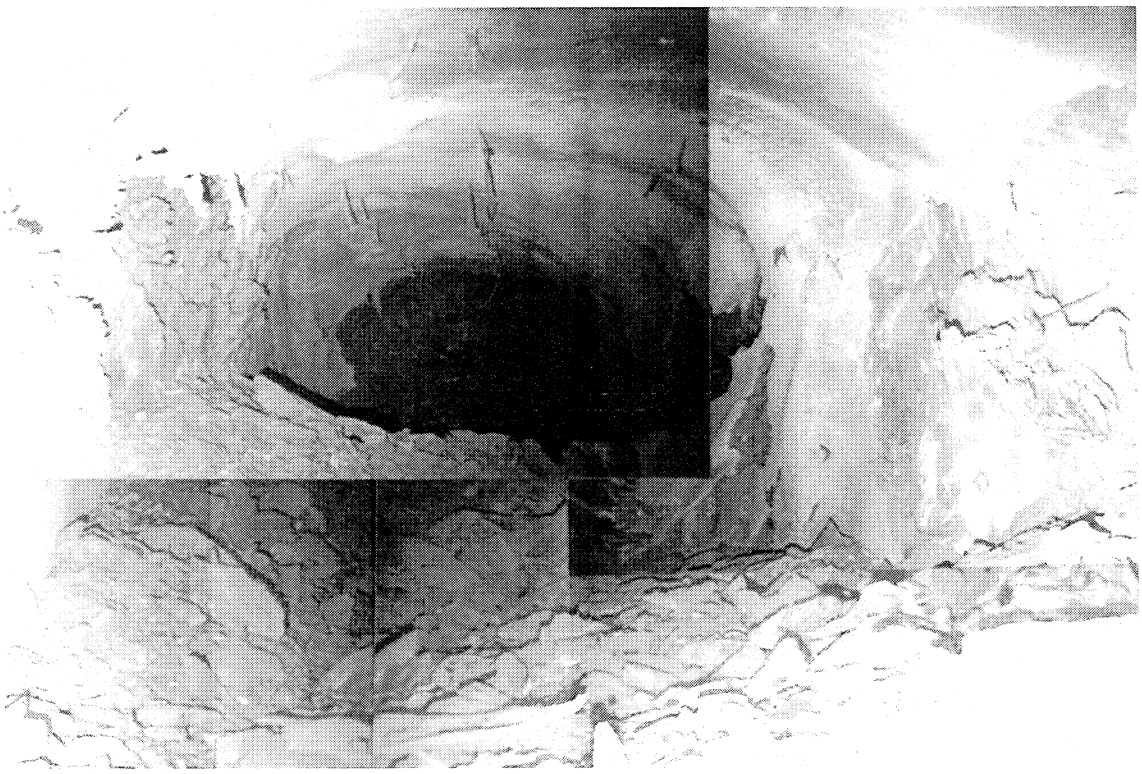

Figure 1 – Photo composite d'un coup de terrain dans la galerie d'accès 230-7 à la mine Brunswick.

Les méthodes de renforcement et de support de tunnels, comme l'utilisation de boulons d'ancrage, de plaques de réaction et de maillage d'acier sont bien adaptées pour des conditions de chargement gravitaire lorsque les systèmes de support sont soumis à des charges statiques et quasi-statiques. La performance des systèmes peut à tout moment être vérifiée, à l'aide de tests d'arrachement des éléments de support et des unités de maillage par exemple. Les patrons de boulonnage et la conception du système de support peuvent être inspirés d'un bon nombre de publications (e.g. Stillborg, 1986; Choquet, 1987; Charette, 1991; Hoek et al., 1995; Charette and Hadjigeorgiou, 1999) pour atteindre des objectifs de performance spécifiques.

La conception d'une stratégie de support en mode de chargement dynamique est pour le moment moins facile. Les lignes directrices publiées (Ortlepp, 1992a, 1992b, 1993, 1994; Stacey et Ortlepp, 1994, 1999; Kaiser et al., 1996) suggèrent d'attribuer un fardeau à chaque tendon ainsi qu'une vitesse d'éjection arbitraire. Ces facteurs peuvent être utilisés pour calculer la capacité d'absorption d'énergie nécessaire d'un système de support et pour le comparer à celui du travail épuisé lors d'un test d'arrachement en mode de chargement quasi-statique. Cette méthode a été proposée faute de données disponibles (Kaiser, 2000), particulièrement en tests d'arrachement en mode dynamique sur des systèmes de support par tendons. Une proposition du Geomechanics Research Centre (GRC ; Maloney et Kaiser, 1996) visait à combler ce vide; elle suggère un appareil permettant le chargement dynamique de systèmes de boulonnage et de mesurer la charge et le déplacement du boulon en chargement rapide.

Dans le contexte de ce mémoire, la capacité d'absorption d'énergie d'un système de support prototype par tendons a été testée en utilisant un bâti de tests d'impact issu des propositions du GRC et modifié pour le programme. Ce bâti était situé sur le site du Centre de Technologie Noranda Inc (CTN). Les modifications ont porté sur le monte-charge, le système d'aquisition de données, le système de traitement de signal, le choix

du type de cellule de charge et de transducteur de déplacement utilisé et son emplacement. Le bâti de tests d'impacts du CTN est illustré à la figure 2.

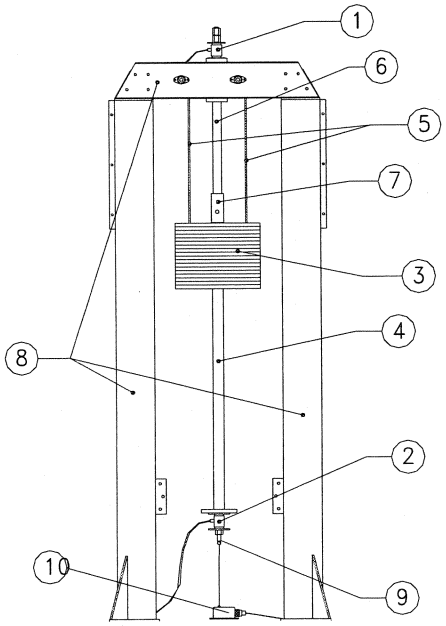

1-Cellule de charge 1
2-Cellule de charge 2
3-Charge d'impact
4-Contenant de l'échantillon
5-Tiges de retenue
6-Espaceur
7-Tige d'accouplement
8-Bâti
9-Tendon (dans le contenant)
10-Transducteur de déplacement

Figure 2 – Bâti de tests d'impacts

Le système de boulonnage analysé dans le cadre du mémoire est le tendon prototype Modified Cone Bolt (MCB). Tel qu'illustré à la figure 3, le boulon (4) est muni d'une tête conique (2) à un bout et d'une section filetée (5) à l'autre bout. Le MCB est installé en perçant un trou dans le roc (13). Le trou est rempli de cartouches de résine de polyester (14), puis le boulon est poussé et tourné dans le trou dans le but de mélanger les composantes contenues dans la cartouche de résine (15) à l'aide de la plaque à mélanger (1) assujettie à la tête conique. Une fois la résine mélangée, elle se solidifie par polymérisation. Lors de chargement dynamique, le boulon a la capacité de fissurer la matrice de résine, ce qui lui permet de se déplacer sous l'effort sans se briser immédiatement, comme c'est le cas (à différents degrés) pour certains systèmes de boulonnage.

Les tests de vérification du système de support prototype MCB en chargement quasi-statique et en impact ont été utilisés pour proposer une méthode de calcul du déplacement

du tendon en chargement rapide. Cette méthode de calcul repose sur des paramètres qui peuvent être mesurés à partir de tests d'arrachement, relativement faciles à exécuter sous-terre. L'amortissement de la vitesse est introduit dans le modèle d'interprétation du mouvement avec d'autres sources de dissipation d'énergie via l'utilisation d'un système de mouvement harmonique amorti. Il a été montré que les résultats de calculs avec la méthode proposée correspondent bien aux données expérimentales. Les paramètres d'entrée de la méthode sont la rigidité plastique du système de support ainsi que sa limite d'élasticité, tel qu'obtenues à partir de tests d'arrachement. En choisissant le fardeau par tendon et la vitesse d'éjection, il est possible de calculer le déplacement maximal du tendon en impact ainsi que la charge axiale maximale dans le tendon. Puisque la courbe complète charge-déplacement peut être évaluée à l'aide des calculs, on peut estimer la quantité d'énergie dissipée durant l'impact du système de boulonnage pour un fardeau et une vitesse d'éjection donnés. Cela pourrait être utile pour des études de cas d'effondrements dus à la sismicité, mais aussi pour la détermination du patron de boulonnage étant donné une profondeur de rupture probable et une vitesse d'éjection arbitraire.

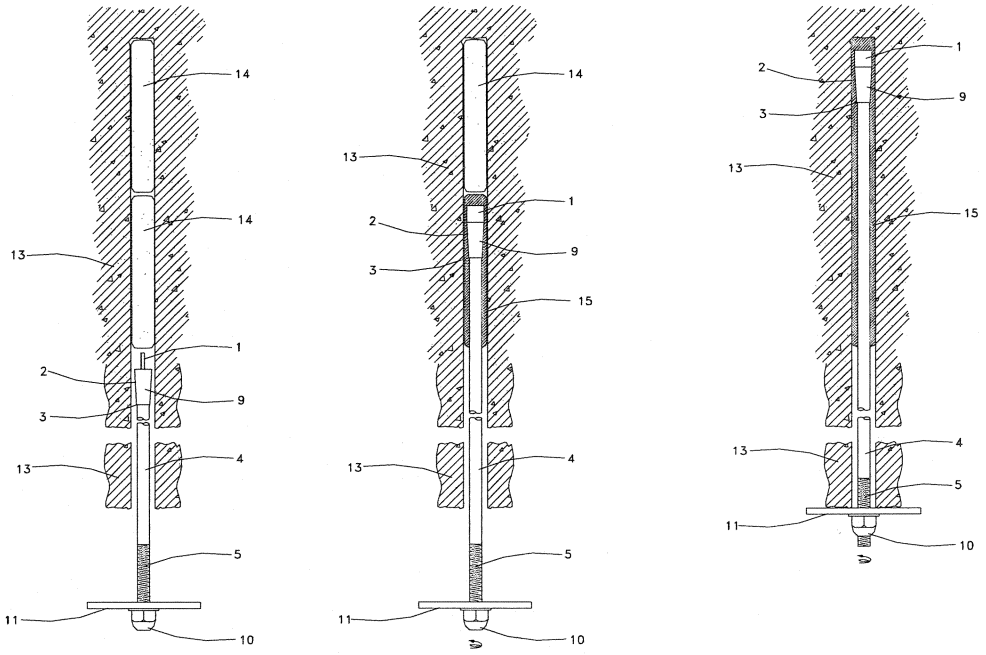

Figure 3 – Système de boulonnage prototype MCB (US 6,390,735 B1)

Les équations du modèle proposé de calcul de déplacement d'un tendon en chargement en impact sont présentées dans le mémoire. Les principales équations peuvent s'écrire comme suit:

$$w = \sqrt{\frac{k_p}{m}} \tag{4.11}$$

$$x_g = (C_1 \cdot t + C_2) \cdot e^{-wt} - \frac{F_y}{k_p} \tag{4.21}$$

$$C_2 = x_0 + \frac{F_y}{k_p} \tag{4.27}$$

$$C_1 = v_0 + w \cdot (x_0 + \frac{F_y}{k_p}) \tag{4.28}$$

où:

- m est le poids du fardeau (N)
- k_p est la rigidité plastique du système telle qu'évaluée à l'aide de tests d'arrachement (N/m)
- F_y est la force constante globale définie par la somme de la limite d'élasticité du tendon (N) et un facteur de friction F_f (N)
- x_g est le déplacement en impact du tendon (m) à la plaque de réaction en fonction du temps t (s)
- C_1 et C_2 sont les constantes de conditions initiales
- x_0 (m) et v_0 (m/s) sont respectivement le déplacement et la vitesse initiale du tendon au moment de l'impact; dans la majorité des cas, x_0 est nul et v_0 égale la vitesse d'éjection du fardeau ou la vitesse de la charge d'impact au moment de toucher la plaque.

La méthode de calcul proposée nécessite quelques itérations où l'énergie potentielle et le travail doivent être balancés en utilisant le facteur de friction F_f. À cet effet, les paramètres requis F_{bar}, E_{bar} et We peuvent être calculés suivant:

$$F_{bar} = x_g \cdot \mathrm{k_p} \tag{4.29}$$

$$E_{bar} = \frac{\mathrm{m} \cdot \mathrm{v}_0^2}{2} + \mathrm{m} \cdot \mathrm{g} \cdot \max x \tag{4.30}$$

$$\mathrm{We} = \int \mathrm{F} dx \tag{4.4}$$

où F_{bar} (N) est la charge axiale dans le tendon, E_{bar} est l'énergie potentielle (J), We est le travail (J) et max x est le déplacement maximal (m) calculé.

En vue d'obtenir la charge en tension maximale dans le tendon de même que la quantité d'énergie absorbée par le système de boulonnage, on suggère de suivre les étapes suivantes (l'usage d'un chiffrier électronique est recommandé):

1. Définir une "force de friction" $\mathrm{F_f}$ arbitraire représentant les pertes de charges par friction et autres sources de dissipation. Pour la première itération, il est suggéré d'utiliser la limite d'élasticité mesurée au test d'arrachement, sinon la limite d'élasticité du tendon seul.
2. Calculer le déplacement x_g pour différents incréments de temps, typiquement dans l'ordre des millisecondes, utilisant les équations (4.11), (4.21), (4.27) et (4.28).
3. Calculer la force dans le tendon F_{bar} utilisant l'équation (4.29).
4. Construire un graphe charge-déplacement représentant la réaction du tendon. Le graphe doit être conçu pour que si la force dans le tendon F_{bar} ne dépasse pas le niveau de force de friction arbitraire $\mathrm{F_f}$, alors la force dans le tendon F_{bar} à ce point dans le temps égale la force de friction $\mathrm{F_f}$.
5. Calculer la dissipation d'énergie potentielle dans le tendon E_{bar} utilisant l'équation (4.30).
6. Calculer le travail accompli durant l'arrachement We utilisant l'équation (4.4).
7. Répéter les étapes 1 à 6 jusqu'à ce que l'énergie potentielle E_{bar} soit approximativement égale au travail We.

Ce mémoire contient une description des mécanismes menant aux coups de terrain et à la sismicité dans les mines, ainsi que des méthodes de tests en chargement dynamique pour les systèmes de support par tendons. Certaines procédures de tests d'arrachement en mode quasi-statique et en impact ont été revues, avec une emphase sur les essais de validation du système de support prototype MCB. Les résultats et observations de la phase d'essais ont été utilisés pour proposer le modèle de déplacement de tendons sous chargement en impact. La figure 4 illustre le schéma d'un test d'arrachement en mode quasi-statique. Lors d'un tel test, le boulon est installé dans le roc, puis on tente de l'arracher à l'aide d'un cylindre hydraulique de forte capacité muni d'un adapteur pouvant s'accrocher à la tête du boulon d'ancrage au moyen d'une goupille et d'un écrou. Le déplacement du tendon ainsi que la charge axiale sont mesurés à la fois électroniquement à l'aide de transducteurs de pression et de déplacement, et de façon analogue à l'aide d'une règle graduée et de la jauge de pression. Les tendons n'ont pas été testés jusqu'à leur limite à la rupture puisque le système de cylindre hydraulique doit être enchainé à la face de travail pour ce faire. Les résultats d'un test d'arrachement et les paramètres mesurés sont illustrés à la figure 5.

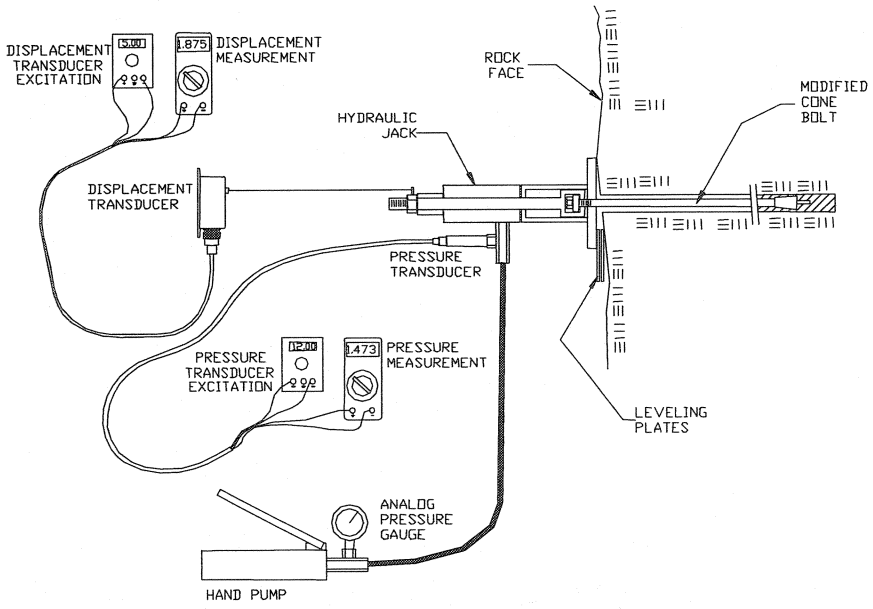

Figure 4 – Schéma d'un test d'arrachement en mode quasi-statique.

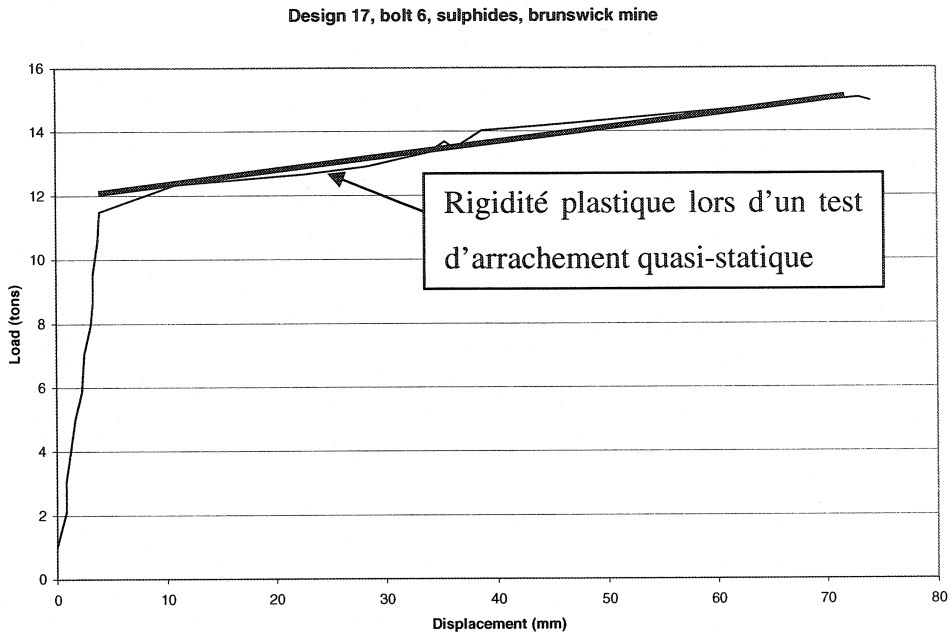

Figure 5 – Résultat d'un test d'arrachement et paramètres mesurés sur un spécimen prototype MCB.

L'estimation de la charge dans le tendon en fonction du temps à l'aide du modèle proposé est illustrée à la figure 6. La courbe illustrée à la figure 6 repose sur un calcul basé sur une rigidité plastique de 775 kN/m, tirée des résultats de tests d'arrachement, une force de friction de 89 kN et 1000 kg de fardeau à une vitesse d'impact de 5.4 m/s. L'allure de la courbe de la figure 6 peut être comparée à celle de la figure 7 (modèle Force 2). Puisque le modèle emprunte le mécanisme d'un mouvement oscillatoire harmonique amorti, il convient de négliger le calcul du mouvement de la charge d'impact après le maximum.

Un résultat-type de test en chargement dynamique sur un spécimen prototype MCB à l'aide du bâti de tests du CTN est illustré à la figure 7. À noter sur cette figure la course du trajet de la plaque de réaction du tendon vers le bas, tel qu'illustré sur la courbe de déplacement, qui se redresse lors de la récupération élastique de l'acier à la fin du cycle de chargement. Aussi, la courbe Force 1 representant la cellule de charge située au haut

du bâti de tests d'impacts montre des oscillations de plus forte amplitude que la courbe Force 2 située sous la plaque de réaction. L'amplitude des oscillations mesurées par la cellule 1 est moins prononcée lors de la décélération du mouvement. La figure 6 contient un schéma décrivant la tendance générale des courbes forces calculées à l'aide du modèle proposé pour fins de comparaison.

La figure 8 illustre un test d'impact type représenté sous la forme d'un graphe contrainte-déformation. Une fois de plus, la charge mesurée au-dessus du bâti de chargement Force1 montre des oscillations plus amples que la courbe de force mesurée sous le tendon Force2. Lors du déplacement initial du tendon, il a été observé en laboratoire que peu de dommages étaient faits à l'acier. Tout semble indiquer que l'effort en traction dans l'acier se produit à la fin du chargement en impact lors de la décélération du fardeau du boulon.

L'intégration de la courbe force-déplacement illustrée à la figure 8 donne la valeur du travail absorbé par le système de boulonnage. À noter que beaucoup d'énergie est dissipée dans le boulon avant que l'acier du tendon soit sollicité en déformation plastique. Finalement, l'estimation de la courbe contrainte-déplacement pour les paramètres du test de la figure 8 à l'aide de la méthode de calcul proposée est illustré à la figure 9.

La courbe force-déplacement illustrée à la figure 9 repose sur un calcul basé sur une rigidité plastique de 775 kN/m, une force de friction de 89 kN et 1000 kg de fardeau à une vitesse d'impact de 5.4 m/s, correspondant aux paramètres du test d'impact affiché à la figure 8. La charge maximale dans le tendon telle que calculée à l'aide du modèle est de 133 kN. Lors du test du spécimen 17-1-1, une force de 131 kN a été mesurée lors d'un impact à 1000 kg et une vitesse de frappe de 5.4 m/s.

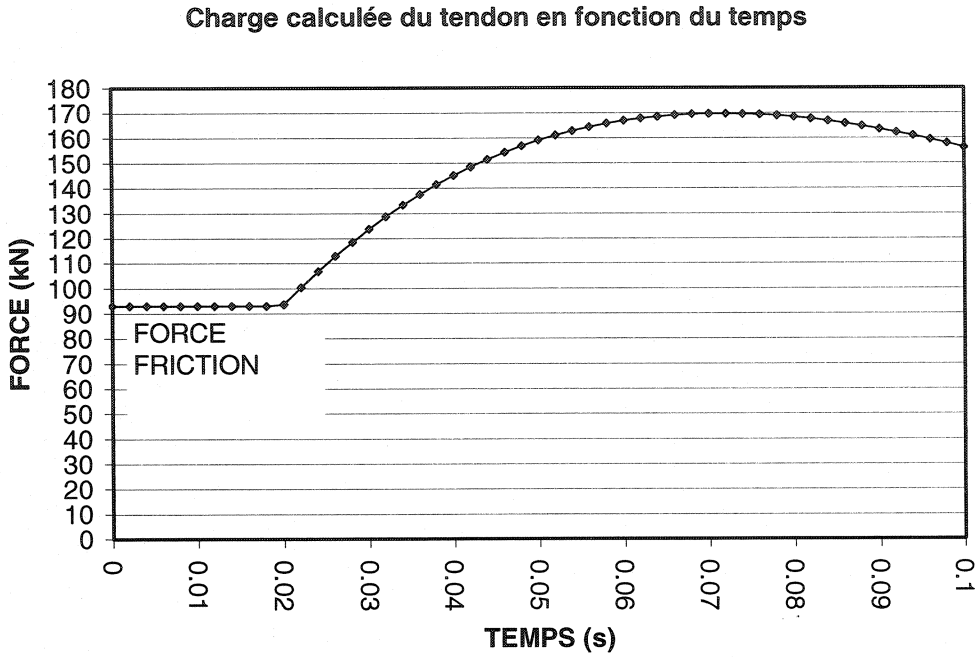

Figure 6 – Calcul de la charge axiale du tendon en fonction du temps selon la méthode de calcul proposée.

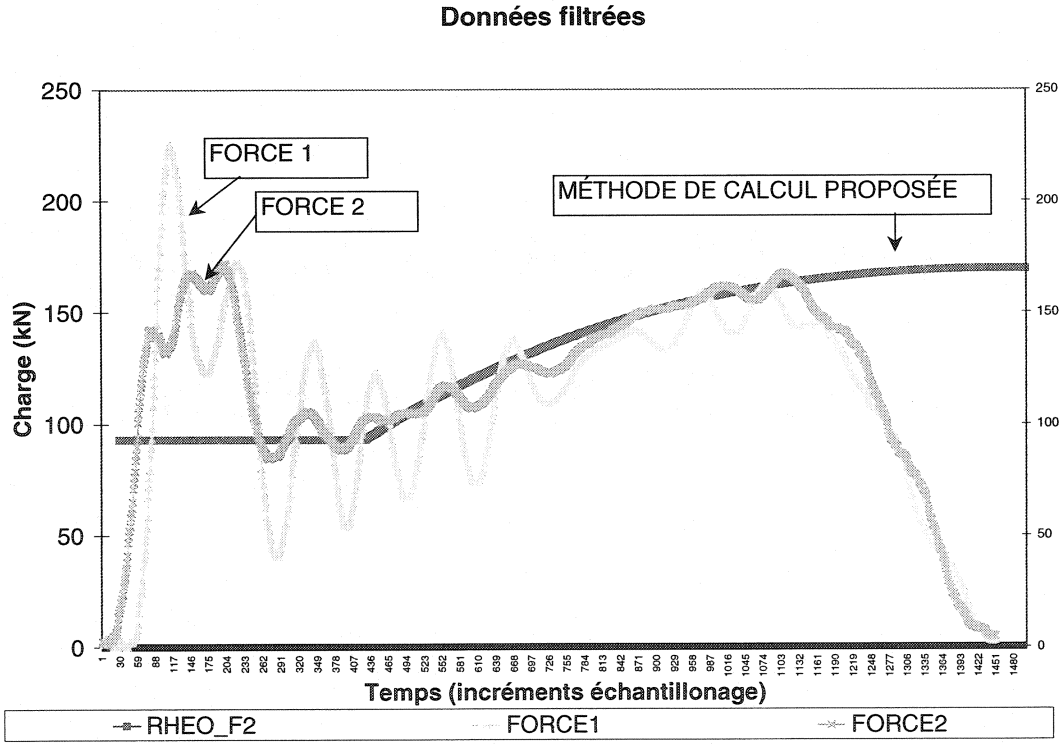

Figure 7 – Données du test 17-11-2. L'abscisse indique le temps par ordre de mesure et l'ordonnée la charge ou le déplacement (en Volts).

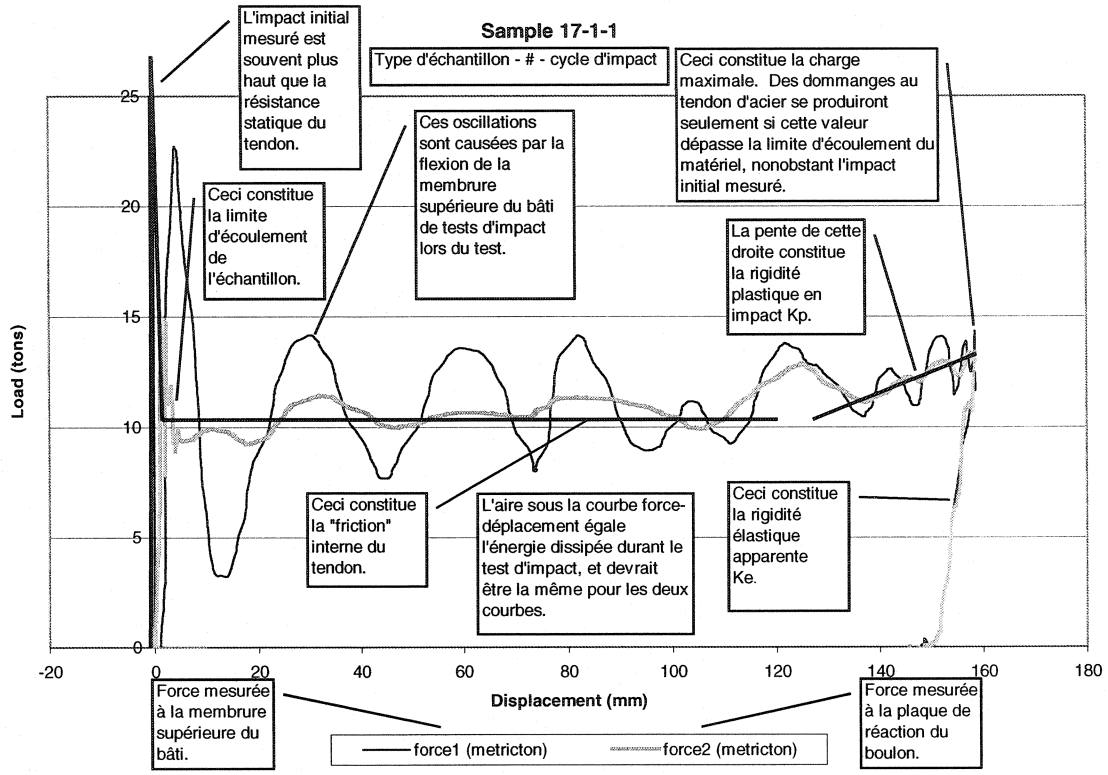

Figure 8 –Courbe contrainte-déformation typique résultant d'un test d'impact en laboratoire. L'abcisse représente le déplacement et l'ordonnée la charge axiale dans le tendon.

Les essais d'arrachement du système prototype MCB en chargement quasi-statique ont révélé une rigidité plastique de l'ordre de 630-775 kN/m. Si le modèle proposé de déplacement du tendon en chargement en impact est utilisé pour le prototype MCB, sa capacité maximale d'absorption d'énergie est de 32-40 kJ à une vitesse d'éjection de 5.4 m/s. À une vitesse d'éjection du fardeau de 3.0 m/s, la capacité du tendon augmente à une valeur de 45-50 kJ. Les prototypes MCB ont été testés en impact avant la construction du modèle proposé. Le modèle correspond bien avec les observations faites en laboratoire. Le bâti de tests d'impact utilisé pour les tests d'arrachement en impact était limité à une capacité de 15 kJ, aucun des tendons MCB n'a été brisé avec un seul impact pour une masse de 1000 kg et une hauteur de charge correspondant à une vitesse d'impact de 5.4 m/s. Le modèle proposé pourrait fournir un moyen de calculer la

capacité maximale en absorption d'énergie de tendons pour la conception de systèmes de support pour les coups de terrain.

L'estimation de l'effet de renforcement fourni par le confinement additionel dans la zone boulonnée *durant* le chargement en impact du massif rocheux pourrait contribuer à améliorer les méthodes de conception de systèmes de renforcement pour les coups de terrain. De plus, il est à noter que la conception d'un système de support pour le chargement dynamique ne s'arrête pas au choix du tendon mais repose aussi en grande partie sur le choix du système de recouvrement de la galerie, comme par exemple le choix du maillage d'acier se trouvant tissé entre les tendons sous les plaques de réaction. Un exemple de système de renforcement pour le chargement dynamique est illustré à la figure 10. Le système comprend les tendons MCB tels que forgés par Mansour Mining Inc., des plaques de réaction épaisses déformées en forme de dôme, et un maillage d'acier de grosseur 6 assujetti de maillage de grosseur 00 entre les tendons.

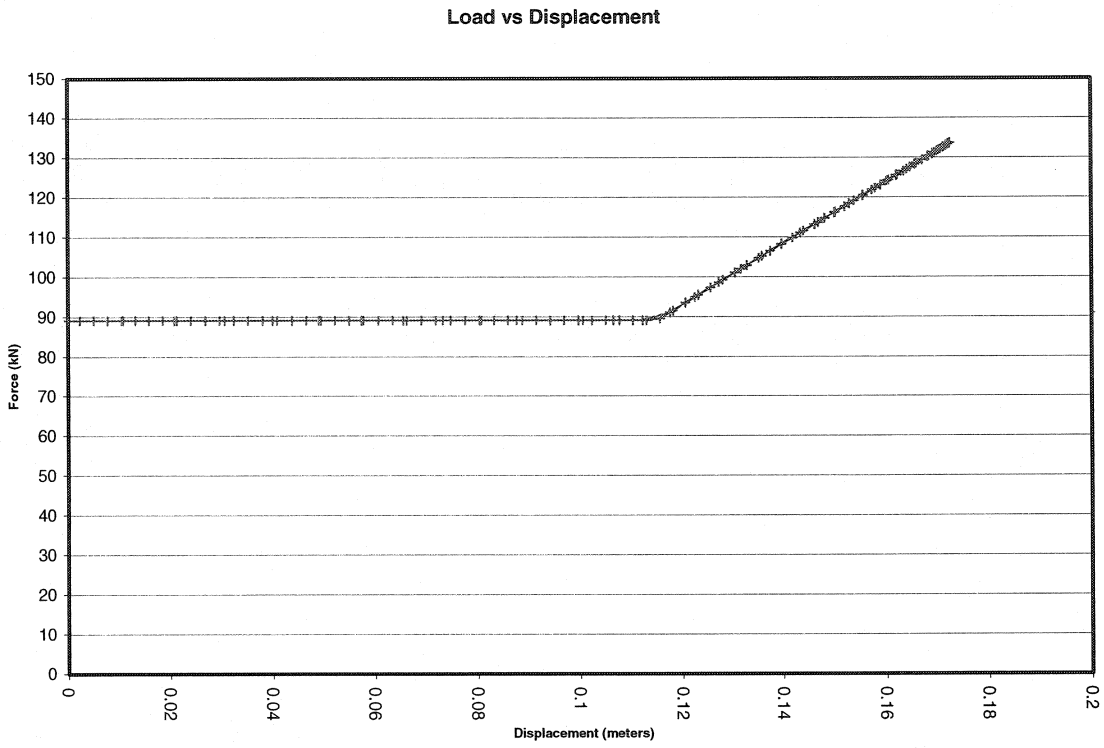

Figure 9 – Estimation de la courbe contrainte-déformation à l'aide de la méthode de calcul proposée.

Figure 10 – Système de renforcement pour le chargement dynamique à la mine Brunswick.

TABLE OF CONTENTS

LIST OF TABLES

LIST OF FIGURES

LIST OF SYMBOLS

a	Acceleration
a	Constant (magnitude calculation)
A	Seismic source area or surface area or cross-sectional area of bar
b	b-value constant (magnitude calculation)
b	Constant (harmonic motion)
B	Width of unstable element
c	Damping factor
C_1	Solution constant
C_2	Solution constant
$(C_0)_{mass}$	Uniaxial compressive strength of rock mass
δ	Tangential displacement
D	Displacement
Disp	Total displacement
dt	Small time increment
dx	Small displacement increment
E	Young's modulus
E	Elastic modulus of bar
E_{bar}	Potential energy absorption through the bar
E_x	Excess energy
E'_m	Post-peak stiffness of rock mass
ElasticDisp	Elastic displacement
F	Force
F	Impact load
$Fbar$	Axial force in the bar
F_f	Friction factor
F_y	Overall constant yield force
g	Gravitational constant
GRC	Geomechanics Research Centre
h	Drop height
h	Height
H	Length of unstable element
KE	Kinetic energy
K_e	Elastic stiffness
K_p	Plastic stiffness
K_r	Pre-peak stiffness
K_r'	Post-peak stiffness
K_{sc}	Loading system stiffness
k_e	Stiffness of the loading system
k_{pr}'	Post-peak stiffness
k'$_p$	Post-peak stiffness
l	Length of bar
LC1	Load cell 1
LC2	Load cell 2
LowerLimit	Smallest probable value of sample mean
m	Mass, tendon burden or impact mass

max x Maximum calculated displacement

MCB Modified Cone Bolt

M_o Seismic moment

M_L Seismic event local magnitude

M_m Seismic event magnitude

n number of samples

NB Province of New Brunswick

NTC Noranda Technology Centre

ν Poisson's ratio

ON Province of Ontario

P Load

P_i Applied pressure

PlasticDisp Plastic displacement

q Unit weight of bar

QC Province of Quebec

R Solution form

s standard deviation

sigma 1 Maximum principal stress

sigma 2 Intermediate principal stress

sigma 3 Minimum principal stress

σ Normal load v peak particle velocity

t Time

$t_{\alpha/2,n-1}$ t-distribution value

τ Tangential load or threshold for wavelet filter

TensileStrength Ultimate tensile strength

$\bar{u}$ Average displacement on slip

μ Seismic constant

u Displacement

UTS Ultimate tensile strength

UCS Intact rock uniaxial compressive strength

UpperLimit Highest probable value of sample mean

v Speed

v_0 Initial velocity

w Constant (harmonic motion)

W Drop weight

We Work

x Downwards displacement

$\bar{x}$ Sample mean

x_p Particular solution

x_h Homogeneous solution

x_g General solution

x_0 Initial displacement

YieldLoad Yield load

YieldPoint Yield point

FOREWORD

The choice of the thesis subject was this of the author who wanted to investigate the performance of tendon support systems under dynamic loading. Concurrent with the investigations, the opportunity arose after months of work in a seismically active mine to develop the Modified Cone Bolt, a bolting system for dynamically loading ground. The development of the Modified Cone Bolt is not presented in this thesis but methods and equipment used to validate its performance to failure are. There is much progress in the field of dynamic testing of tendon support systems and it is hoped that this snapshot in time can be of use to those interested.

CHAPTER 1
INTRODUCTION

1.1 Tunnels in highly stressed ground

Underground tunnel excavations have various functions such as accessing ore bodies, storage areas, etc. Tunnels excavated underneath the surface need to be stable, i.e., self-supporting structures that will not collapse, for a given period of time corresponding to the period of utilisation of the tunnel. Most often, the tunnel will be reinforced using rock support.

Principal factors influencing tunnel stability are its shape, the quality of the material it has been excavated in, the magnitude and orientation of the ground stresses, and the support added to insure stability.

In a mining environment, external factors including the mining of ore bodies near the tunnel can also affect its stability over time. These factors are further enhanced when mining in highly stressed ground. This can lead to sudden violent failure around the tunnel. Other external factors influencing the long-term stability of the tunnel can be the presence of water seepage or environmental and usage-related material wear.

The design of tunnel support systems thus needs to satisfy many criteria in order to obtain a stable shape and an economical support system. In highly stressed ground, the need arises to adapt support solutions and mining strategies aimed at reducing the risk of tunnel damage. These can be based on time-dependent load distribution capabilities of rock masses and support.

The tendon energy absorption testing methodology presented in this thesis was developed concurrently with Noranda Inc.'s Technology Centre (NTC) research project R2-9684. The project related to the design of support systems able to sustain rapid loading conditions. In 2002, a patent application (US 6,390,735 B1) has been granted for Noranda Inc. regarding a new bolt called the Modified Cone Bolt (MCB). This new tendon can yield in its polyester resin grout matrix. The bolt's mechanical response in rapid loading has been evaluated using an impact test rig located inside its NTC premises. Impact testing on different bolt types called for an energy absorption calculation method that could describe the tendon's impact behaviour through time for two reasons. The first is due to limitations on the test rig's maximum drop weight load and height. Certain types of support require more than one impact to break the tendon. Thus drop heights and impact velocities were not constant from one test to another. The second reason pertains to the purpose of the impact testing. The characteristic response of each tendon had to be summarised in such a fashion that it could be used for rockburst load simulation purposes. This thesis report focuses on the selected method for testing and assessing the response of different systems to impact loading, by proposing a methodology for the verification of the MCB capabilities.

Tendon support is most often used with other support elements, such as wire mesh and straps, as a system for drift support in mines. Tendon support consists of a stiff rod of a given geometry, length and diameter installed in a bore hole. Different tendon support systems are available; cable bolts, rock bolts, rebars and Split Sets (e.g. Hoek et al., 1995) to name a few. Each type of tendon will react differently when subjected to slow or rapid loading.

Stiffer support systems can provide immediate resistance to the deformation of openings. If the deformations become too large or if the drift sustained damage, the tunnel is rehabilitated, usually by removing loose parts and installing new rock support devices. Certain support systems are better suited to carry massive deformation through time, and

can avoid the rehabilitation process. By definition, a yielding tendon support system has enhanced load-time distribution properties when subjected to large displacements, while providing resistance to the movement. An example is given here for clarity. A massive impact load is suffered by a supporting structure at the periphery of a tunnel, due to the violent failure of a wall. If the wall support system is stiff, it will carry the full load in a very short amount of time. Hence, the steel tendons will elongate elastically then break, leaving a large amount of energy available that may be imparted to mobile rock particles. The smaller ejected masses will likely be ejected at high velocity, the heavier ones will be found near the toe of the wall. If this wall was supported using yielding support, the impact load received by the reaction plates through strapping and screening materials will be transferred to the tendon unit. If the tendon unit can move and follow the wall displacement with some resistance, the load will be transferred to the tendon, until the wall comes to a full stop. It is near the end of the deceleration that the tendon will sustain the most damage if the dynamic load is too large. But during the controlled movement of the wall, a quantity of work energy will have been absorbed, which could decrease the damage to the opening. The load absorbed inside the tendon is a complex mechanism dependent on the characteristics of the support system and of the bonding materials inside the borehole. One can speculate that the pressure of the reaction plate and straps on the wall in reaction to the tendon displacement inside the borehole can reduce the size of the failure zone since rock is stronger when confined. The extra confinement given by the movement resistance of the tendons could change the size of the failure zone *during* the impact.

All support systems available commercially have limitations. The choice of the proper one depends on factors such as the in-situ stresses, the expected rate and amount of deformation of the drift walls, the nature and quality of the rock mass, the presence of structural features in the rock as well as the tunnel function and utilization time.

Cook and Ortlepp (1968) suggested the use of yielding support in the deep gold mines of South Africa. The concept was further developed by Jager et al. (1990), who introduced the South African Cone Bolt (Jager, 1992), a groutable tendon equipped with a cone anchor. Preliminary impact testing of resin and cement grouted Cone Bolts was conducted in May of 1998 at the Noranda Inc. Technology Centre. Testing results and other industry results suggested that the Cone Bolt was not reliable when installed with cartridged polyester resin, but seemed effective for use with cement grout. This was mainly due to the bolt's inability to mix the cartridged resin in a reproducible fashion.

1.2 Background of the Modified Cone Bolt project

In 1996, the Ground Control Group at Brunswick mine, located near Bathurst in New-Brunswick, initiated a project with the Geomechanics Research Centre (GRC) directed at the control of rock mass failure in highly stressed and seismically active ground. Those efforts involved the design and installation of an impact test facility underground at Brunswick (Maloney and Kaiser, 1996).

The Group was interested in the Cone Bolt after a recent visit from Dave Ortlepp (SRK Consulting) at Brunswick mine, and decided to investigate the use of resin grouted Cone Bolts with help from the GRC. The testing facility was successfully installed on the 1000 m level. Unfortunately, logistical problems prohibited the use of the facility underground.

In 1997, the impact test rig was moved and installed inside NTC premises in Pointe-Claire, QC, Canada. The research mandate then was, in part, to investigate the use of the South African Cone Bolt as a yielding support system in a resin matrix. Results pertaining to this investigation showed that these yielding tendon support systems were well suited for use in cement grout, but unreliable in resin grout.

Yielding support systems must sustain large deformation while absorbing excess energy that may cause a failure to one of its functional components. For the Cone Bolt, the excess energy is dissipated when the anchor (the cone) plows through the filling material confined in the rock hole, until the force on the face is no greater than the residual strength of the system.

Efforts started at NTC in 1998 to engineer a yielding tendon appropriate for use in resin grout. A list of design criteria was established to select the tendon geometry and the testing program was completed in 2000. The resulting product is the MCB. The latter is a smooth bar threaded at its outer end, with a forged cone at the inner end. When installed in a borehole and plated, it can sustain large tunnel deformation by transferring loads from the plate to the cone. If the load is large, the cone will plow through the grout, to ease the tension in the steel bar. The conical head is capped with a resin mixer, and the tendon is greased.

The selection of the tendon's grouting matrix was based on its physical properties, its cost and the curing time of the agent. Brunswick mine uses primarily resin cartridges and type 30 cement grout. The use of these grouts was examined at NTC in 1997 and 1998 for different tendon types. Polyester resin, if properly mixed, can be three times stronger than cement grout, and presents good residual strength. Since the conical head of the bolt requires grout failure to release energy, stronger grout having residual strength can be a disadvantage for the bolt mechanism. But fast setting resin present undeniable advantages when installing yielding support with hand held tools in burst prone ground. This material was selected as the grouting matrix for the yielding tendon support system in 1999. During that year, it was also found that tendon de-bonding agents were required in order to obtain a "softer" mechanical response of the tendon. The adhesion of the bar with the resin can cause the steel to prematurely elongate plastically near the threaded end. The impact wave requires time to travel to the conical head. If that time is spent dislodging the bar from its matrix, the wave returns to the plate without travelling to the

conical head, which causes severe elongation of the steel bar. An industrial grease product is currently used as de-bonding agent for the MCB, but in early 2000, a commercial wax product was used as de-bonding agent for testing purposes. This agent had the advantage of having a fast curing time and performed as well as the industrial grease product. However, the wax product was unable to provide corrosion resistance to the tendon, as opposed to the grease product, and its cost was prohibitive for mass usage. Pull testing in 2000 was done using greased and waxed tendons. Validation results in quasi-static and impact loading are presented in Chapter 3 of this thesis.

The MCB is manufactured by Mansour Mining Inc., based in Sudbury. So far, more than 100,000 units have been installed in various sites, including Brunswick, Bell Allard, Louvicourt and Craig mines, located respectively in Bathurst, NB, Matagami, QC, Val d'Or, QC and Onaping, ON.

1.3 Thesis objective and contents

This thesis objective is to present experimental procedures and results pertaining to the evaluation of tendon support performance in impact loading. More specifically, the experimental results and procedures will be descriptive of the validation tests for the Modified Cone Bolt (MCB) developed at Noranda Inc. Technology Centre (NTC), which were led by the author.

Chapter 2 contains a literature review on seismicity in mines, load-deformation-time behavior of tendon support, and testing methods thereafter. Chapter 3 contains experimental procedures used to test MCB prototype tendons at various loading rates, as well as the testing results. Chapter 4 elaborates on the results analysis, and contains a proposed displacement evaluation method for tendons submitted to dynamic loading.

A proposed displacement evaluation method for tendons submitted to dynamic loading is presented in Chapter 4. It represents a means for incorporating observed data collected during impact testing of tendon support in a mathematical formulation that can be applied to various situations, using input of the quasi-static loading mode. The method could be applied to such calculation as the spacing of a given tendon support package in a highly stressed tunnel for an arbitrary velocity of ejection. It could also be applied to the calculation of the maximum tolerable velocity of impact for a known anchoring means in a mining engineering application, such as loads in ore silo feeders. Finally, it could also be used as a means of corroborating impact test results performed in different parts of the world.

CHAPTER 2
NOTIONS OF MINE SEISMOLOGY AND REQUIRED PERFORMANCE OF TENDON SUPPORT

2.0 Introduction

In this chapter, factors influencing the selection of rockburst support systems for tunneling will be discussed by themes, to shed some light on mechanisms affecting tendon performance in an underground environment. Design aspects such as the quasi-static and rapid loading performance of off-the-shelve tendons will be presented. Also, rockburst damage mechanisms will be depicted along with some introductory concepts of mine seismology.

2.1 Nature of seismic events

By definition, seismic events happen as part of an earthquake, or as the result of an earthquake (e.g. Collins, 1987). An earthquake is a shaking of the ground caused by movement of the earth's crust (Collins, 1987). It generally refers to the movement of large masses of ground on the face of the earth that collides in different ways or large faults that lock and slide. A similar phenomenon can occur around underground excavations but on a smaller scale. The creation of underground openings next to sensitive discontinuities or in areas under high stress can affect the stress field sufficiently enough to induce seismic events. In an underground mining environment, these can be considered as a sudden inelastic deformation within a given volume of rock that radiates detectable seismic waves (Mendecki, 1997).

There are several necessary conditions for seismic events to occur in a rock mass. Salamon (1983) summarized them as such:

- A region in the rock mass must be on the brink of unstable equilibrium, either because of:
    - the presence of an appropriately loaded pre-existing geological weakness plane such as a joint, fault, dyke or bedding plane;
    - the changing stresses are driving a volume of rock towards sudden failure;
    - some support system approaches an unstable state in which its collapse is imminent.

- Some induced stresses must affect the region in question and the magnitude of these stress changes, however small, must be sufficiently large to trigger off the instability.

- Sudden stress change of sizeable amplitude must take place at the locus of instability to initiate the propagation of seismic waves.

- Substantial amount of energy must be stored in the rock around the instability to provide the source of kinetic or seismic energy. The origin of this stored strain energy is work done by:
    - gravitational forces and/or
    - tectonic forces and/or
    - stresses induced by mining.

When instability develops in a material, it can be either gradual or violent. Gradual instability is associated with "slow" energy dissipation in the rock mass, by fracturing and by loading of existing rock support. Violent instabilities occur when external work promote a disruption of a state of equilibrium in the rock mass, and energy is suddenly released in the form of strain waves, so that the material becomes stable again.

Brittle rocks usually behave more or less elastically until they fail, but the elastic theory cannot explain the sudden release of energy characterizing rockbursts in a rock mass (Cook, 1965). Bursting mechanisms are related to the post-peak behavior of the rock. The violent instability of a rock mass can be compared to the behavior of a rock sample in a soft-testing machine. Here, the specimen under a uniaxial compression state of stress acts as the fractured rock and the loading system, as the surrounding rock mass. Figure 2.1 shows the analogy, where K_r is the pre-peak stiffness of the rock, K_r' is its post-peak stiffness and K_{sc} is the loading system stiffness.

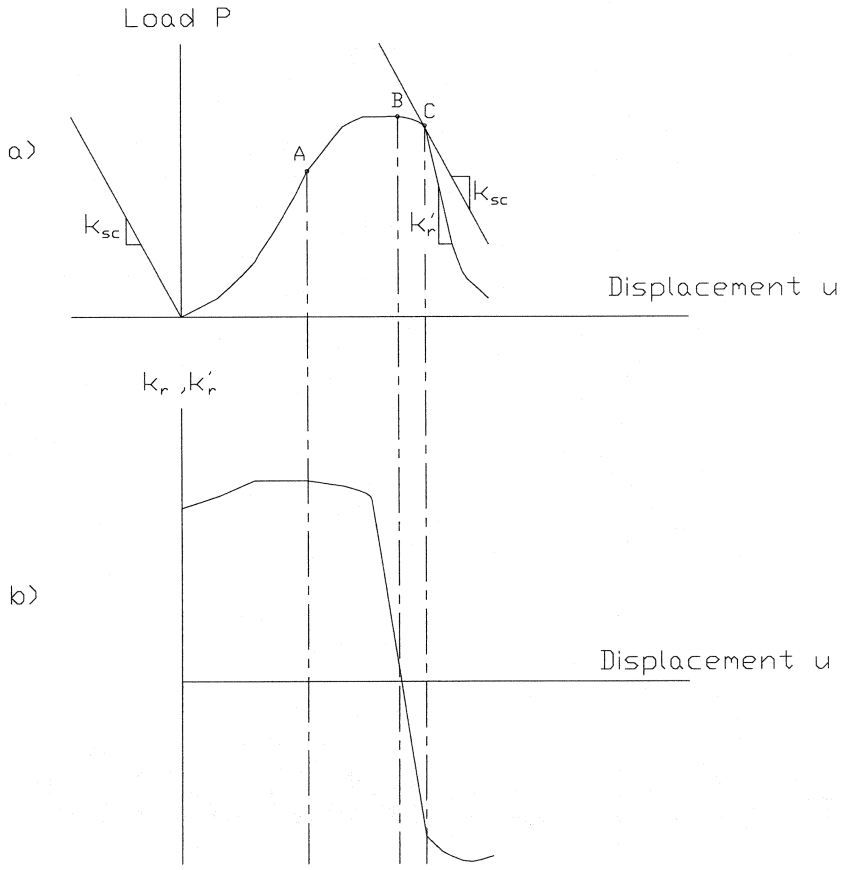

Figure 2.1 – a) Schematic load-deformation curve of a rock sample under uniaxial compressive strength test. b) Specimen's apparent stiffness behaviour as a function of the displacement of the press platen (adapted from Salamon, 1974).

When violent failure occurs, the amount of stored strain energy in the loading system is larger than the amount of energy that rock can dissipate over a certain increment in its post-peak phase. In other terms, there is a sudden failure when the surrounding rock mass stiffness is less than the post-peak stiffness of the fractured rock (in absolute values). With the same analogy, there is a gradual failure when the surrounding rock mass stiffness is higher than the post-peak stiffness of the fractured rock (Cook, 1965), given that the load on the rock mass exceeds the strength of the material. A somewhat similar analogy has been proposed by Salamon (1974) for seismic events caused by movements along a discontinuity plane. Figure 2.2 illustrates the loading system's relative stiffness influence on the rate of failure, where k_{sc} is the loading system stiffness and k'_p the post-peak stiffness of the fracture specimen submitted to tangential loading.

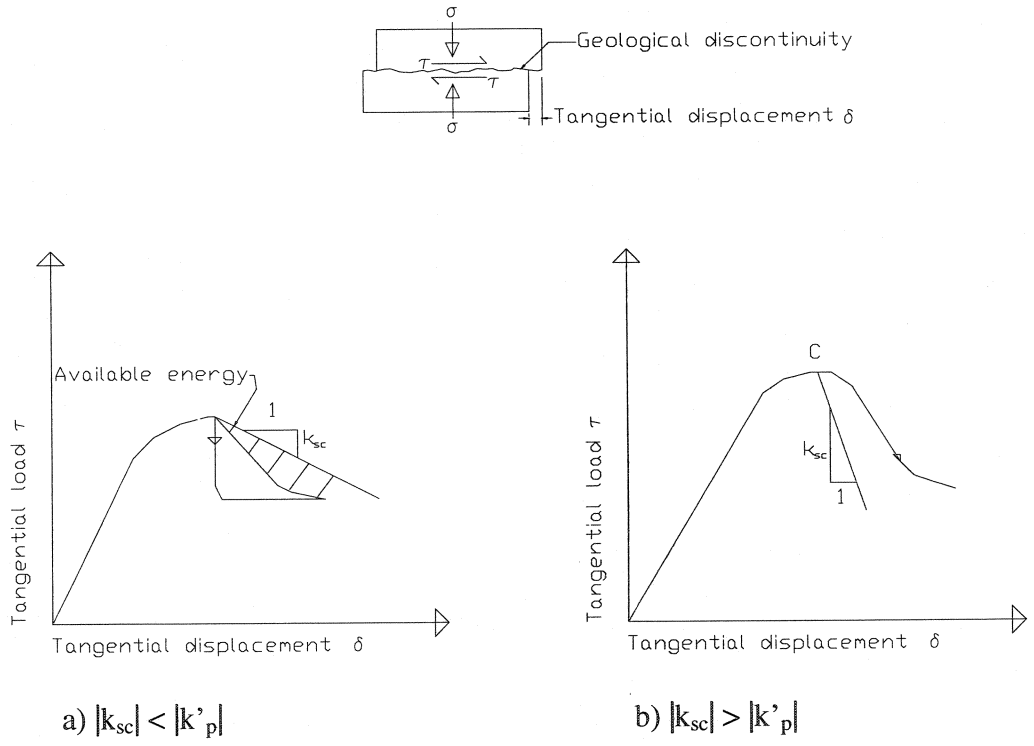

a) $|k_{sc}| < |k'_p|$ b) $|k_{sc}| > |k'_p|$

Figure 2.2 – Loading system's relative stiffness influence on the rate of failure. a) For a violent failure. b) For a gradual failure (adapted from Salamon, 1974).

It can be assumed that violent failure of a rock mass or along a geological discontinuity will produce a release of excess energy detectable through seismic waves. This concept will be elaborated further in Section 2.4.

2.2 Seismic event source parameters and classification

Seismic sensors detect waves caused by inelastic deformation within a certain distance. Since the attenuation of seismic waves increases with their frequency, the higher the amplitude and the lower the frequency, the longer the distance over which one can receive waveforms at a reasonable signal to noise ratio (Mendecki, 1997).

Seismic sensor arrays, data acquisition systems and processing software are used to decipher the recorded waveforms and generally provide at least an event location and time of occurrence.

The seismological classification of seismic events depends on the failure mechanism at the source of the tremor. Two broad types of mine tremors are observed almost universally – those directly connected with mining operations, that is, those associated with the formation of fractures at stope faces, and those associated with movement on major geologic discontinuities (Gibowicz, 1988, 1993).

Seismic source parameters are conventionally found from the spectra of each record of an event and then averaged (Gibowicz, 1993). In the next sub-sections, factors affecting the nature and intensity of mining seismic activity are presented.

2.2.1 Focal mechanism of mine seismicity

Before introducing the nature and calculation of source parameters, a general description of focal mechanisms is presented. These focal mechanisms relate to the damage

mechanisms of tunnels. Mine tremors can be classified by two generally accepted mechanisms, double-couple and non-double-couple mechanisms (Gibowicz, 1988). Double-couple mechanism is associated with movement along major geological discontinuities. These events are usually larger in magnitude than non-double-couple events. They often occur at some distance from openings and their time distribution is erratic. They seem to respond to mine-wide stress redistribution and can rarely be pinpointed to any specific area of mining. Physically, they are represented by a double-couple point source, consisting of two opposing force couples with no net force on torque.

Non-double-couple mechanism is suggesting the convergence of the surrounding rock mass on a volume of rock that fails suddenly near an excavation (Joughim and Jager, 1983). They are generally of lower magnitude than double-couple mechanisms.

For large seismic events, it is possible to approximate a fault-plane solution from the seismic event recorded at each sensor. This can be done by plotting the seismic event at the center of a lower hemisphere, equal area projection net, and then pole positions of each sensor relative to their axis to the event. The stereographic projection provides a convenient mean of calculating the orientation of planes in space. First motion analyses of the seismic trace will determine if the wave transmitted by each sensor had a compression or dilatation front. By identifying each pole with the proper polarity, it is then possible to find solutions for the fracture plane. A seismic event near the open face of an excavation would show dilatancy at each pole. A geological discontinuity plane would show compressional and dilatant poles with some sensors being attracted by the discontinuity movement, some others being "pushed" away from it.

Other methods for focal mechanism analyses, designed for small tremors, are composite fault-plane solutions, use of amplitude data, seismic moment tensor inversions and principal component analysis. The seismic moment tensor inversion is the approach most

generally used for the determination of a point source mechanism. Figure 2.3 illustrates moment tensor inversion solution. A review of its rather complex mathematical solution can be found in Gibowicz (1993) and Mendecki (1997). The moment tensor solutions can be quite helpful in identifying structural features at play in the particular surroundings of an excavation in highly stressed ground. Once identified, excavation methods, rates and means of rock support can be pro-actively altered in the surroundings of the structure. In essence, the moment tensor inversion and its decomposition can provide information about the nature of the seismic event relatively to the inherent displacement mechanism at the source.

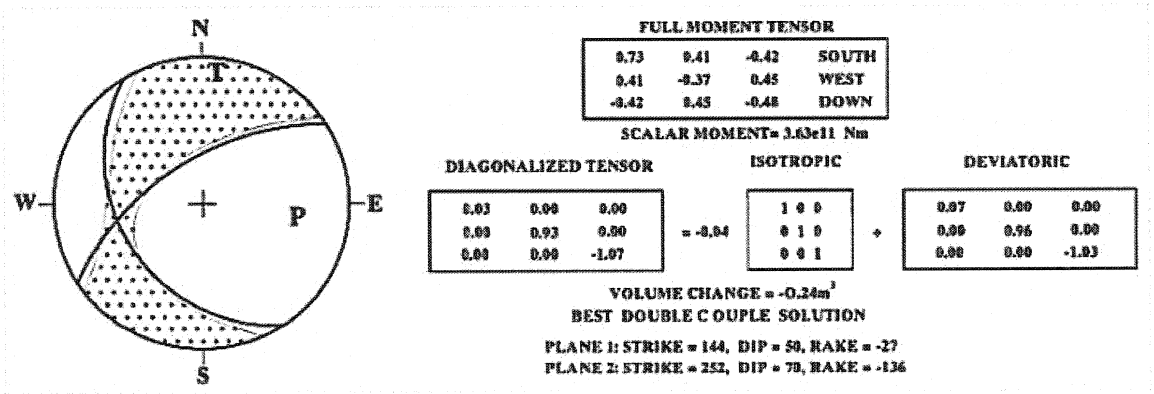

Figure 2.3 – Example of moment tensor inversion using ISS system (ISS International, 2002).

The stereographic projection shown in Figure 2.3 depicts the two possible fault plane solutions of a seismic event. Having compiled a number of these solutions, typically from large moment magnitude events, the seismic analyst can isolate the fault plane most likely to have been subjected to movement. This is done in light of known geological discontinuities in the rock mass.

2.2.2 Seismic moment, event magnitude and seismic energy

The seismic moment M_o, in contrast to the moment tensor, is a measure of the earthquake strength defined in terms of the double-couple shear dislocation source model (Gibowicz, 1993). It can be defined as (Mendecki, 1997):

$$M_o = \mu \bar{u} A \tag{2.1}$$

where $\bar{u}$ is an average displacement (slip) over the source area A, and μ is a constant.

Seismic event magnitude is most generally measured using the well-known local magnitude M_L (or M_m), introduced by Richter. Its general form:

$$\log M_o = aM_m + b \tag{2.2}$$

where M_m can be any magnitude and a and b are constants (Gibowicz, 1993). Parameters a and b in Canada are generally calibrated to match the relative scale of the regional seismic system maintained by the Geological Survey of Canada.

The fundamental scaling relation for earthquakes and seismic events is expressed in their frequency-seismic moment distribution. The number $N(M_m)$ of earthquakes with moment magnitude M_m obeys a relation:

$$N(M_m) = aM_m^{-b} \tag{2.3}$$

where a and b for a given set of observations are constants, although in general they are variable in space and time (Gibowicz, 1993). This relation is known as the Gutenberg-Richter relation. Since the moment magnitude of a seismic event is expressed as the

logarithm of its seismic moment, every increase in moment magnitude significantly increases the relative size of the shear displacement involved in the seismic event. Given a sample of seismic data, and using the Gutenberg-Richter relation between frequency and magnitude of seismic events, one can characterize the distribution of the data in terms of the b value. The latter is often used as a measure of regional seismicity. A low b value indicates that there are several small events in the distribution and few large ones, and inversely a high b value indicates that there are proportionally less small events in the distribution and more large ones.

The radiated seismic energy represents the total elastic energy radiated by an earthquake. The seismic energy better describes the potential for earthquake damage to artificial structures (buildings, etc.) than the seismic moment, although the seismic moment provides a better description of the overall size of an earthquake (Gibowicz, 1993). The seismic energy is calculated from the spectral analysis of the waveforms. The rock fracture and frictional sliding rates will affect the magnitude of the seismic energy. In terms of fracture mechanics, the slower the rupture velocity, the less energy is radiated; a quasi-static rupture would radiate practically no energy (Mendecki, 1997).

2.3 Rockburst definitions

In Eastern Canada rockbursts are often called "bumps". A 1920 definition of a bump is "a sudden breaking sometimes accompanied by a setting or upheaval of the strata in the mine, accompanied by a loud report. (...) often interpreted as a sudden squeeze, or buckling of the floor or walls of the mine passage-ways. It has its origin in the shocks accompanying earth movements" (Fay, 1947).

Rockbursts are violent failures of rock that result in damage to excavations (e.g. Cook, 1965). Only those events that cause damage in accessible areas of the mine are called

rockbursts (Gibowicz, 1993). Out of thousands of bumps recorded in Canadian mine seismic networks, only a few can be considered as rockbursts.

The rockburst phenomenon has many appellations, not to be confused with mine gas explosions or sulfur blasts. Cook et al. (1966) defined a rockburst as "damage to underground workings caused by the uncontrolled disruption of rock associated with a violent release of energy additional to that derived from falling rock fragments". The energy release can be in the form of seismic waves, sound waves or others. Damage can range from the expulsion of small fragments of rock from the sidewall of an excavation to the collapse of many square kilometers of pillared areas (Obert and Duvall, 1967).

A seismic event is a broader term referring to all occurrences that are associated with the release of kinetic energy, with the exclusion of blasting. Salamon (1974) suggested that a rockburst could be described as a seismic event that adversely affects the operation.

The Chamber of Mines of South Africa (Anon., 1982) suggested these definitions for seismic activity (Hedley, 1992). A seismic event is a transient earth motion caused by a sudden release of potential or stored strain energy in the rock. As a result, seismic energy is radiated in the form of strain waves. A rockburst is a seismic event that causes injury to persons, or damage to underground workings. The general and essential feature of rockbursts is their sudden, violent nature causing visible damage to underground openings.

2.4 Rockbursts source mechanisms, size and classification

Rockbursts can be classified as (Gill and Aubertin, 1988; Gill et al., 1993):
-Type I: "Fault-slip rockbursts" resulting from the slippage of major geological discontinuities,

-Type II: "Strain bursts and pillar bursts" resulting from the failure of portion of a rock mass.

Kaiser (1993) distinguish rockbursts as events triggered by these *modes* (Kaiser et al., 1996):

I- self-actuated ejection of fractured rock "strain burst",

II- ejection of part of a fractured, broken or jointed rock mass (driven by some seismic event in vicinity of excavation, or inertia or stress waves),

III- displacement of broken rock with gravity as dominant driving force component (seismically triggered falls of ground).

Ortlepp (1992a) depicted his interpretation of the main source mechanisms of rockbursts in underground haulages as shown in Table 2.1.

Table 2.1 – Suggested classification of seismic event source with respect to tunnels (Ortlepp, 1992a)

Seismic event	Postulated Source Mechanism	Source Mechanism from seismic record	Local Richter Magnitude
Strain bursting	Superficial spalling with violent ejection of fragments	Usually undetected, could be implosive	-0.2 to 0
Buckling	Outward	Implosive	0 to 1.5
Face crush	Violent expulsion from tunnel face	Implosive	1. to 2.5
Shear rupture	Violent propagation of shear fracture through intact rock areas	Double-couple shear	2.0 to 3.5
Fault-slip	Violent renewed movement on existing fault	Double-couple Shear	2.5 to 5.0

In Table 2.1, the top four mechanisms would relate to Type II rockbursts. The last mechanism describe slippage on discontinuities, such as Type I events.

Here, the author suggests a slightly different rockburst mechanism classification in Table 2.2 (Gaudreau, 2001). This classification was derived from Ortlepp (1992a). It aims to better reflect the relative calibration of Noranda Inc.'s mine seismic systems in relation to the observed seismic damage in some Canadian mines. The classification is illustrated in Figure 2.4. Note that this classification is somewhat arbitrary. Its intent is only to illustrate the relative magnitude of what could be "felt" by someone near the affected area, in terms of a fairly well known moment magnitude scale, namely the Richter scale. In fact, damage may be crudely estimated directly from the moment magnitude of the event and is obviously affected by the type of ground support in the heading. Gibowicz (1993) suggested that seismic energy was a better indicator for potential damage to artificial structures than seismic moment (or moment magnitude).

Table 2.2 - Classification for rockburst source mechanisms and associated damage.

Type of failure	Postulated mechanism at the source of the seismic event	Local Richter Magnitude
Stress-induced fracture	Energy dissipation in the rock mass by creation of new fractures	-3.0 to –1.0
Strain bursting	Superficial spalling of tunnel surface and violent ejection of rock particles.	-2.0 to 0.0
Buckling	Bending of rock slabs inwards the tunnel due to the pressure on both ends	0.0 to 1.5
Face crush/Pillar burst	Violent and deep expulsion of rock from a tunnel surface or multifaceted structure (pillar, rib, "skin" pillar, remnant)	1.0 to 2.5
Shear rupture	Violent propagation of a shear surface in a solid or healed area	1.0 to 3.0
Fault-slip	Violent slip on a pre-existing shear surface.	2.0 to 3.0

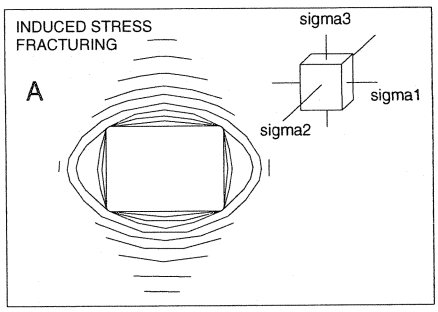

A-Responsible for the most part of recorded seismic events on a sensitive detector array.

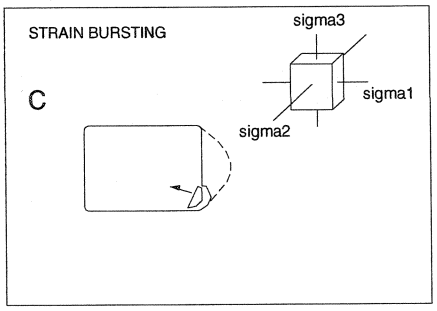

C- Violent failure of rock face due to the absence of confinement in highly stressed ground.

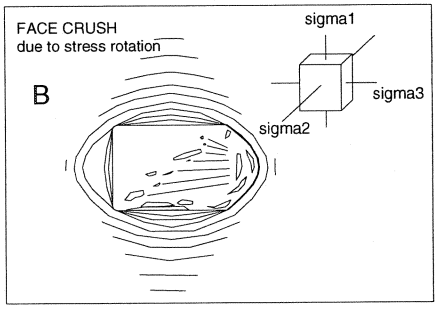

B- Usually triggered after some stress rotation due to mining in close proximity.

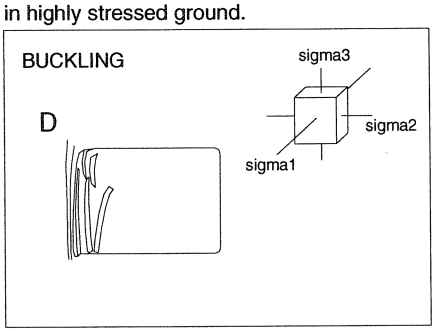

D- Induced stress fracturing will often occur striking along the excavation axis and dipping parallel to its walls when facing maximum principal stress direction. If a stress rotation occur, the slabs can be pinched out violently.

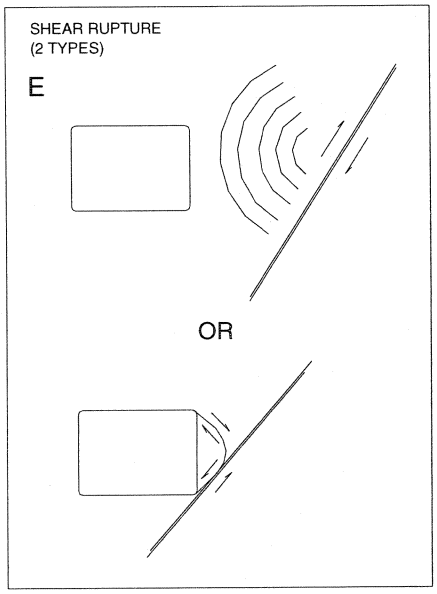

E- Usually associated with event of large scale along a healed geological discontinuity. Will be triggered relatively to regional stress changes.

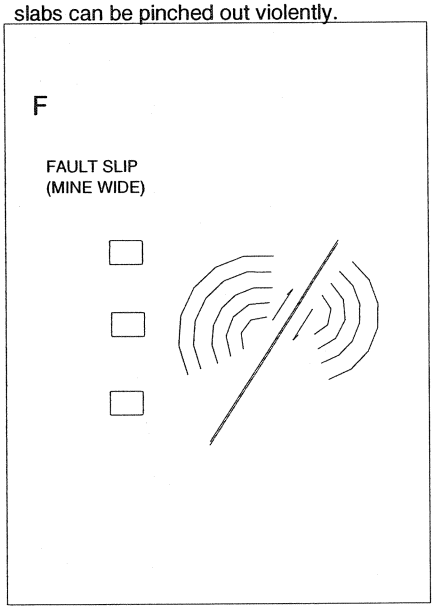

F- Triggered from mine wide stress changes on extensive geological discontinuities.

Figure 2.4– Tunnel damage classification (Gaudreau, 2001).

Simon et al. (1998) derived potential energetic considerations for Type II bursts "strain bursting", as a function of rock mass and loading system stiffness comparisons, in the context of developing a method for the evaluation of rockburst potential (called ERP method). These considerations are only valid if it is assumed that the portion brought near failure is under uniaxial compressive stress. They demonstrated that:

$$E_{x(\min)} = \frac{(C_0)_{mass}{}^2 A^2}{2}\left(\frac{1}{|k_e|} - \frac{1}{|k_{pr}'|}\right) \tag{2.4}$$

$$E_{x(\max)} = \frac{(C_0)_{mass}{}^2 A^2}{2|k_e|} \tag{2.5}$$

where E_x is the excess energy that can be dissipated in the burst, $(C_0)_{mass}$ the uniaxial compressive strength of the pillar, A its surface area, k_e the stiffness of the loading system and k_{pr}' the post-peak stiffness of the pillar. Following these equations, one can calculate the potential bursting energy of a tunnel abutment assuming that its lateral confinement is null. According to the equations, the larger the pillar, the higher is the excess potential energy.

The stiffness of the loading system k_e can be approximated using numerical modelling of the excavation. For this, Hoek and Brown's approach (1980) can be used, as depicted by Simon et al. (1998). This approach is valid if it can be assumed that the confinement on a given unstable structural element is small enough to be neglected. Thus a first model run is done to capture the geometry of the unstable element within the grid. The unstable structural element, such as a rock wall or a pillar, is then removed from the model and replaced by a uniformly applied pressure P_i at its loading extremities. Figure 2.5a depicts an example of such a situation. In this figure, the back (or roof) of the excavation is deemed unstable. Points A and A' delineate the axis for which displacement D is approximated with the simulation. The user can proceed with several runs of the

numerical model and modify the magnitude of pressure P_i for each run. Then, the simulation results can be used to trace the graph of $B*P_i$ as a function of D (see Figure 2.5b). Parameter *B* represents the width of the unstable structural element perpendicularly to the loading axis. It can be demonstrated that the slope of the curve represents the equivalent stiffness of the loading system. The latter can thus be calculated as a function of material properties, far-field stresses, and the unstable element geometry as well as the excavation's. Once the loading system stiffness k_e is known, it can be compared with the post-peak stiffness of the unstable element k_{pr}' as discussed in Section 2.1 to determine if the failure can release excess energy. Essentially, if the absolute value of the unstable element's post-peak stiffness is larger than the loading system stiffness, the failure can potentially be a rockburst.

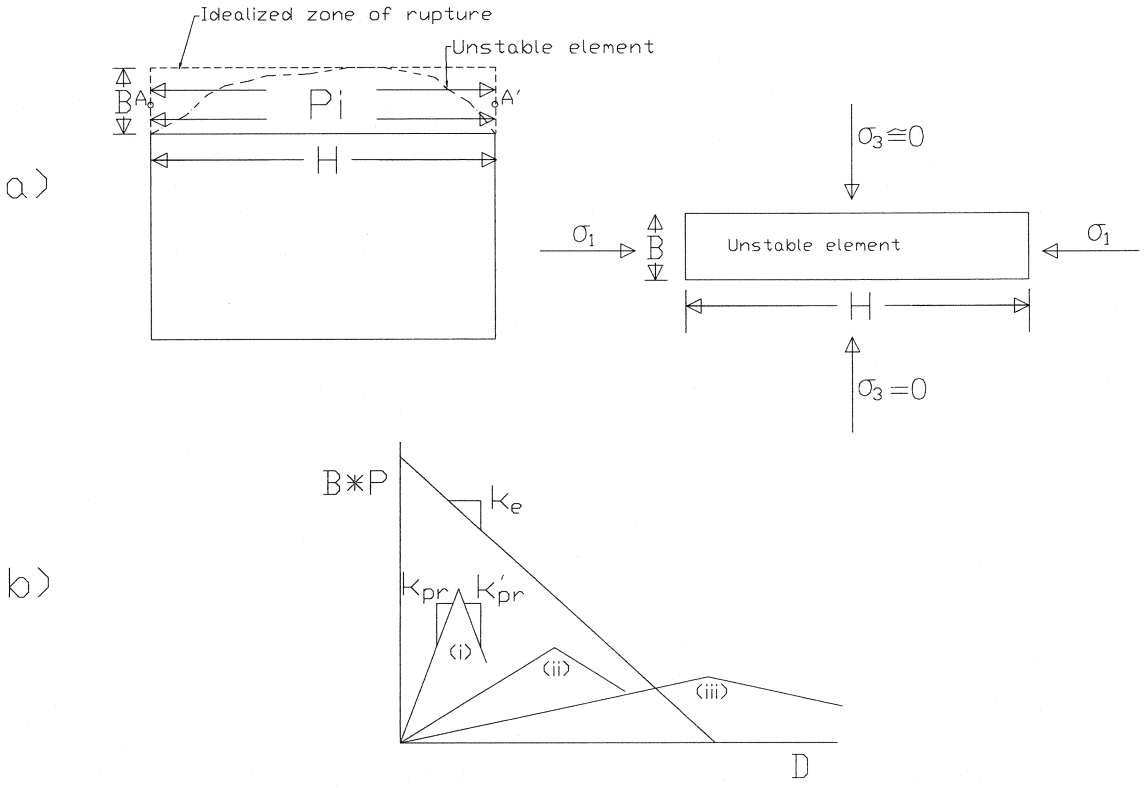

Figure 2.5 – a) Model used for estimating the equivalent stiffness of the loading system. b) Load-deformation curve illustrating i) violent failure ii) gradual failure iii) no failure. (After Simon et al., 1998).

The post-peak stiffness of the unstable element can be estimated using:

$$k_{pr}^{'} = \frac{E_m^{'} B}{H(1-\nu^2)} \tag{2.6}$$

where E'_m is the post-peak stiffness of the rock mass, B and H the width and length of the unstable element and ν Poisson's ratio, assuming uniaxial loading of the element.

The ERP method is useful to evaluate the rockburst potential of existing or planned excavations against Type II bursts. Type I bursts or violent slippage on discontinuities can be analysed with a somewhat similar process (Simon, 1999).

2.5 Performance requirements of yielding support

Progressively, the Canadian mining industry has witnessed increasing problems related to burst-prone ground, particularly large-scale underground base metal mines (e.g. Gill and Aubertin, 1988; Kaiser et al., 1996; Talebi et al., 1997; Simon et al., 1998; Simon, 1999; Simser et al., 2001). This led to vast research efforts to delineate the best support packages for extreme loading conditions.

This Section contains a review of the performance requirements of tendon support under quasi-static and impact loading in tunnels driven into burst-prone ground. Measurable parameters such as tunnel convergence, failure excess energy and block ejection velocity will be discussed, then compared with mechanical tendon performance for commercial tendons in Section 2.6.

2.5.1 Quasi-static loading requirements

Tunnels driven into highly stressed ground typically suffer from stress-induced damage (e.g. Wagner, 1984; Mühlhaus, 1990; Ortlepp, 1992a; Dyskin and Germanovich, 1993; Langille et al., 1995; Maxwell and Young, 1997). Stress-induced damage can form from either creation of new fractures or reactivation of existing fractures in the rock mass. This phenomenon is depicted in Figure 2.4a, showing an exaggerated profile of the induced fracture lines relative to the influence of the principal stress direction. The extent of the induced fracture zone can affect the amount of "dead load" in the back of the tunnel. Static loading performance of tunnel support in highly stressed ground must reflect this aspect. Further to this, the tunnel support must be able to tolerate relative convergence of tunnel walls, or swelling and squeezing rock conditions (Stillborg, 1986). Sidewall dilations in excess of 500 mm have been recorded under both static and dynamic conditions. However, when such large movements occur, the dimensions of conventional tunnels are reduced to such an extent that the basic functions of these tunnels cannot be maintained. Wojno et al. (1987) recommended a static tendon yield force greater than 100 kN to control wall movement. Moreover, these same authors suggested that the distribution of the dilation within the fractured zone is an important factor to the design of support tendons for yielding ground. They observed average values of dilation in a highly stressed tunnel to be such that 46% occurred within 2 m of the tunnel wall, 16% between 2-3 m and 38% at depths greater than 3 m from the tunnel sidewall. They thus recommended that the yielding range due to sidewall/hangingwall movement within the supported rock thickness for non-rockburst conditions be:

-230 mm for a tendon length of less than 2 m,

-310 mm for a tendon length of 2 m to 3 m

-500 mm for a tendon longer than 3 m.

Langille et al. (1995) have set the following criteria for the selection of a one-pass support system (i.e. that is installed in one cycle) for use in a high stress mining environment at Creighton Mine in Sudbury:

-immediate support of loose rock blocks for protection of men and equipment at the face,

-yieldability of at least 50 mm in the short term,

-long term rigid reinforcement of the broken rock mass

-corrosion resistance to heat, humidity, fumes, smoke and percolating mine water.

The quantity of material that could potentially be statically contained by a rockburst support package after a dynamic event can be in the order of 10 tons. Kaiser et al. (1992) have proposed a Rock Damage Scale for which levels of displaced rock range from a few kilograms to amounts greater than 10,000 kg.

2.5.2 Dynamic loading requirements

Dynamic loading implies physical forces producing motion. Stress changes and blast vibrations after mining to a new stope geometry can produce dynamic loading of a nearby tunnel. The stress regime at its periphery can fluctuate rapidly.

Wojno et al. (1987) have set these guidelines for the capacity of tendons in dynamic loading:

-The amount of work to be done during yielding of the tendon must be greater than 25 kJ (in worst conditions, this energy will be transferred from rock to tendon in a fraction of a second).

-The mean dynamic yield force must be in excess of 50 kN.

-The maximum dynamic yielding range must not exceed 500 mm of displacement.

-The dynamic strength of the tendon should exceed the static yield load of the tendon by at least 25 per cent.

Gaudreau (2000) set the design criteria for the components of a yielding support system for Noranda Inc. at:

-peak reaction load of less than 11.3 tons (25,000 lbs) and greater than 6.8 tons (15,000 lbs) for an impact energy of 15 kJ;

-tendon system plasticity limit at load greater than 6.8 tons (15,000 lbs);

-pull-out displacement greater than 150 mm (at maximum static capacity and at impact loading of 15 kJ);

-ability to install in cement or polyester resin grout using mechanized or non-mechanized means of installation;

-support must not creep if load below plasticity limit after initial movement of the anchor;

-better corrosion resistance than resin-rebar installation;

-support can be pre-tensioned at installation;

-support to be installed in a 38 mm hole with a 17 mm smooth bar of grade C1060.

These criteria were set to match energy absorption and wall control requirements from damage observed underground at Brunswick Mine and from other operational restrictions including compatibility with the mine's machinery and rapidity of installation. The choice of the smooth bar was made based on two assumptions:

-it is preferable for the full rock load transfer in the steel rod from the reaction plate to the bolt's inner end,

-there is a possibility for creating an "active" support effect, i.e., additional clamping charge transferred to the rock mass during the event of a strain burst from a tunnel face.

The second assumption could be verified if it can be demonstrated that the volume of rock subjected to failure decreases with the instantaneous clamping provided by the bolt during the burst.

2.5.3 Ground vibration and velocity

Ground vibrations from major pit and stope blasts nearby underground tunnels at Kidd Creek Mine, Timmins, Ontario were measured using a blast vibration monitor. Yu (1980) compiled peak particle velocity measurements and rock damage observations as summarised in Table 2.3. The maximum range of 150 cm/s results in unmanageable damage.

Stillborg (1986) identified the maximum particle velocity affecting the load bearing capacity of fully cement grouted cable bolts at 50 cm/s. This is in good agreement with Table 2.3. Wojno et al. (1987) have set a design criterion of 300 cm/s relative to peak ground velocity and rockburst support based on seismological analyses.

Wagner (1984) compiled case studies of damage to underground openings and estimated peak velocities for a set of deep South African mines (Table 2.4).

Ortlepp (1993) compiled block ejection velocity observations and measurements near sources of major seismic events. He supports that only seismic failure in the vicinity of the workings is likely to generate the peak velocity necessary to cause the support failure, but that the design values could range from 3-10 m/s for the performance of rockburst support in that area.

Kaiser et al. (1996) proposed a series of charts to calculate the demand on support using peak particle velocity. The charts (or abacuses) correlate moment magnitude and distance from the source to the expected peak particle velocity. In these charts, very high peak particle velocities are ranging above 1 m/s.

Table 2.3 – Blasting ground vibration and damage criteria (Yu, 1980).

Peak Particle Velocity (cm/sec)	Type of Damage
25	No noticeable damage to underground workings. Maximum tolerable vibration level for permanent drifts.
30	Fall of rock in unlined tunnels.
50	Minor scabbing failure observed. Maximum tolerable vibration level for main drifts.
75	Development of cracks in weak ground. Timber sets required to support scabbing wall. Maximum tolerable vibration level for temporary accesses.
100	Possible formation of cracks 1.5 cm wide along weak plane of geologic structures causing severe dripping of water and potential failure.
125	Major scabbing failure in an entire drift leading to failure of pillars associated with strong geological features.
≥150	Possible formation of cracks 1.5 cm wide in drifts of competent rock resulting in abandoned accesses.

A maximum peak particle velocity criteria is useful to derive guidelines relative to the required energy absorption capacity of tendon support. The estimated maximum ground velocity can be combined with an estimation of the probable ejected weight assigned to the surface area of the support system. The energy absorption capacity can be calculated using the kinetic energy imparted to the block (Ortlepp, 1994):

$$KE = 0.5 * m * v^2 \qquad (2.7)$$

where KE is the kinetic energy (in Joules), m is the mass of the block or unstable element (in kg) and v is the peak particle velocity or block ejection velocity (in m/s).

Table 2.4 – Summary of rockburst damage information (Wagner 1984).

Mining district	Magni-tude of event	Distance of damaged areas from source of event	Nature of damage	Estimated peak velocity
Klerksdorp	4.4	200 m	Faces within 100 m source completely closed. Extensive damage to sidewalls and tunnels.	at 200 m v = 2 m/s at 100 m v = 3.5 m/s
Klerksdorp	5.0	up to 750 m	Faces within 250 m from source completely closed. Stope faces up to 750 m from source showed appreciable damage.	at 750 m v = 0.9 m/s at 250 m v = 2.6 m/s
Klerksdorp	3.9	100 m	Extensive sidewall damage in tunnels.	at 100 m v = 1.7 m/s
Klerksdorp	2.7	±100 m	40 m of stope face damaged. 90 m from event extensive roof falls in tunnel.	at 100 m v = 0.4 m/s at 50 m v = 1 m/s
Klerksdorp	1.1	±10 m	Stope travelling way collapsed.	at 10 m v = 0.4 m/s
Carletonville	4.0	±100 m	Total closure of stope for a distance of 100 m either side of focus of event. Follow low-on tunnels not effected.	at 100 m v = 1.7 m/s at 50 m v = 3.5 m/s
East Rand	2.9	±50 m	Stope face completely closed for a distance of 30 m and extensive falls for another 10 m. Cross-cut to stope collapsed but post developed footwall tunnels undamaged.	at 50 m v = 1 m/s at 15 m v = 3 m/s
Central Rand	2.0	±50 m	Main haulage almost completely closed over a distance of 20 m and showing appreciable damage for over a total distance of 90 m.	at 50 m v = 0.26 m/s at 10 m v = 1.2 m/s

2.6 Performance of yielding support

Quasi-static and dynamic mechanical performance for commercial tendons is presented in this sub-section in light of performance requirements of yielding support. Failure of tendon support can be induced by the four failure inducing agents listed below (Collins, 1993):

- Force : Steady, transient, cyclic or random.
- Time: Very short, short, long.
- Temperature: Low, room, elevated, steady, transient, cyclic or random.
- Reactive environment: chemical, nuclear.

Different failure modes (e.g. Collins, 1993) can be observed on failed tendon support and can be induced by static, quasi-static or dynamic loading. Failure modes can be characterised as brittle, ductile, due to fatigue or corrosion, to impact loading or due to stress corrosion.

Brittle failure occurs when the elastic deformation is carried to the extreme so that the primary inter-atomic bonds are broken and the member separates into two or more pieces. Pre-existing flaws or growing cracks form initiation sites for very rapid crack propagation to catastrophic failure, leaving a granular, multifaceted fracture steel surface.

Ductile rupture failure occurs when the plastic deformation is carried to the extreme so that the member separates into two pieces. Initiation and coalescence of internal voids propagate to failure, leaving a dull, fibrous rupture surface.

Fatigue failure of tendon support can occur at the threaded end due to the method of installation (e.g. Hedley and Whitton, 1987). It results in the separation of a tendon part as a result of the application of fluctuating loads or deformations over a period of time.

This is the case during the installation process of some tendon types such as threaded rebars. These tendons are installed with rotating dollies that often do not perfectly align with the tendon axis. The steel grains are thus pulled apart one from another next to the dolly and the tendon is permanently damaged.

Corrosion failure implies that a tendon part is rendered incapable of performing its intended function because of the undesired deterioration of the material as a result of chemical or electrochemical interaction with the environment.

Impact failure occurs when a tendon member is subjected to non-static loads that produce stresses or deformations of such magnitude that the member is no longer capable of performing its function. The failure is brought about by the interaction of stress or strain waves generated by dynamic or suddenly applied loads, which may induce local stresses and strains many times greater than would be induced by static application of the same loads.

Stress corrosion failure occurs when the applied stresses on a tendon part in a corrosive environment generate a field of localised surface cracks, usually along grain boundaries, that render the part incapable of performing its function, often because of triggering some other failure mode.

2.6.1 Failure of materials in quasi-static loading and relaxation mode

Quasi-static loading relates to bodies or forces at rest or in equilibrium. The loading is fixed or changes very slowly. Quasi-static loading or convergence of underground openings occurs when stresses in the region of the excavation are large enough to cause relaxation of the rock material. Typically, displacement vectors are larger when closer to the tunnel walls, where the confinement is minimal.

Important characteristics of tendon support systems (e.g. Stillborg, 1986; Hoek and Wood, 1987) for quasi-static load considerations are the steel designation, yield stress, steel diameter, hole diameter and tendon length. These will serve as indicators of tendon performance for applied reinforcement designs.

2.6.2 Quasi-static loading testing methods for tendons

Quasi-static pull testing is generally used to evaluate the in-situ reaction of tendon support. This consists in extracting pre-installed rock support from its installation site using a hydraulic ram while measuring the force given to the ram and the displacement of the tendon at the collar of the hole. The pull test procedure is further depicted in Chapter 3.

The instrumented pull test result consists of a load displacement characteristic curve representing the possible performance of tendons under the same relative displacement. Such a schematic characteristic curve is illustrated in Figure 2.6.

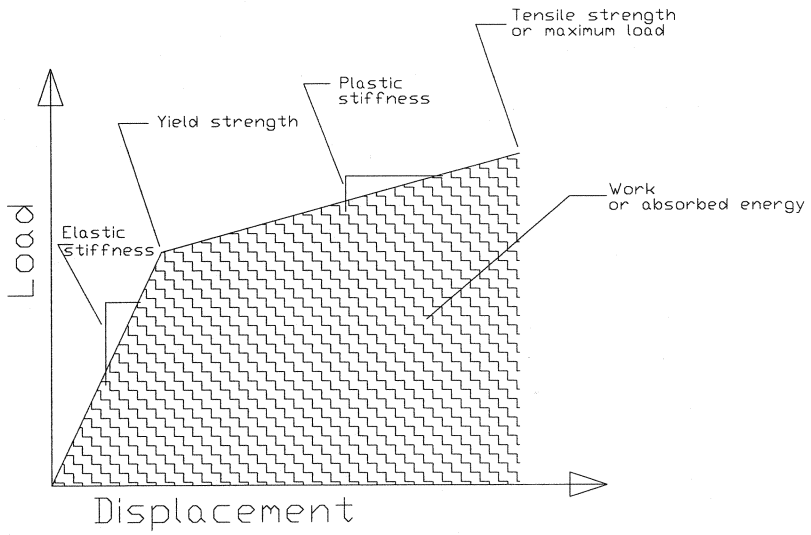

Figure 2.6 – Schematic of typical pull test result curve.

2.6.3 Commercial bolt characteristics in quasi-static loading

Tables 2.5 to 2.10 present pull test results presented by various authors. These Tables are shown to illustrate the different characteristics of a selection of products for underground tunnel stabilisation in highly stressed ground. Table 2.5 depicts stiffness ranges of a selection of tendon support systems used in Québec mines. Note that illustrations of most tendons described in Chapter 2 are given in Appendix. Charrette (1991) used a relative stiffness scale to compare support systems. The stiffness scale was calculated as the slope of the load-displacement graph of a tendon going in a straight line from zero loading to its typical maximum load and displacement specification, disregarding the transient tendon deformation response. From this Table, resin-anchor bolts offer the stiffest mechanical response.

Table 2.5 – "Stiffness" scale for different bolting systems (After Charette, 1991)

Bolt type	Stiffness (kN/m)
Split Set	2000 to 3000
Mechanical anchor bolt (diameter=19mm)	3500 to 5250
Mechanical anchor bolt (diameter=22mm)	5250 to 8500
Resin anchored bolt (diameter=22mm sealed in a 32mm hole)	7800
Standard Swellex bolt in a 32 mm hole	8500 to 12000
Standard Swellex bolt in a 38 mm hole	22000 to 26000
Cement grout anchored bolt (diameter=22mm sealed in a 32mm hole)	26000 to 35000
Resin anchored bolt (diameter=22mm sealed in a 25mm hole)	70000

The role of each support component in a support system depends on its characteristics. Stiffer tendon types (Table 2.5), such as rebars, are generally strong and provide immediate support with little ability for the walls to deform. Softer rock tendons will yield to ground movement, to some degree, while providing a certain level of support to

the walls. Table 2.6 contains specifications of Split Set bolts as manufactured by Ingersoll-Rand. It can be seen that although the Split Set support's characteristic curve is "softer" than a resin-rebar installation, it is not as strong (compare with Table 2.10).

Table 2.6 – Split Set specifications (After Hoek, 2000)

Split Set stabiliser model	SS-33	SS-39	SS-46
Recommended nominal bit size	31 to 33 mm	35 to 38 mm	41 to 45 mm
Breaking capacity, average	10.9 tonnes	12.7 tonnes	16.3 tonnes
Minimum	7.3 tonnes	9.1 tonnes	13.6 tonnes
Recommended initial anchorage (tonnes)	2.7 to 5.4	2.7 to 5.4	4.5 to 8.2
Tube lengths	0.9 to 2.4 m	0.9 to 3.0m	0.9 to 3.6 m
Nominal outer diameter of tube	33 mm	39 mm	46 mm
Domed plate sizes	150 X 150 mm 125 X 125 mm	150 X 150 mm 125 X 125 mm	150 X 150 mm

Tannant and Buss (1994) have tested and compared different tendons in search of an off-the-shelve yielding tendon support system for burst-prone ground. Table 2.7 to 2.9 summarise these results. The authors have tested cut-off tubular bolts (i.e. smooth bars) and grooved tubular bolts. The grooved tubular bolts were machined near the expansion shell location to break loose of the point anchor and then slide like the smooth bar. The Cone Bolt developed by Jager (1992) is amongst the tested specimens (Table 2.8). Results in Table 2.9 show that the bolt is closer to compliance with the performance criteria of yielding support set by Wojno et al. (1987) when installed in cement grout.

Table 2.7 – Dimensions and properties of Stelpipe tubular rockbolts (After Tannant and Buss, 1994)

Shank diameter	Tube wall thickness	Yield Strength	Min. Tensile Strength	Min. Breaking load for bolt
17.3 mm	4.3 mm	620 MPa	758 MPa	133 Kn

Table 2.8 – Load, displacements, and work energy for cut-off and grooved tubular rockbolts (After Tannant and Buss, 1994)

Bolt type	Length (m)	Initial Peak		Sliding and Steel Elongation		
		Peak Load (kN)	Disp. (mm)	Peak Load (kN)	Max. Disp. (mm)	Energy (kJ)
Cut-off	0.5	46	1.5	NA	200	4
	1.0	70	1	120	317	24
	1.5	85	1	136	52*	6
Grooved	0.20	97	6	61	164	6
	0.50	106	4	70	285	12
	0.75	90	4	138	312	28
* bolt failed						

Table 2.9 –Loads, displacements, and work energy for 16 mm cone bolts (After Tannant and Buss, 1994)

Grout	Initial Peak		Steel Elongation		
	Peak Load (kN)	Disp. (mm)	Peak Load (kN)	Max. Disp. (mm)	Energy (kJ)
Cement	121	6	156	253	33
Resin	119	6	160	107	15

The 1.8 m long Cone Bolts in Table 2.9 were resin grouted using 2-4 min. set time DuPont Fasloc resin, and cement grouted using Portland cement at a 0.4 water to cement ratio. In Table 2.10, all support types were 1.8 m long and installed in 32 mm boreholes. The resin grouted rebar had one 0.45 m long fast setting (10-15 sec.) resin cartridge at the toe of the hole and two 0.6 m long cartridges (2-4 min. gel time) to the collar of the hole. The cartridges had a 29 mm diameter. Cement and resin grouted rebar consisted of rebars installed in boreholes with fast setting resin at the toe of the hole with the remainder of the bolt grouted in slow setting cement grout. Jager et al. (1992) Cone Bolt tested were installed in a water based "modified resin" product.

Kaiser et al. (1996) proposed pull strength parameters for tendon support and mesh as shown in Table 2.11. The energy absorption values were derived from the work energy based on static pull testing curves. The different tendons are classified by their ability to yield. Split Sets, Swellex and Cone Bolts were classified within the best yielding tendons available on the Canadian market, thus would be better suited for use in rockburst-prone areas to prevent damage. A pull-testing program should be designed at the mine site to compare tendon support elements to one another where it is intended for them to be used. Table 2.11 also contains data on various types of meshing. Meshing and/or liners have importance in the design of a rockburst support package, since they are required for the rock load transfer to the bolting system. Tendons alone cannot contain rockburst damage.

Table 2.10 – Summary of pull-test results (After Langille et al., 1995)

Bolt type	Bolt No.	Age (days)	Peak Load (kN)	D_{150}* (mm)	Results	Comments
Resin-	std1	5	170	6.2	bolt broke	-
grouted	std2	5	165	4.4	test stopped	-
rebar	std3	5	169	151	bolt broke	poorly grouted
cement and	cmnt1	5	170	13.6	bolt broke	poorly grouted
resin-	cmnt2	7	172	8.8	bolt broke	-
grouted	cmnt3	7	159	11.0	test stopped	well grouted
rebar	cmnt4	9	163	11.8	test stopped	-
	cmnt5	9	165	7.8	test stopped	-
resin-	cone1	1	127	94	adapter fail.	bolt bent
grouted	cone2	13	156	115	bolt broke	well grouted
cone bolt	cone3	13	152	89	test stopped	-
	cone4	15	110	>430	test stopped	load oscillations
	cone5	15	157	141	bolt broke	-

*D_{150}=displacement (mm) at load of 150 kN.

Table 2.11 – Load-displacement parameters of support elements (Kaiser et al., 1996)

Description	Peak load (kN)	Displacement limit (mm)	Energy absorption (kJ)
19 mm resin-grouted rebar	120-170	10-30	1-4
16 mm cable bolt	160-240	20-40	2-6
16 mm, 2 m mechanical bolt	70-120	20-50	2-4
16 mm, 4 m debonded cable bolt	160-240	30-50	4-8
16 mm grouted smooth bar	70-120	50-100	4-10
Split Set bolt	50-100	80-200	5-15
yielding Swellex bolt	80-90	100-150	8-12
yielding super Swellex bolt	180-190	100-150	18-25
16 mm cone bolt	90-140	100-200	10-25
#6 gauge welded-wire mesh	24-28	125-200	2-4/m^2
#4 gauge welded-wire mesh	34-42	150-225	3-6/m^2
#9 gauge chain-link mesh	32-38	350-450	3-10/m^2
shotcrete and welded-wire mesh	2 X mesh	< mesh	3-5 X mesh*
Displacement limit and energy absorption are taken at the point of failure for rock bolts and at peak load for mesh or shotcrete * at displacements below 100 to 150 mm			

2.6.4 Failure of materials under impact

This section contains an overview of materials performance under impact or rapid loading.

Table 2.12 provides reference literature pertaining to the strength of steel materials having similar properties to the materials tested in Chapter 3.

Table 2.12 - Impact strength of selected materials (after Oberg et al., 1996)

AISI #	Treatment	Strength		% Elongation at failure	% Reduction in Area
		Tensile	Yield		
		Mpa			
1050	As-rolled	724	413	20	40.0
	Normalized 1650F	748	427	20	39.4
1060	As-rolled	813	482	17	34.0
	Normalized 1650F	775	420	18	37.2

Under dynamic loading, steel material properties may be changed from their quasi-static values. Most of the increase in ultimate strength is achieved in the range of loading rates corresponding to impact velocities up to 7.6 m/s. Further increase of the loading rate above this level seems to produce very little additional change in ultimate strength (see Collins, 1993). Table 2.13 shows a list of material properties from Collins (1993) where samples were tested in axial impact loading. Dynamic ultimate strength shown were tested at 7.6 m/s.

Table 2.13 - Properties of selected steel materials loaded at a displacement rate of 7.6 m/s (Collins, 1993).

Material	Condition	Static Yield Strength MPa	Ultimate Strength (MPa)	
			Static	Dynamic
SAE 1015	Annealed	201	348	437
1045	Normalized	382	674	728
1045	Annealed (low)	332	561	806
1045	Annealed (high)	356	650	911
1045	Spheroidized	457	528	678
1045	Q.&T.	911	985	1165
1095	Normalized	510	997	1041
1095	Q.&T.	937	1216	1175

Table 2.13 shows that for most steels, the impact strength is greater than the quasi-static ultimate strength at 7.6m (25 foot) per second loading rate. Collins (1993) suggests that there is also a critical impact velocity for which the steel material will fail in a brittle fashion. This velocity corresponds to the loading rate for which the struck end would move faster than the plastic deformation wave could propagate through the material, thus causing failure of the material. This velocity is in the order of 25 m/s for annealed 1020 steel (Collins, 1993).

2.6.5 Rapid load testing methods for rock tendons

Most tendon rapid loading testing methods depicted in the literature can be classified under explosive loading or impact loading categories.

2.6.5.1 Controlled explosive testing

Ortlepp (1992b) discussed the blast testing approach where a tunnel half-section is bolted with conventional end-anchored bolts and the other half with yielding end-anchored bolts. These trials were conducted by Ortlepp in 1969. The test was used to demonstrate the relative performance of both support systems under dynamic loading. Given the complex nature of a blast deflagration, critics could demonstrate that the nature of a ponctual explosion and a seismic event are distincively different. For example, gazeous emmissions during an explosive test are expelled through cracks and rock joints, thus making it difficult to calculate the real energy absorption of the support package. Furthermore, an explosive impact will not show the distincive shear wave component of a seismic event. Ortlepp (1992b) also indicated that it is difficult to visually distinguish rockburst damage from explosive damage.

Another widely published experiment concerns the explosive testing of the COMRO Cone Bolt, developed and manufactured by Strata Control Systems, and now

manufactured by Steeldale in South Africa (see Ortlepp, 1994; Stacey & Ortlepp, 1994, 1999, 2000; Ortlepp & Stacey, 1998). In this experiment, six different sets of support tendons, namely two distinct sets of 16 mm Cone Bolts, and one set of each 16 mm rebars, 16 mm smooth bars, 25 mm rebars and 22 mm Cone Bolts (see Table 2.14) were installed in a quarry. Each set was installed and grouted into bedrock through a 0.3 X 0.45 X 0.5 m independent concrete slab. Explosive charges were then inserted in horizontal cavities consisting of rows of PVC pipes laid on the bedrock before the casting of concrete. Each slab was tested separately and monitored using a high-speed camera and a velocity transducer consisting of a velocity of detonation electronic timer. The objective of the experiment was mainly to compare the performance of a stiff support system to a yielding one. The explosive jolt was not the same from one test to another, making it difficult to estimate the energy absorption of each set. Gases from explosive charges did not burst out from the fractured ground in exactly the same way every time, thus inducing a different energy at each test.

Tannant et al. (1992) used a different approach when a test drift, located near a large stope, was instrumented in the expectation of a large blast susceptible of triggering seismic activity. Accelerometers were set up directly on Split Sets, mechanical bolts and Swellex bolts. The performance of tendon support under these events was thus measured. The peak particle velocity measured was in the range of millimetres per second, whereas ejection velocities during a rockburst are in the order of 1 to 10 meters per second. Although this technique measures the impact of real seismic events on tendon support, it carries a disadvantage, the uncertainty of expectation. One must wait until a natural seismic event hits a particular instrumented area to get results.

Ansell (1999) and Tannant et al. (1994) have worked on an approach were the dynamic damage is simulated in a tunnel by using a blasthole drilled at a small angle to the axis of the haulage. The maximum ejection velocities were no greater than 2 meters per second, but were successful in creating damage to the haulage. The tests showed that loading by

explosives close to bolts causes cracking of the surrounding rock and thereby inadequate loading of the bolts. Furthermore, it would be preferable to test support packages at velocities higher than 2 m/s for rockburst support design.

2.6.5.2 Impact testing

Special impact test rigs have been used to test tendons at impact velocities and loads that are comparable to these of yielding support system requirements.

Ansell (1999) grouted yielding tendon support inside a large cylindrical concrete mass. The mass, attached to an horizontal H-beam, was dropped from the ceiling of a two story high pilot plant, to a receiving structure were it was suddenly stopped (see Figure 2.7. The set-up was used for fully grouted bolts (as in the figure) and for ungrouted steel bars coupled to steel weights.

Stacey and Ortlepp (1999) used a swing-beam mechanism and a large mass to provoke the separation of a test tube where the tested tendon is installed (see Figure 2.8).

Maloney and Kaiser (1996) have designed the test rig that has been installed at Brunswick mine in 1997 and was later modified by Noranda Inc. (see Figure 2.9). The test rig was never used at the mine site due to operational difficulties.

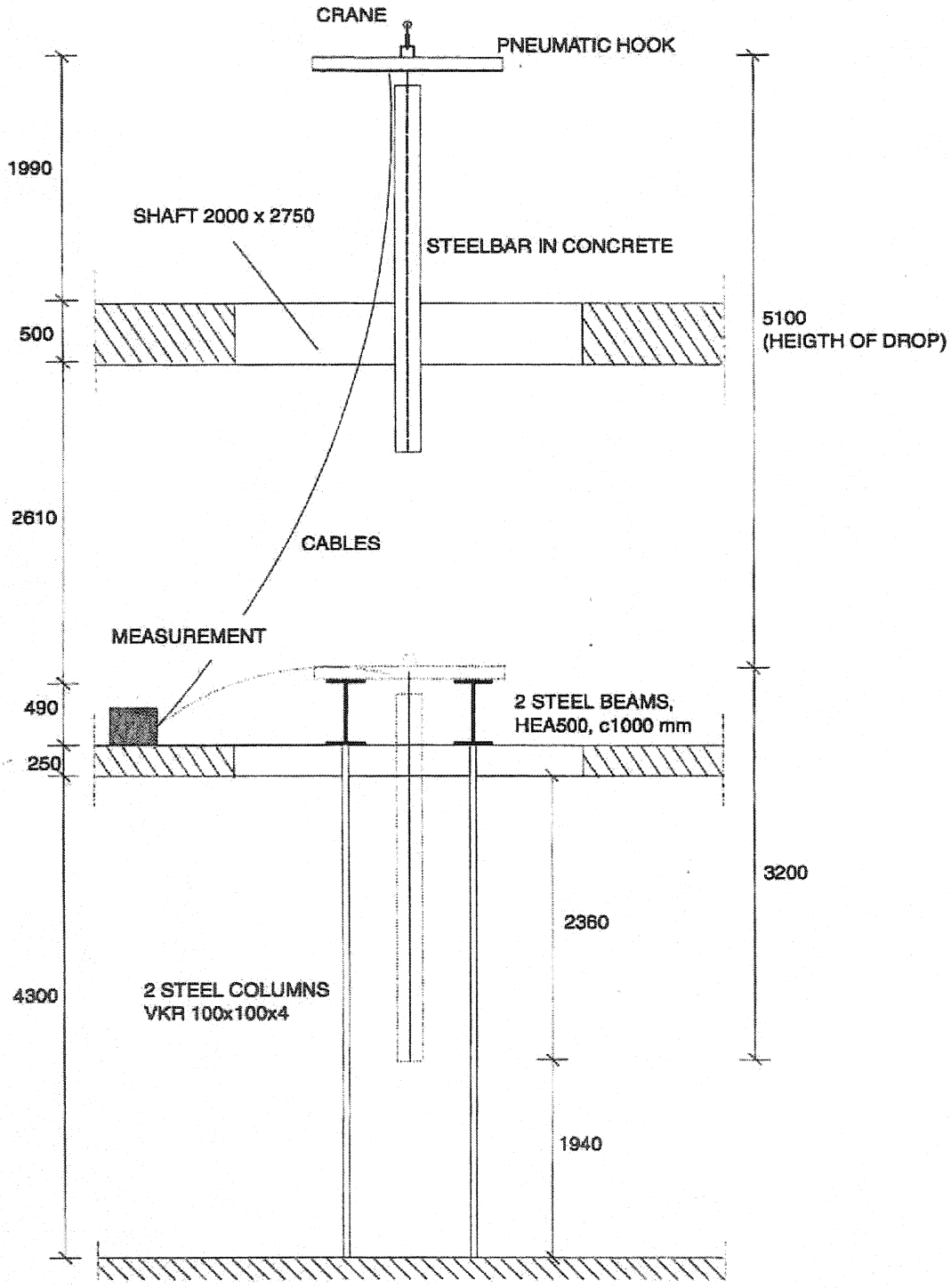

Figure 2.7 – Test set-up for dynamic testing of rock bolts (from Ansell, 1999).

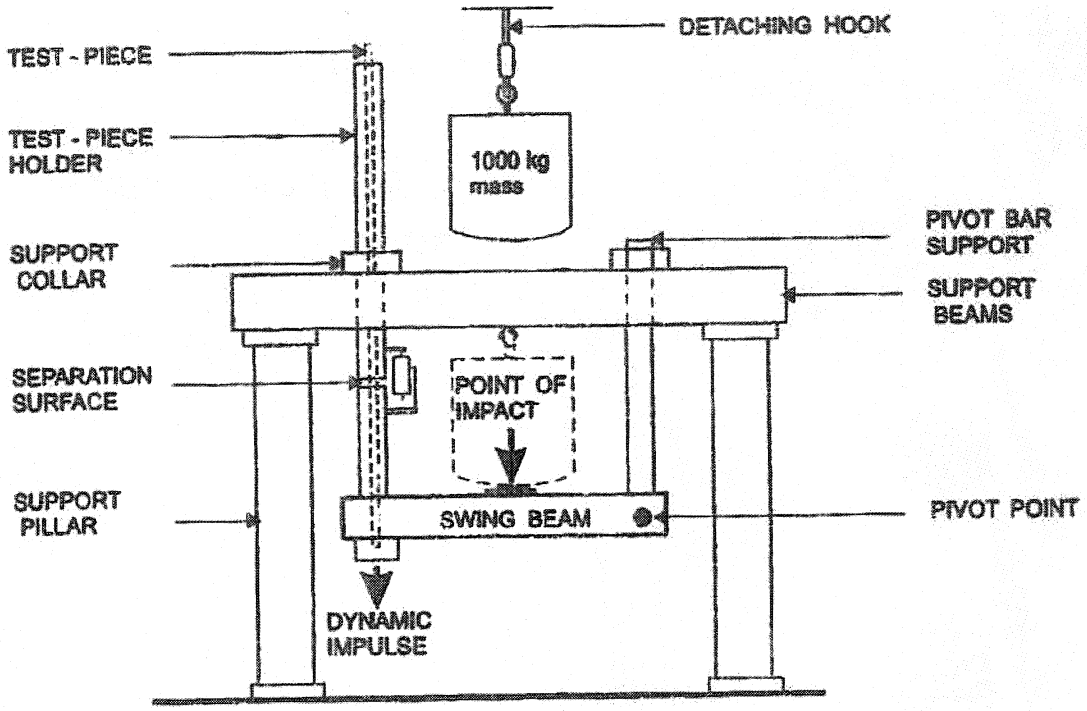

Figure 2.8 – Dynamic testing facility (from Stacey and Ortlepp, 1999).

2.6.6 Compilation of impact testing results from commercial units

This section contains a compilation of impact testing results on tendon support. Table 2.14 presents test results obtained from controlled explosive testing of tendon support. The calibration tests give an appreciation of how high the test blocks ascend without support for explosive charges of 0.5 kg and 1.0 kg. From the perspective of controlling vertical displacement of the slab, "softer" support systems such as smooth bars and Cone Bolts seem to perform better compared to "stiffer" systems such as rebars under such loads. The comparative test can at least illustrate that point. Looking at these figures, it can be observed that the 16 mm rebar had apparently no effect on the movement of the concrete pad, since the pad flew higher than for the calibration test.

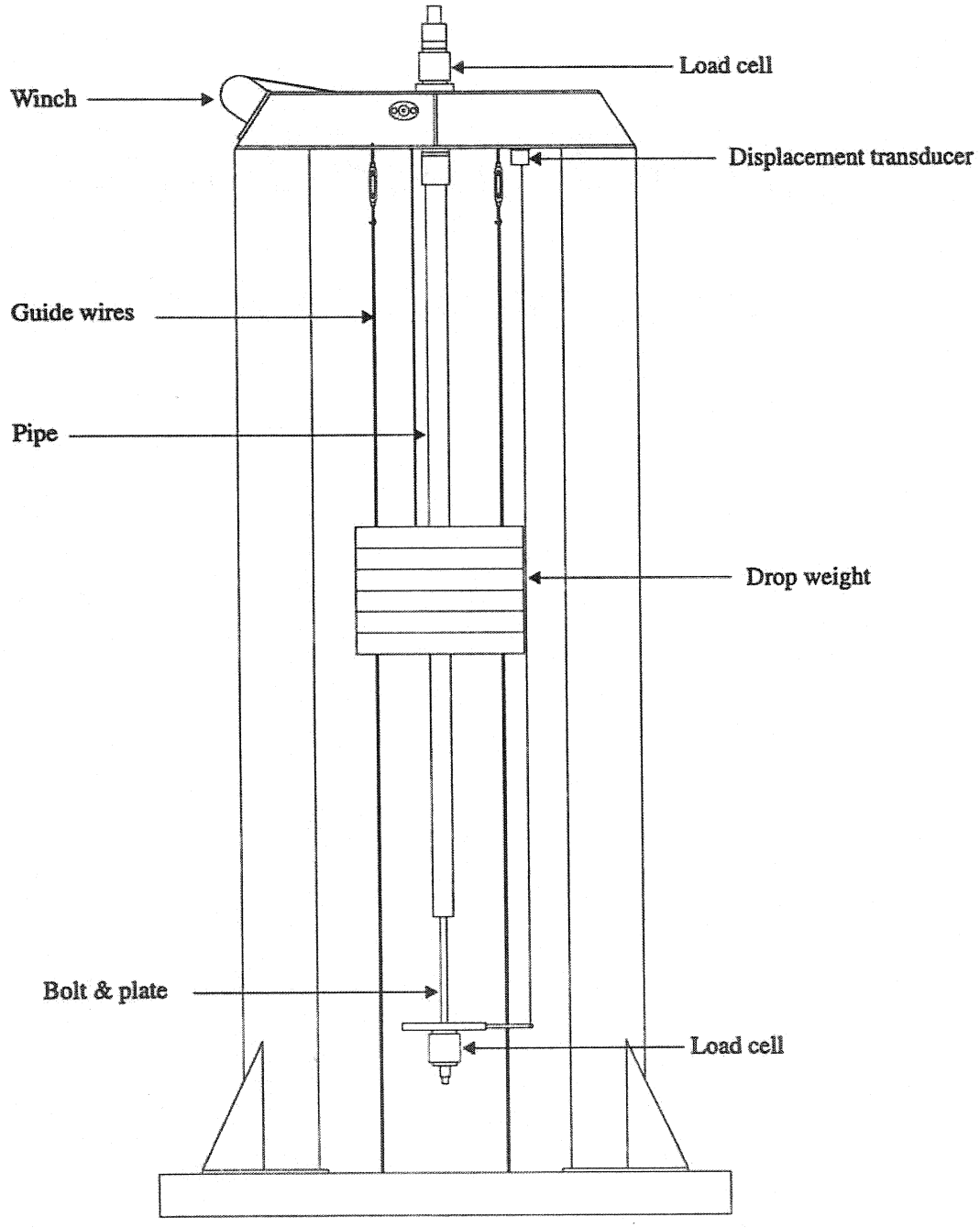

Figure 2.9 – Prototype of dynamic load frame (from Maloney and Kaiser, 1996).

Table 2.14 – Results of impulse load testing of rockbolts (Ortlepp, 1994; Stacey and Ortlepp, 2000).

Rockbolt type	Total resistance (kN)	Amount of explosives (kg)	Maximum Height (m)	Maximum Velocity of Ejection (m/s) at distance S mm	Damage to Tendons
16 mm cone	290	0.5	0.33	6.5/180	Nil
16 mm cone	290	1.0	1.80	8.6/80	All pulled out but totally undamaged
16 mm smooth	700	0.5	0.38	7.3/20	Nil
16 mm rebar	725	0.5	2.03	8.0/50	All broken
22 mm cone	1035	1.0	0.50	12.8/55	Nil
25 mm rebar	1350	1.0	4.65	10.2/500	Two pulled out three broken
Calibration tests	-	0.5	1.8	6.5/20	-
	-	1.0	5.20	10.2/100	-

Table 2.15 – Results of drop weight testing of rockbolt elements (Stacey and Ortlepp, 1999, 2000)

Rockbolt type	Rupture Energy (kJ)	Elongation Energy (kJ/100 mm)	Sliding Energy (kJ/100mm)
Rebar 16 mm	4.8 ± 0.7	-	-
Smooth bar 16 mm	-	13.9	3.0 X l_e – 0.15
Vall Reef's hoist rope strand	<2.4	-	0.8 to 8.2
18 mm compact strand cable	17.5 ± 2.0	-	-
39 mm diameter Split Sets	11.6 to 15	11.6 ± 1.3	3.0 to 6.3
Standard Swellex	4.6 ± 0.5	9.9	3.0 to 5.8
* l_e is initial embedded length in meters			

Results from drop weight testing on rockbolt elements are shown in Table 2.15. For these tests, Stacey and Ortlepp (2000) characterised the rockbolt performance by components of rupture, sliding and elongation energy. If the rockbolt was strongly bonded, or prevented from slipping, necking of the bolt started at the separation surface,

then the energy component was associated to rupture energy. If failure of the grout/steel bond takes place then yield of the steel with concurrent work hardening also occurs. This takes the form of incipient necking, which advances away from the initiation point. The energy component developed in this progressive elongation of the rockbolt is called the elongation energy. A small decrease in the diameter of the rockbolt accompanies the progressive elongation of the steel. This causes debonding and, for smooth rockbolts, allows sliding to take place. In the case of friction rockbolts, the hollow steel tube makes it relatively easy for the pressure normal to the interface to relax sufficiently for sliding to take place. The energy component in this mechanism was termed the sliding energy. As seen in Table 2.15, rebars show the least energy absorption capacity compared to "softer" support types.

2.6.7 Performance of tendon support in static and dynamic shear

Finally, the performance of tendon support under shear loading is discussed. Tendons can be loaded not only in pure traction, but also in shear or by a combination of both loading modes. This can occur during the course of induced stress fracturing (Figure 2.4a) and dislocation of fracture surfaces thereafter. The shear movement can be significant if combined with stress changes due to mining of excavations in proximity.

Haile et al. (1995) have studied the phenomenon using two types of apparatus to perform shear tests on tendon support. Devices used were a double shear and a single shear apparatus as illustrated in Figures 2.10 and 2.11. The single shear device was used for most experiments. Results from the double shear device when used on certain tendon types presented interpretation problems due to the lack of symmetry of loading forces. The tests were performed under both static and dynamic loading. The results are shown in Table 2.16.

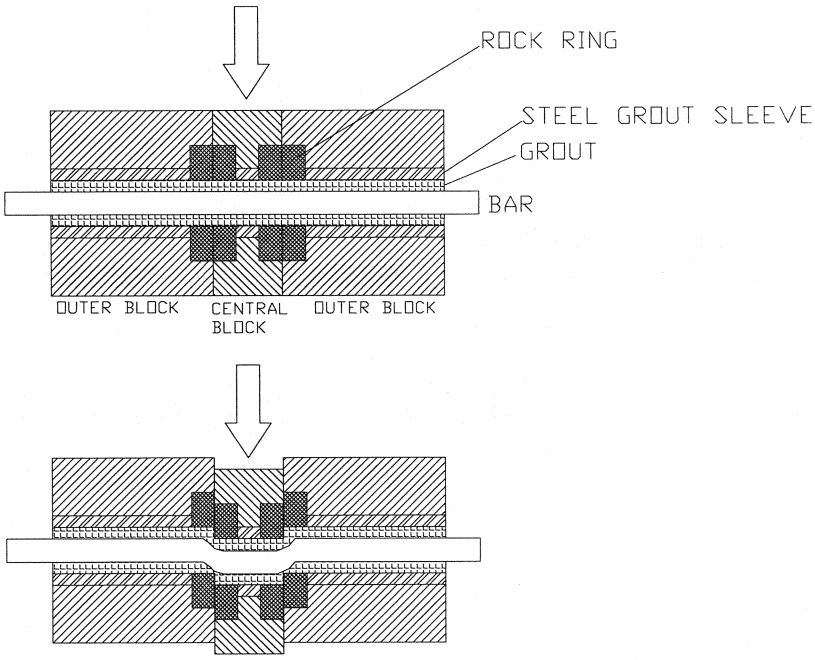

Figure 2.10 – Schematic of double shear test rig (After Haile et al., 1995).

Table 2.16 – Static and dynamic shear strengths and displacements for tested tendons (after Haile et al., 1995)

Tendon	Ulti-mate Tensile strength (kN)	Static shear strength (kN)	Static shear strength (% of UTS)	Dyn. shear strength (kN)	Dyn. shear strength (% of UTS)	Dyn. shear strength (% of static)	Loss in strength Stat. to Dyn. (%)	Static disp. at failure (mm)	Dyn. disp. at failure (mm)
Smooth bar (16mm)	116	120	103.4	122	105.2	101.7	0	34	33
Rebar (16 mm)	156	140	89.7	124	79.5	88.6	11.4	33	32
Twist bar (12mm sq.)	139	137	98.6	63	45.3	46	54	33	32
V-bar (16 mm)*	120	85	70.8	38	31.7	44.7	55.3	11-20	10-15
Cone bolt (16 mm)	116	190	163.8	120	103.4	63.2	36.8	68	33-65
Rope #1 (12 mm)	117	116	99.1	76	65	65.5	34.5	40	-
Rope #2 (12 mm)	135	142	105.2	73	54.1	51.4	48.6	42	23-30
Rope #3 * (14 mm)	243	242	99.6	179	73.7	74	26	37	33
Rope #4 (16 mm)	221	227	102.7	118	53.4	52	48	39	-
Split set (SS39)	110	97.7	88.8	60	54.5	61.4	38.6	31	26-33
*Results are for double shear tests									

*UTS = Ultimate Tensile Strentgh

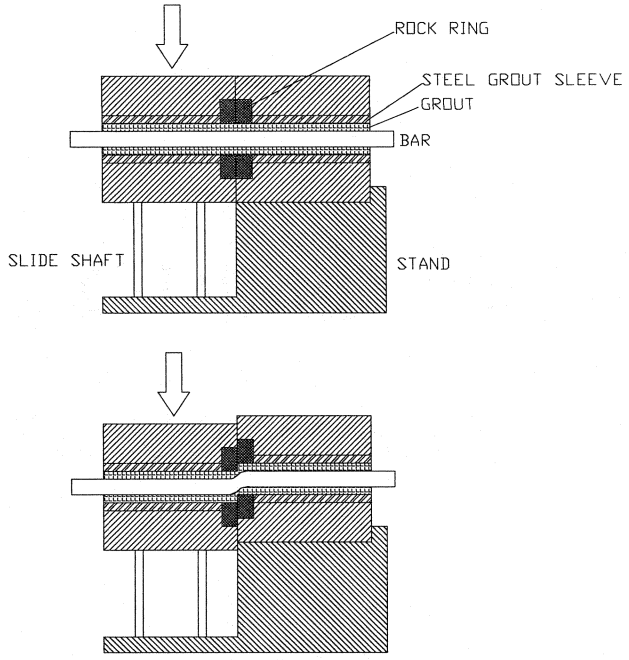

Figure 2.11 – Schematic of the single shear test rig (After Haile et al., 1995).

There are little details in Haile et al. (1995) report on the loading rate for quasi-static and for dynamic shear loading. The ends of the tendons were clamped with the intention of representing a crack dislocation well inside the tendon's critical encapsulating length on both sides of the crack. From Table 2.16, it appears that the 16 mm Cone Bolt and the 16 mm smooth bar performed equally well under dynamic shear. The 16 mm Cone Bolt showed better shear resistance in static shear than the smooth bar. Haile et al. (1995) recommended the Cone Bolt over the smooth bar, rebar, Split Set and twist bar in applications where shear movements in the rock are predicted. They recommended further work before using larger diameter bars for shear loading but argued that it would not be necessary to increase the diameter size of the Cone Bolt for such a use. The strength of the Cone Bolt in shear loading mode lies in its ability to alter the loading mode. In essence, the Cone Bolt installed in a dislocating wall would be loaded in a combined shear and traction mode.

Gillerstedt (1999) experimented on the ability of the Cone Bolt to perform in mixed loading mode using the test arrangement schematised in Figure 2.12. His results are presented in Table 2.17. The bolts were installed through two concrete blocks and loaded in shear. The resulting axial load on the tendon was measured using a load cell mounted under the bolt's reaction plate. Electronic displacement transducers were used to measure the cone displacement in the grouted bore hole and the crack aperture. Wire potentiometers were used to monitor shear movement of the concrete block. The deformation rate was approximately 0.1 mm/s. Figure 2.13 illustrates the tendons after combined axial and shear load testing. The designated Cone Bolt 2 was not tested to failure due to rupture of the concrete block. Results shown in Table 2.17 indicate that the Cone Bolts did transfer some of the shear load into axial loading. Cone Bolt 1 broke in shear after 226 mm of shear displacement having locked in place in its encapsulating matrix. The compressive strength of the cement grout did not seem to influence the Cone Bolt's behaviour by comparing results.

Table 2.17 – Combined axial and shear test results on Cone Bolts and rebar (after Gillerstedt, 1999)

Bolt	Ulti-mate. strain	Yield strength (MPa)	UTS (MPa)	Young's mod. (GPa)	Comp. grout strength (MPa)	Max shear load (kN)	Max shear disp (mm)	Cone/ end disp. (mm)	Joint opening (mm)	Axial load (kN)	Com-ment
Cone Bolt 1 22mm	20%	360	600	200	69	248	226	69	6.5	75-84	bolt failed
Cone Bolt 2 22mm					28	244	225	107	7 *	71-84	test stopped
Rebar 20mm	17%	570	670	210	69	230	43	0	0	1	bolt failed

*manually measured

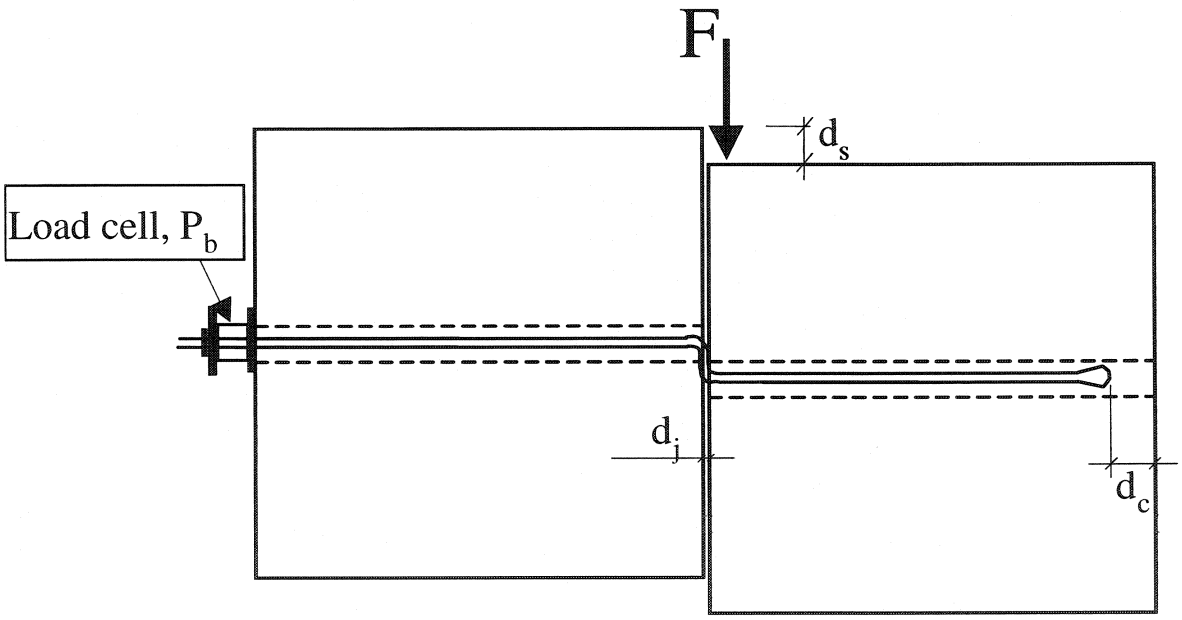

Figure 2.12 – Schematic of the shear test setup used by Gillerstedt (1999).

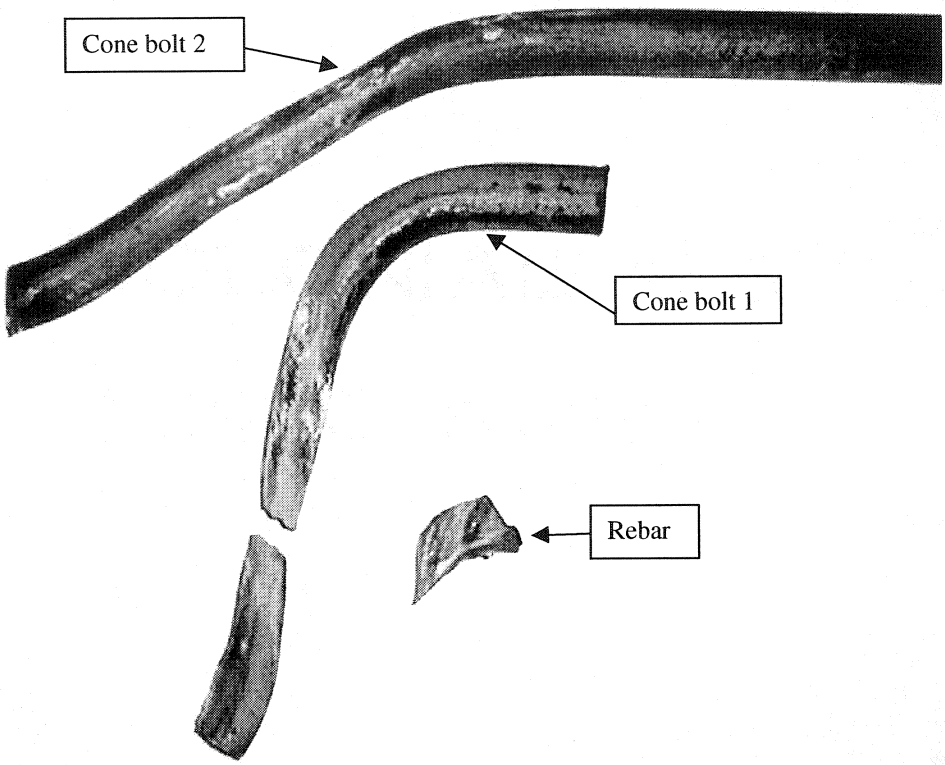

Figure 2.13 – Photography of the three samples sheared in Gillerstedt experiments (1999). Cone bolt 2 was not tested to failure due to the rupture of the encapsulating concrete block. The length of rebar solicited in shear is comparatively shorter than for the Cone bolt samples. These were solicited in combined axial and shear loading.

2.7 Final remarks

The information compiled in this chapter can be useful for the design of a support package that can be suited to given loading modes including dynamic loading resulting from a rockburst. The nature of seismic events was covered as well as the energetic considerations resulting from them. Given a certain rock mass failure energy and considering the chosen support system components, one can postulate on the viability of the support package in a specific environment. Note that rockburst support packages also contain a surface lining system such as wire mesh, straps, shotcrete and possibly cable lacing. These support elements and their performance was not studied in detail in this

review, but are of considerable importance in the design of rockburst support packages. The surface lining system is often the first element of support hit by chunks of rock in the event of a rockburst. The liner will then transfer this load to straps or cable lacing if any, which will then be transferred to the bolt's reaction plate and finally to the tendon itself.

None of the tendons portrayed in the literature review matched the requirements set for performance for use at Brunswick Mine with the major issue being the ease of installation and compatibility with the available equipment and installation practices. As a result, an experimental program was set up at Noranda Technology Centre for the development of a new yielding tendon, the Modified Cone Bolt. The procedures used to develop the tendon are not disclosed here, but the validation tests done in quasi-static and impact loading modes are depicted in Chapter 3.

Impact testing methods used for the development of the Modified Cone Bolt were limited to impact loads of approximately 15 kJ at pre-set impact velocities. A displacement evaluation method for tendons submitted to dynamic loading given a burden, impact velocity and tendon characteristic stiffness was derived and is presented in Chapter 4.

CHAPTER 3
EXPERIMENTAL PROCEDURES AND MAIN RESULTS

3.0 Introduction

This chapter covers general testing procedures and results found through the completion of the Modified Cone Bolt (MCB) design program for the period between November 1999 and April 2000. The program consisted of in situ pull and impact testing on prototype bolts having machined conical anchors whose geometry corresponded to the chosen final geometry of the MCB and threaded onto C1060 TBE (threaded both ends) smooth bars of 17 mm diameter. The thread size of TBE bars was of a nominal ¾ inch rolled type 10-UNC-LHT. C1060 rolled steel has a tensile strength (Oberg et al., 1996) of 813 MPa (118,000 lb/po^2) and a yield strength of 482 MPa (70,000 lb/po^2).

Earlier in the testing phase, design of experiment (commonly called DOE) tools were used at Noranda Technology Centre (NTC) to determine the relative importance of the different materials, geometric and mechanical characteristics on the performance of the MCB yielding system. The MCB support system design protocol will not be presented here.

The objective of this specific testing program was to confirm the MCB final geometry settings and its compliance with the required performance for rockburst support tendons. The testing protocol covered two mechanical performance categories: in situ quasi-static tendon performance using prototype bolts, and impact tendon performance at NTC's pilot plant. The in situ prototype MCB installation was also a good opportunity to monitor the ease of installation with hand-held drills.

3.1 Quasi-static underground pull testing

3.1.1 Testing procedure

Underground pull testing was conducted at the end of April 2000 at Brunswick mine, on the 1000 level, second sub-level. Holes were pre-drilled with a 38 mm (1 ½ inch) bit, over a 2.1 meter distance. Prototype cone anchors were machined and threaded onto smooth bars. Each prototype tendon (Figure 3.1) has been coated with car wax just before its installation to prevent adhesion of the tendon shank to the resin. The impact load distribution through time is affected by the adhesion of the steel tendon to the resin; this aspect is further elaborated in Chapter 4.

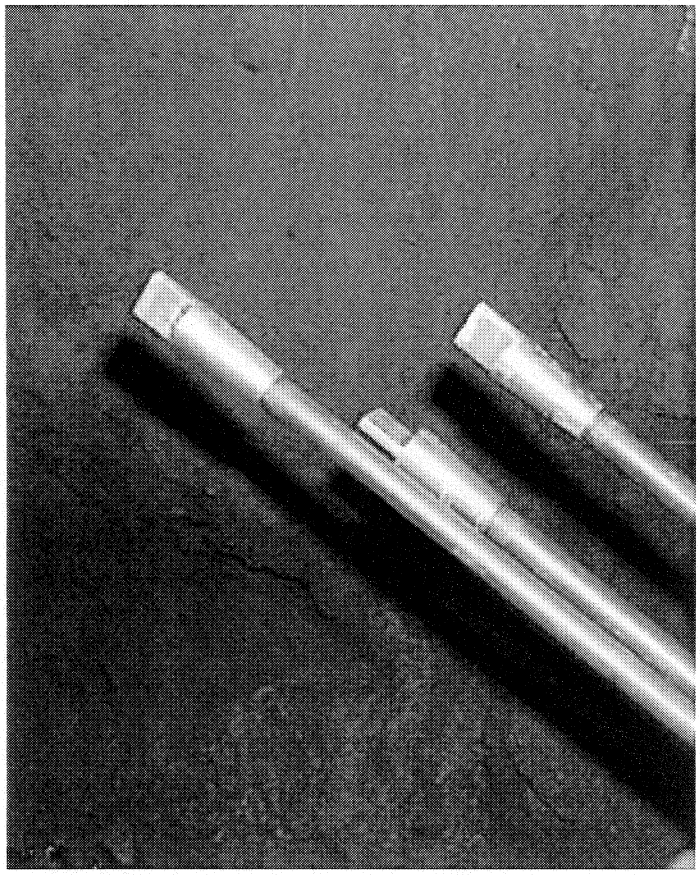

Figure 3.1 – Prototype Modified Cone Bolts installed at Brunswick Mine during the in-situ pull testing campaign.

The prototype MCB jackleg installation procedure was as follows (Figure 3.2):

-Coat each tendon with Maguire Gold Class liquid wax using a small sponge;

-Insert specified lengths of polyester resin cartridges of given set times in the borehole. The length of each resin cartridge was 0.9 meters. Two types of resin cartridges were used, one with a faster set time of 0-30 seconds the other of a slower set time of 1-3 minutes. In all cases at least one fast resin cartridge was pushed to the toe of the hole;

-Push the tendon to a maximum of 0.6 m from the hole end using the jackleg;

-Spin the bolt at the maximum rotation capacity of the machine while pushing the tendon at half thrust until the reaction plate is tight to the face;

-Stop the bolt rotation and keep a pressure on the nut for 5 seconds;

-Remove the dome nut from the threaded end.

Note that a 10 cm spacer was used underneath the reaction plate to keep enough thread length for the pull test adapter. Jackleg drills are used for non-mechanized installation of bolts in tunnel walls. Stoper drills are used for bolt installation in the back (roof).

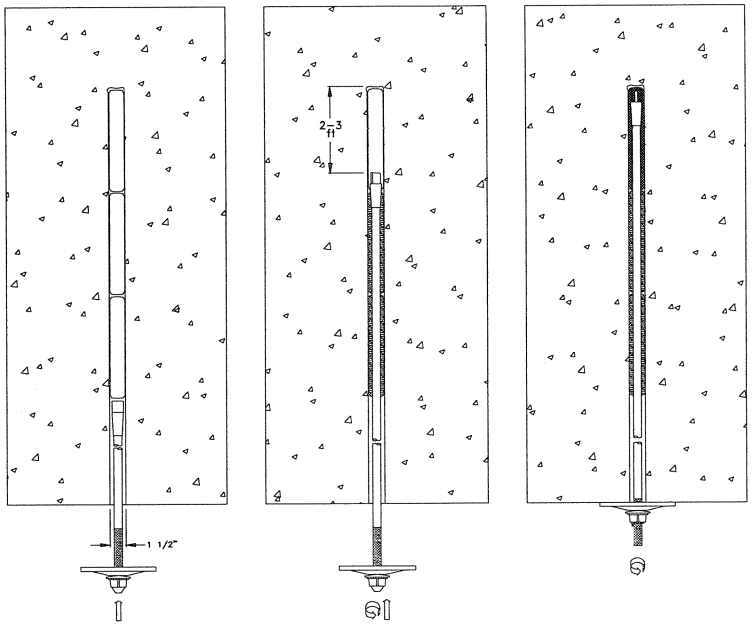

Figure 3.2 – Non-mechanized installation procedure (Gaudreau, 2000b).

All tests were done in the same shift of 8 hours. The time between bolt installation and its pull test varied from 2 to 4 hours. Once all tendons on a single wall were installed, a pull test adapter and a 30 ton capacity hydraulic ram were sequentially installed on each tendon as illustrated in Figure 3.3. A hand pump activated the ram. Each test was instrumented using a displacement transducer and an oil pressure electronic measurement device. An analog gage was fitted to the hydraulic jack assembly to obtain instantaneous readings of the oil pressure as the test was performed. Figures 3.4 to 3.7 show different views of the testing installation. The objective of the testing program was to obtain the MCB in situ deformation curve. In order to do so, tests were performed in two rock types, sedimentary rock and massive sulphides. Rock properties are summarised in Table 3.1. Figure 3.4 shows a bolt being installed in sedimentary rock, through a shotcrete layer. Displacement was measured during pull tests using a potentiometer (see Figure 3.3 and Figure 3.5). Final displacements were also measured manually after each test as shown on Figure 3.6. Figure 3.7 shows the reaction plate used for pull testing.

Table 3.1 – Summary of Brunswick #12 Mine mean rock properties.

Rock Type	UCS (MPa)	Elastic modulus (GPa)	Poisson's ratio	Density (t/m^3)
Massive Sulphides (1)	207	69	0.2	4.27
Footwall Metasediments (1)	50-60	15-20	0.25	2.91
Hangingwall Metasediments (1)	30-40	10-15	0.25	2.65
"Ore" Massive Sulphides (2)	218	105	0.29	-
"Waste" Massive Sulphides (2)	252	156	0.23	-
Metasediments (3)	72	63	0.2	-
Porphyritic Dyke (3)	182	62	0.2	-

UCS = Intact rock Uniaxial Compressive Strength

(1) Kristof, B. (1988). (2) Simon, R., Gaudet, N. (1988). (3) Labrie, D. (1998).

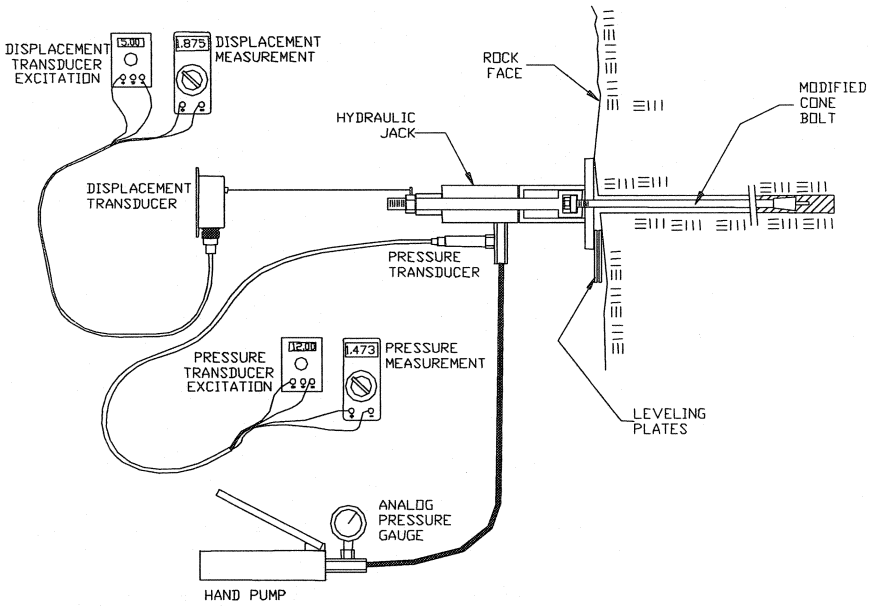

Figure 3.3.- Diagram of pull test assembly.

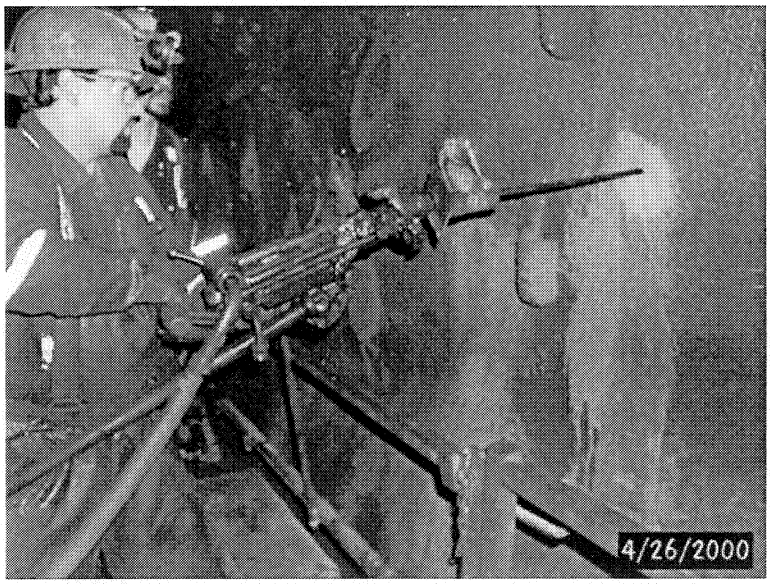

Figure 3.4 – Installation of MCB with jackleg drill for pull testing.

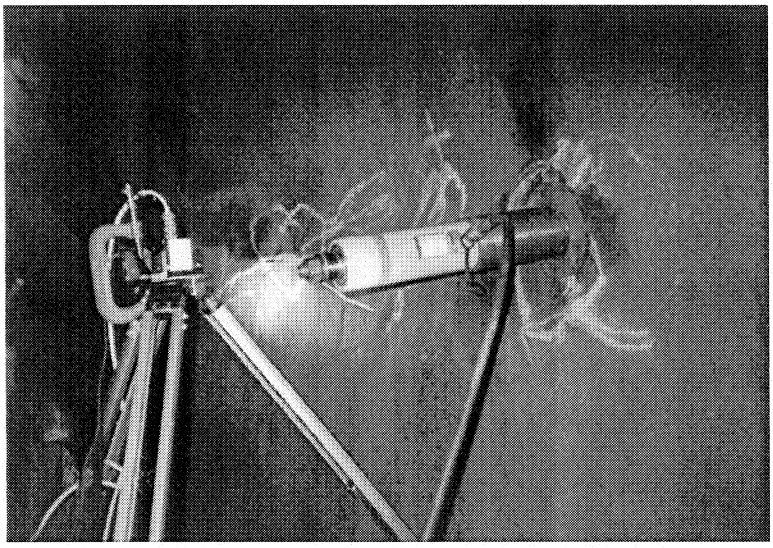

Figure 3.5 – Pull testing of tendon showing 30 ton hydraulic ram and displacement transducer on tripod.

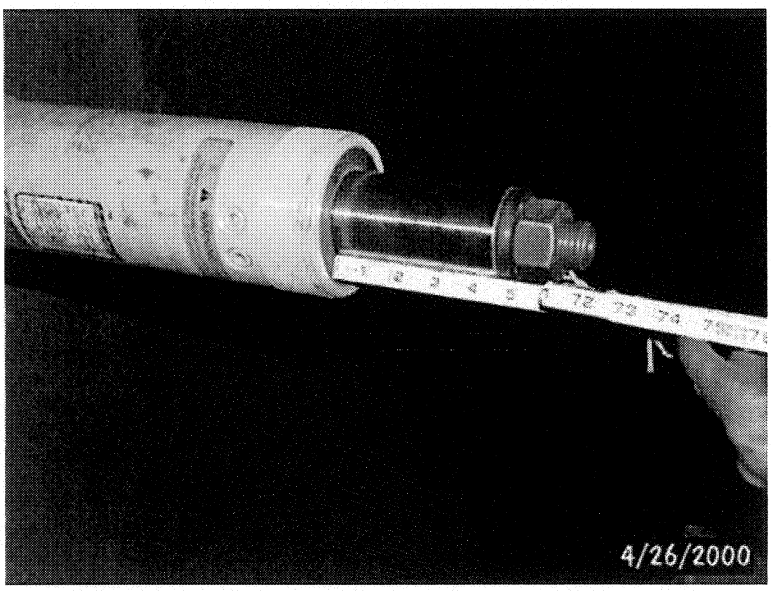

Figure 3.6 – Manual displacement measurement at end of pull test.

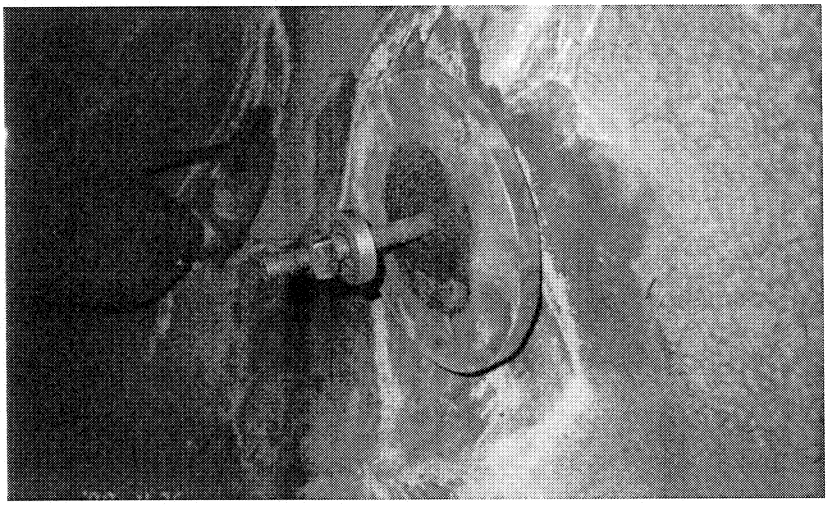

Figure 3.7- Reaction plate, washer, nut and tendon assembly after pull test. The bolt has been extracted from its original location, and it has elongated.

3.1.2 Testing results

All pull testing results shown here are for MCB tendons of 2.1 meter length. Pull testing was performed on April 26th, 2000 at Brunswick mine. Figures 3.8 to 3.15 show in situ testing results. The first three tests were monitored using a Devar Smart Chart recorder model 8100. The device failed after three tests, so the data was then manually recorded at increments of 0.9 tons (2000 pounds) of loading using two voltmeters measuring load and displacement, through a potentiometer and an electronic pressure transducer, as illustrated in the experimental procedures. The polyester resin used was Fosroc 35 mm (1 3/8 inch) diameter cartridges. The testing results showed good agreement with the design criteria. The bolting system was neither too stiff nor too flexible. Further analysis of quasi-static pull testing results is presented in Chapter 4.

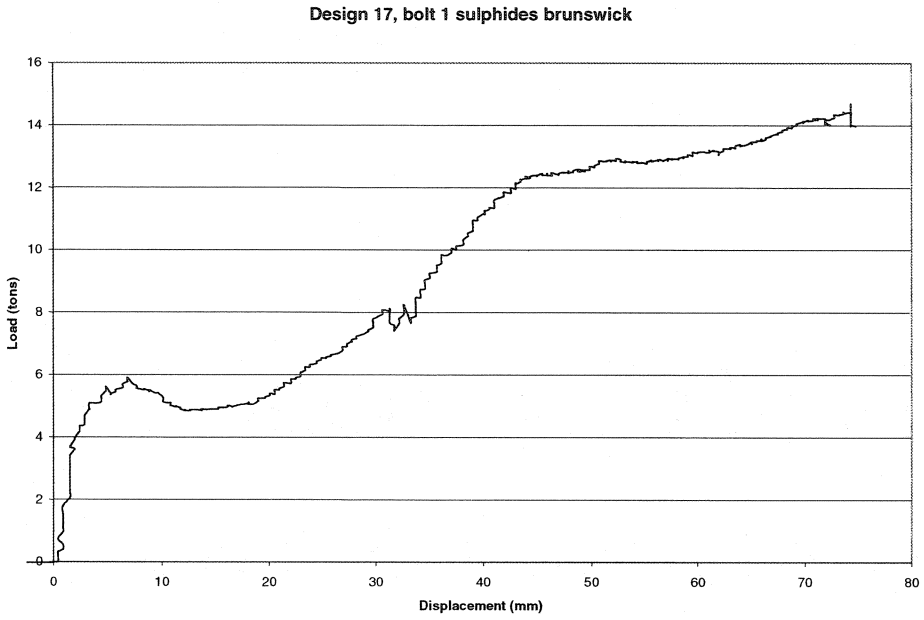

Figure 3.8– Measured load-displacement for bolt #1, which was spun over 0.9 m distance. Two cartridges were used, one of 0.9 m of fast resin at the anchoring point, and one of 0.9 m of slow resin at the collar.

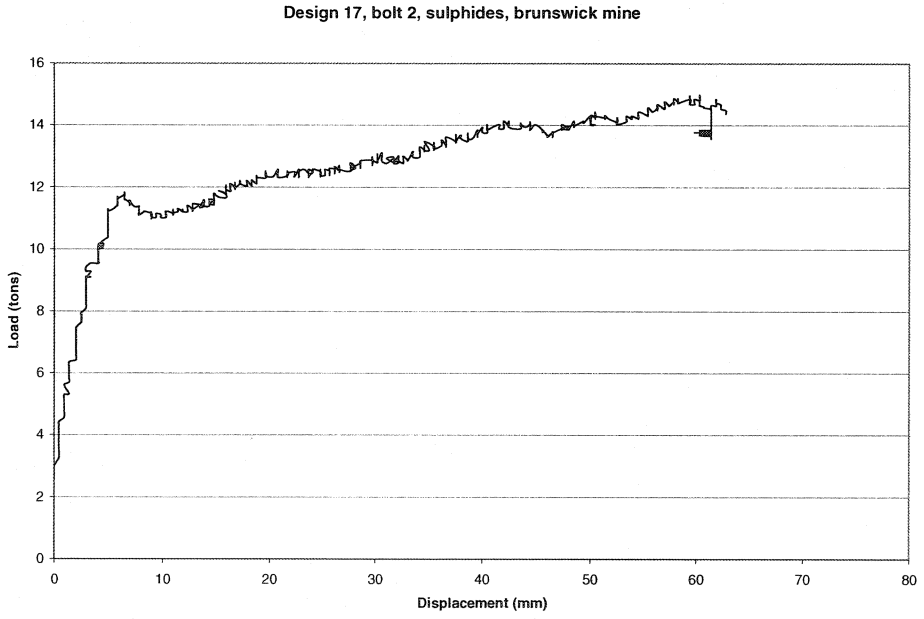

Figure 3.9– Measured load-displacement for bolt #2, which was spun over 0.9 m using 0.9 m of fast and 0.9 m of slow resin.

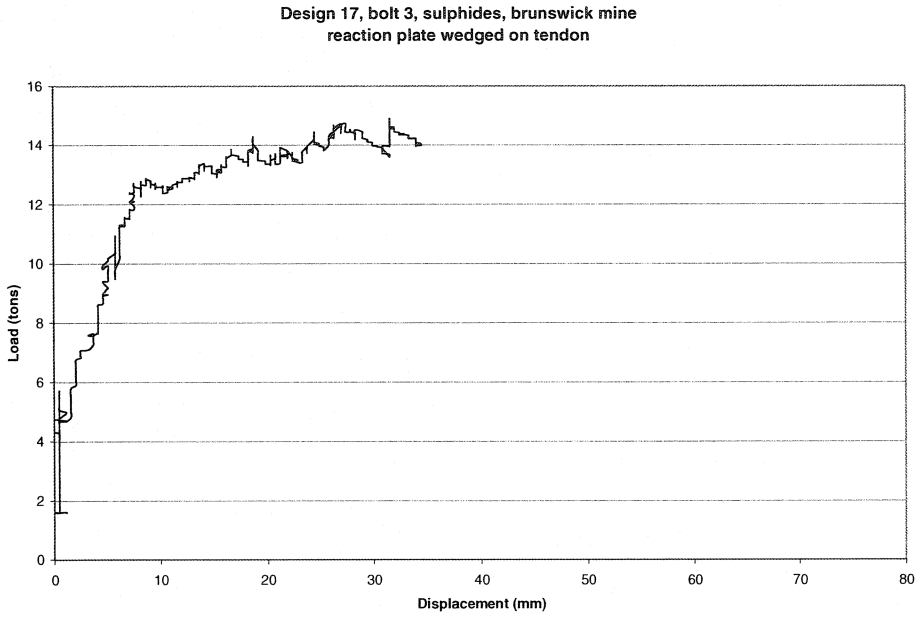

Figure 3.10– Measured load-displacement for bolt #3, which was spun over 0.9 m using 0.9 m of fast and 0.9 m of slow resin.

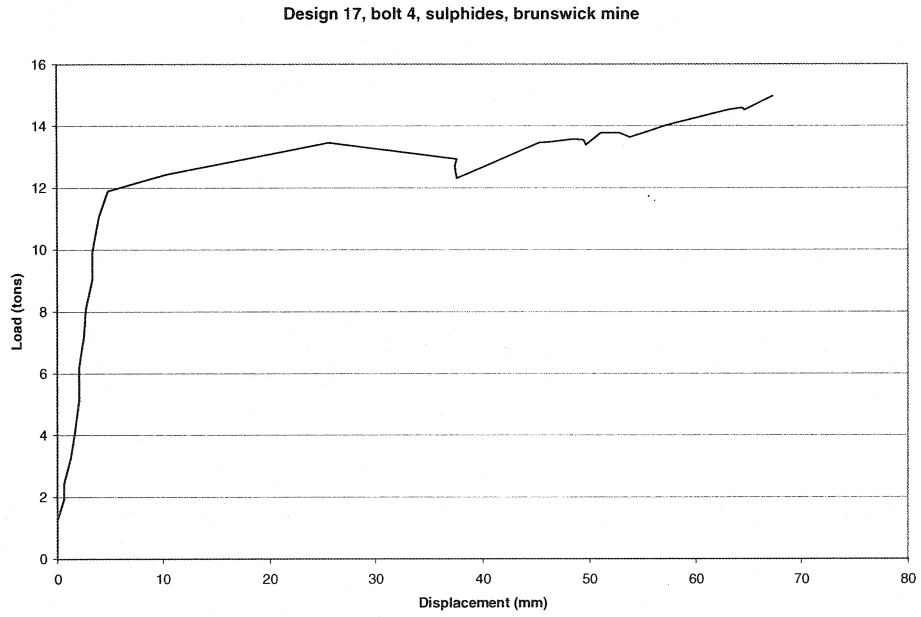

Figure 3.11– Measured load-displacement for bolt #4, which was spun over 0.9 m using 0.9 m of fast and 0.9 m of slow resin. Starting here, readings were done through the voltmeters, without the data acquisition system.

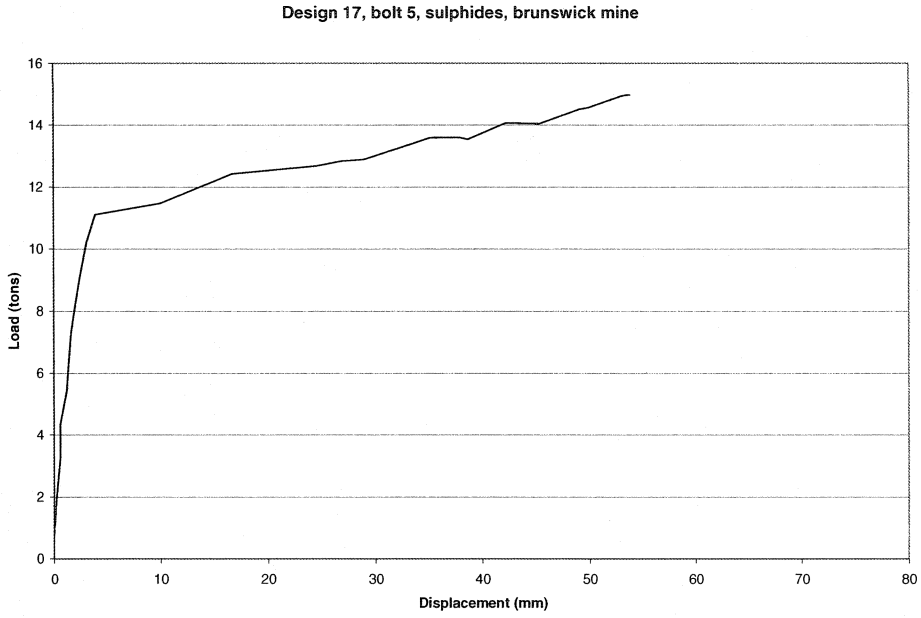

Figure 3.12– Measured load-displacement for bolt #5, which was spun over 0.9 m using 0.9 m of fast and 0.9 m of slow resin.

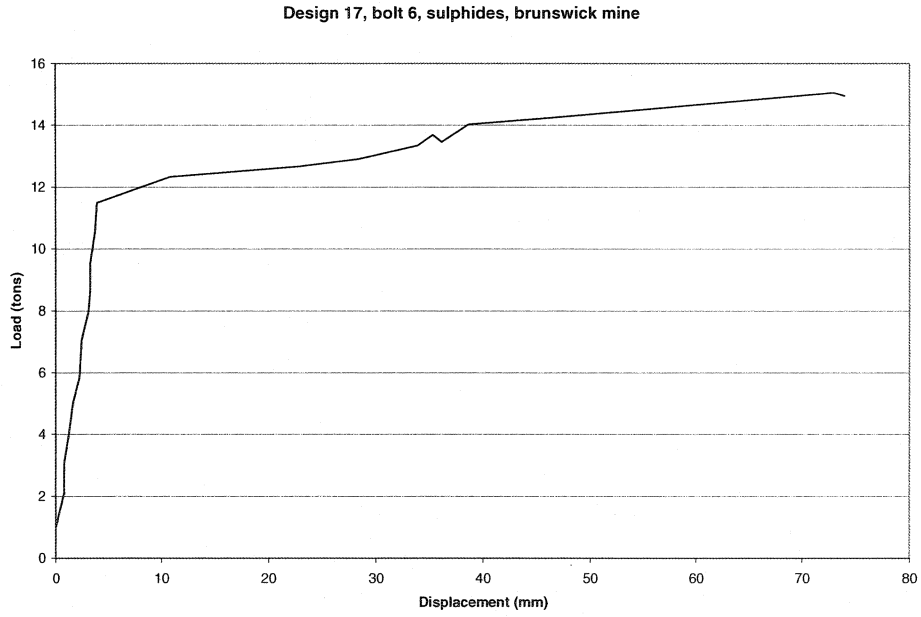

Figure 3.13– Measured load-displacement for bolt #6, which was spun over 0.9 m using 1.8 m of fast resin.

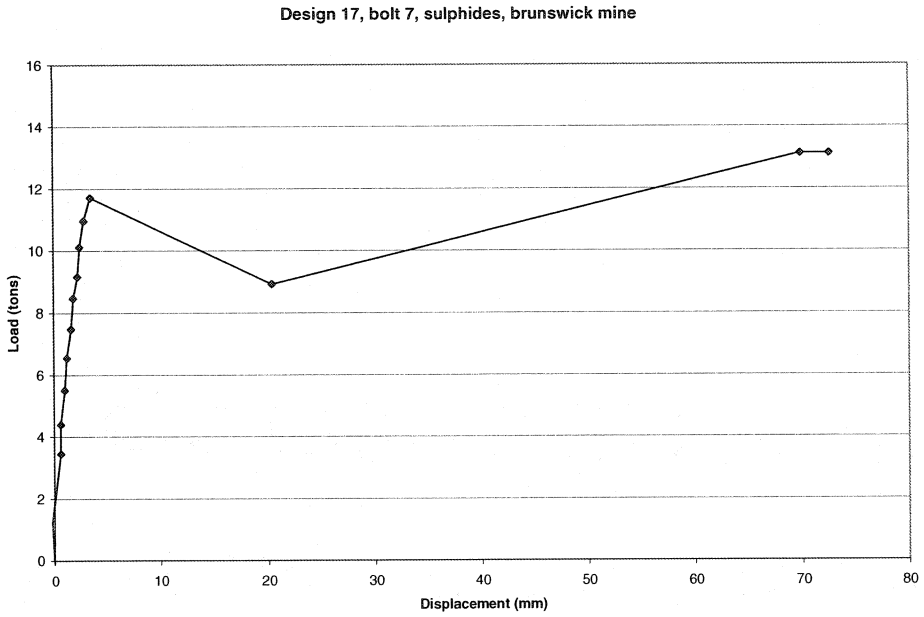

Figure 3.14– Measured load-displacement for bolt #7, which was spun over 0.9 m using 1.8 m of fast resin.

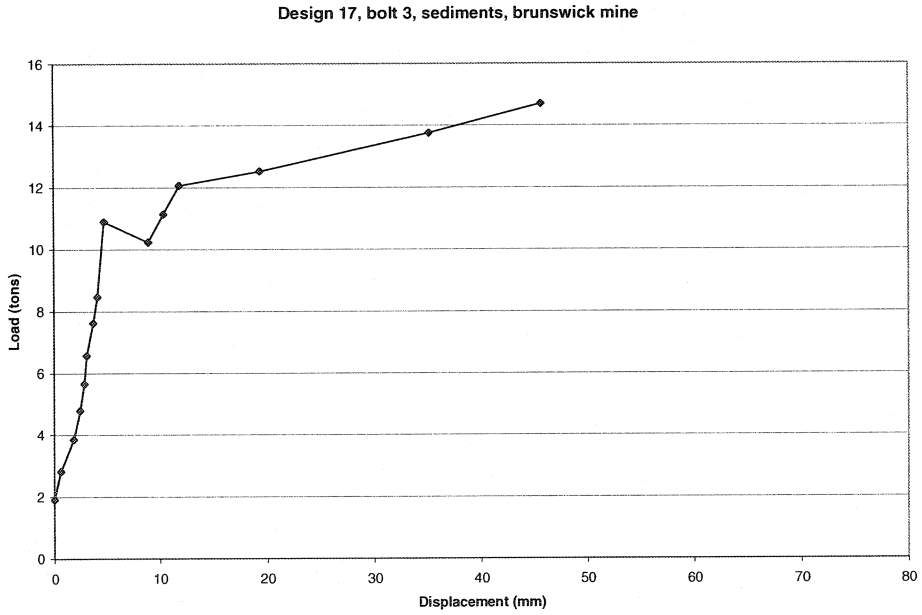

Figure 3.15– Measured load-displacement for bolt #3seds, which was spun over 0.9 m using 0.9 m of fast resin.

3.2 Impact testing

3.2.1 Testing procedure

The impact testing facility located at NTC used a drop weight to induce displacement of the tested tendon at a fixed initial impact velocity. For impact testing, the rig can be set for a drop weight of a maximum of 1000 kg over a fall distance of no more than 2.0 meters. The potential energy is thus of a maximum of 20 kilojoules. Figures 3.16a and b show a frontal view and a back view of the facility, respectively. Figure 3.17 illustrates the details of the impact test rig.

The drop weight is attached to a release system located on the top part of the facility. Once released, the annular shaped impact mass slides along the test tube until it collides with the reaction plate. The latter is supported by the tendon installed in a test tube of an internal diameter of 38 mm and of 9.5 mm wall thickness. Each sample is prepared and installed as it would be underground using a stoper mounted horizontally on a track. A stoper is a hand-held mining drill that can be used to drill boreholes and install roof support.

All tests were instrumented using a load cell located on the top part of the machine, reading load on the test tube, a load cell underneath the reaction plate, reading load on the tendon, and a potentiometer attached on the tendon to read displacement of the bar. The steel mass is hoisted into position using a 5 ton capacity crane, and the straps visible in Figure 3.16.

All 1.7 m long MCB prototype samples were spun into two Fosroc 915 mm length and 35 mm diameter resin cartridges. The first cartridge has a speed index of 30 (for fast), and is of type 35915M35. The second has a speed index of 240 (for slow), and is of type 35910LIF90. All samples were pushed through the slow setting resin, then pushed and rotated through the fast setting resin, to simulate a jackleg installation underground.

Load-displacement curves illustrated in section 3.2.2 are based on the measurements made from the top and bottom load cells. The surface area under the load-displacement curve representing the work energy dissipated is calculated from the bottom load cell when available.

Data was recorded using a LeCroy 9424E Quad 350 MHz oscilloscope. Three channels were used for the test, two for the load cells, and one for the displacement transducer. The top load cell was an RST model SGA-75-1.30, reference RST 90210-100K, serial 961914-1, of 34 ton (75,000 pounds) capacity. The bottom load cell was a Sensotec model TH/1591-01, serial 446250 of 90 ton (200,000 pounds) capacity. Each cell was connected to a Vishay P-3500 strain indicator. The amplified signal was recorded using the oscilloscope. The displacement transducer was a UniMeasure P-20A potentiometer.

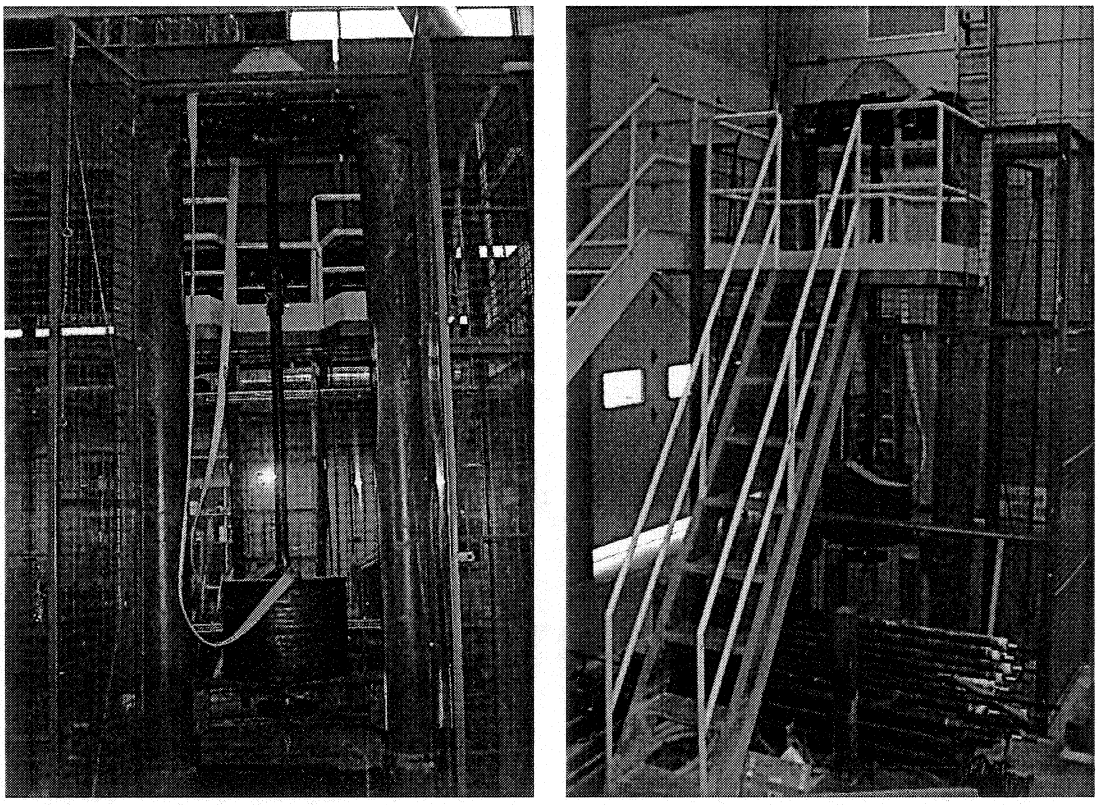

Figure 3.16 a, b – Frontal and back views of impact test rig at NTC.

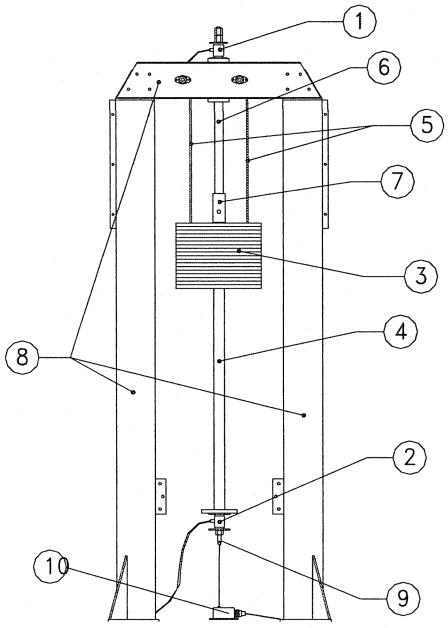

1-Load cell 1
2-Load cell 2
3-Drop weight
4-Sample holder
5-Holding rods
6-Spacer
7-Coupling
8-Frame
9-Tendon (in sample holder)
10-Displacement transducer

Figure 3.17 – NTC impact test rig (see text for more details).

Raw signals for the displacement transducer and the two load cells are illustrated in Figures 3.18a to 3.20a. Although a large number of data points were collected in little time (40, 000 data points in 0.2 seconds), the waveform recorded was noisy. The source of the noise is assumed to be due to environmental electrical and magnetic disturbances whose source was generated by machines and power distribution around the pilot plant at NTC. Voltage jolts often triggered the oscilloscope, and the amplitude and frequency of the ambient noise was erratic. The wavelet filter (Wolfram Research, 1996) provided the ability of rejecting the white noise and was considered well suited for the transient nature of the recorded displacement and load waveforms. The removal of noise from noisy data to obtain the unknown signal is referred to as denoising. The wavelet shrinkage method (Wolfram Research, 1996) was used to suppress the white noise. The procedure is to first represent the data in terms of a wavelet basis, then the coefficients that are below a certain threshold τ are set to zero and those above τ are "shrunk by τ". The threshold τ determines how much noise one wants to suppress, and the larger the variance of the noise, the larger should τ be. The data was denoised using a wavelet transform of spline type and of order 3. The data was then compressed using a threshold τ value of 0.1.

The inverse transform is then applied to the processed signals to give denoised signals such as these represented in Figures 3.18b to 3.20b. On Figure 3.18 to 3.20, the x axis represents the sample points, of which 1 in 10 is displayed, for a total of 4000 data points. The y axis u(x) is the voltage measured by the oscilloscope.

3.2.2 Impact testing results

This section contains impact testing results on the Modified Cone Bolt (MCB). Figures 3.21 to 3.36 illustrate processed filtered signals from each test, in load-displacement graphs. Displacements and loads have been combined on the graph from which work energy can be calculated as the area under the curve. The oscillations may correspond to the natural frequency of the tendon-tube-impact machine system.

Table 3.2 provides details on the impact load and drop height for testing results presented in this chapter. The initial drop height indicated in Table 3.2 corresponds to that of the drop height at the start of the testing. Tendon displacements manually measured after each test are indicated as final drop height in Table 3.2. The numbering system for the samples is GEOMETRY- SAMPLE#- CYCLE#. On impact testing Figures, Force 1 is the load on load cell LC1, located on top of the test frame. Force 2 is for LC2 located underneath the main reaction plate.

The data presented in this Chapter is analyzed in Chapter 4. The "unavailable" data highlighted in the illustration of the impact testing results is either due to difficulties in triggering the oscilloscope at the moment of testing, or to the removal of the displacement transducer. This transducer was generally removed before the last cycles of testing in order to protect the equipment. Available maximum load at failure will be presented in Chapter 4.

Table 3.2 – Impact testing parameters

SAMPLE #	Initial drop height (m)	Final drop height (m)	Drop weight (kg)	Comments
17-1-1	1.51	1.51 + 0.15	1000	waxed tendon
17-1-2	1.51 + 0.15	1.51 + 0.24		tendon not broken
17-2-1	1.51	1.51 + 0.14	1000	waxed tendon
17-2-2	1.51 + 0.14	1.51 + 0.22		tendon not broken
17-3-1	1.51	1.51 + 0.16	1000	waxed tendon
17-3-2	1.51 + 0.16	1.51 + 0.29		tendon broken at outward
17-3-3	1.51 + 0.29	1.51 + 0.36		threaded end
17-3-4	1.51 + 0.36	1.51 + 0.40		
17-10-1	1.51	1.51 + 0.09	1000	waxed tendon not broken
17-11-1	1.51	1.51 + 0.15	1000	waxed tendon
17-11-2	1.51 + 0.15	1.51 + 0.28		tendon broken at outward
17-11-3	1.51 + 0.28	1.51 + 0.37		threaded end
17-11-4	1.51 + 0.46	1.51 + 0.47		
17-12-1	1.37	1.37 + 0.13	750	threads failed
17-12-2	1.37 + 0.13	1.37 + 0.24		
17-12-3	1.37 + 0.24	1.37 + 0.30		
17-12-4	1.37 + 0.41	1.37 + 0.44		
17-13-1	1.37	1.37 + 0.21	750	tendon not broken
17-13-2	1.37 + 0.16	1.37 + 0.28		
17-13-3	1.37 + 0.28	1.37 + 0.39		
17-13-4	1.37 + 0.39	1.37 + 0.56		
17-14-1	1.37	1.37 + 0.07	750	tendon cleaned with acetone
17-14-2	1.37 + 0.07	not available		
17-14-3	not available	1.37 + 0.30		tendon broke at outward
17-14-4	1.37 + 0.30	1.37 + 0.40		threaded end
17-14-5	1.37 + 0.40	1.37 + 0.47		

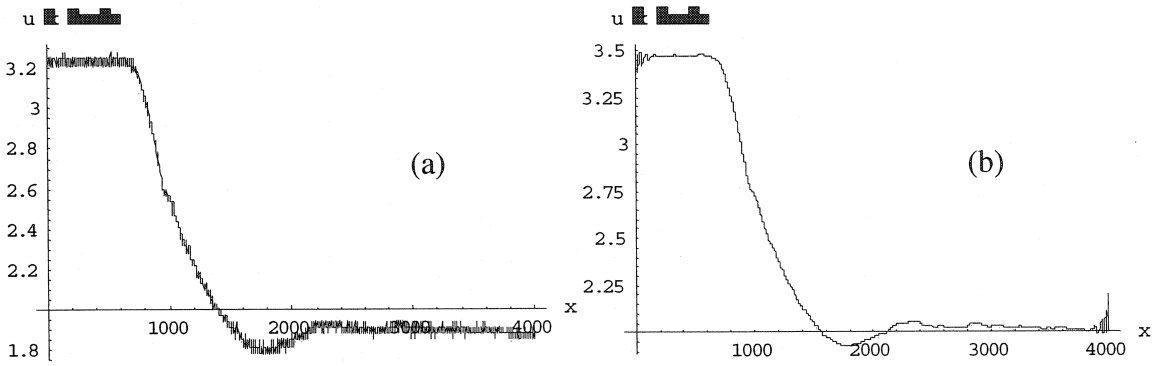

Figure 3.18- Example of raw (a) and filtered (b) displacement data for sample 17-1-1.

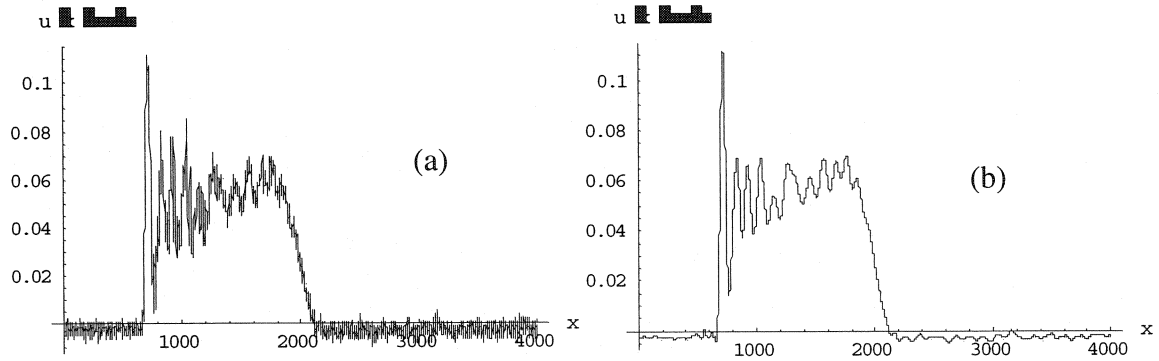

Figure 3.19- Example of raw (a) and filtered (b) load data (top load cell) for 17-1-1.

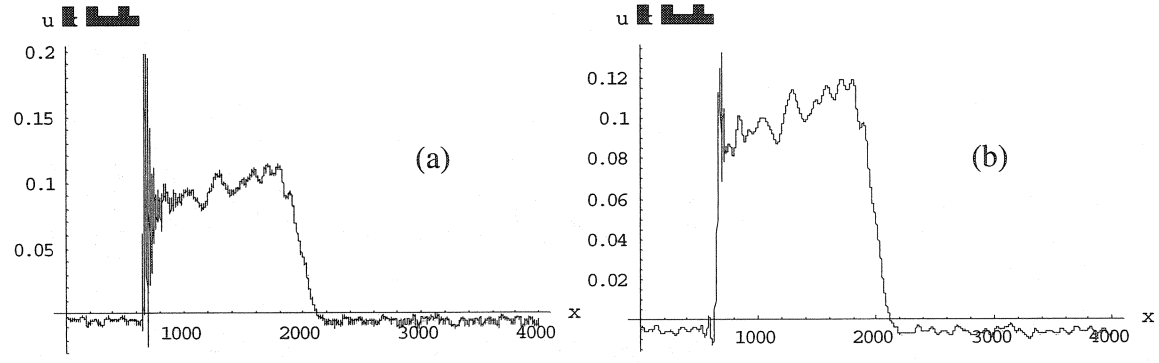

Figure 3.20 – Example of raw (a) and filtered (b) load data (bottom load cell). The x axis is 1/10 of the data recorded in the test. Given the sampling rate it will represent time. The u(x) axis is a voltage reading for each transducer. Data from testing sample 17-1-1.

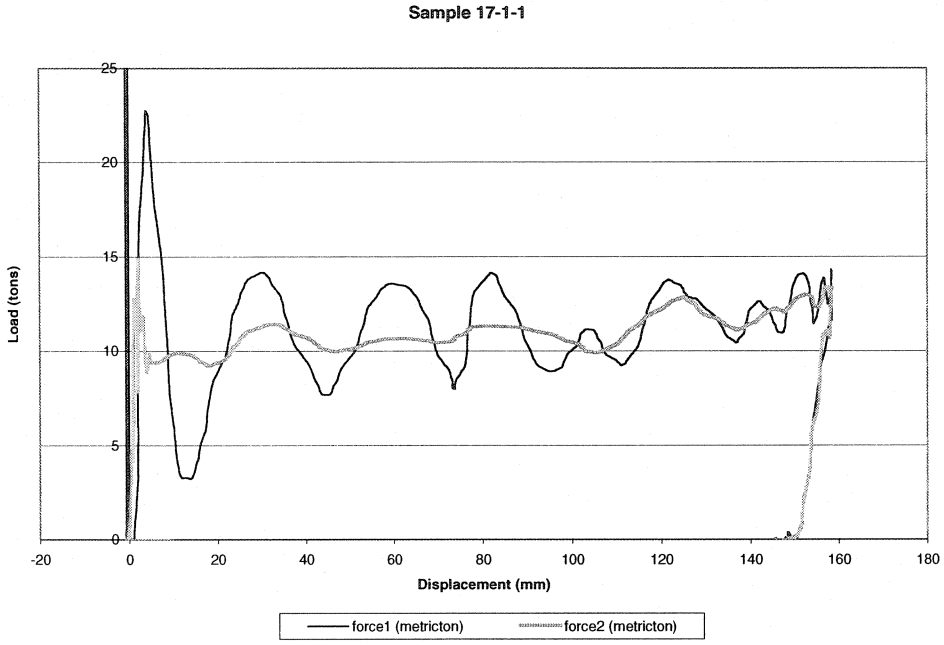

Figure 3.21 – Processed impact data for sample 17-1-1.

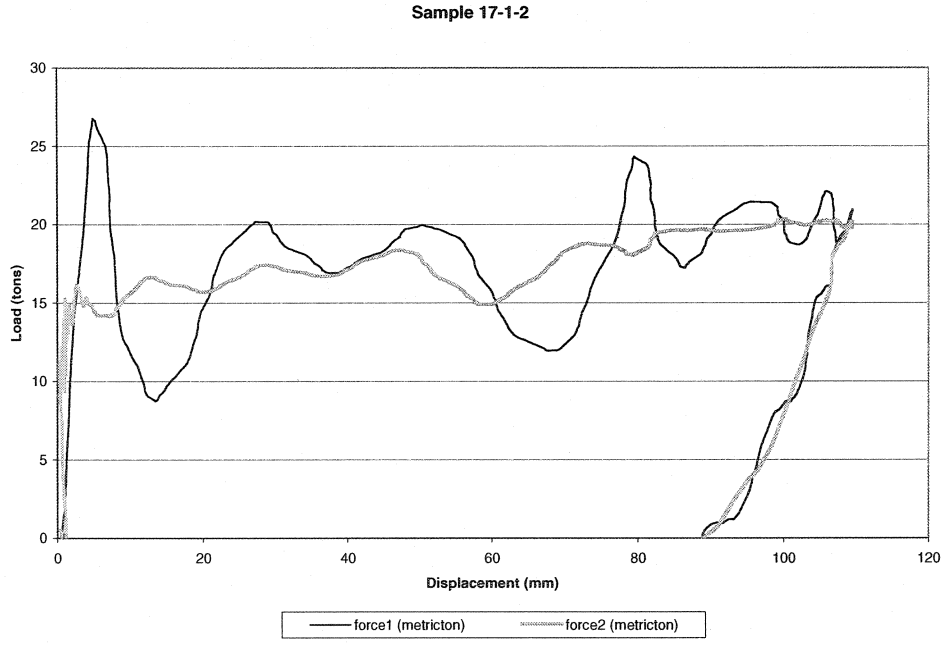

Figure 3.22 – Processed impact data for sample 17-1-2.

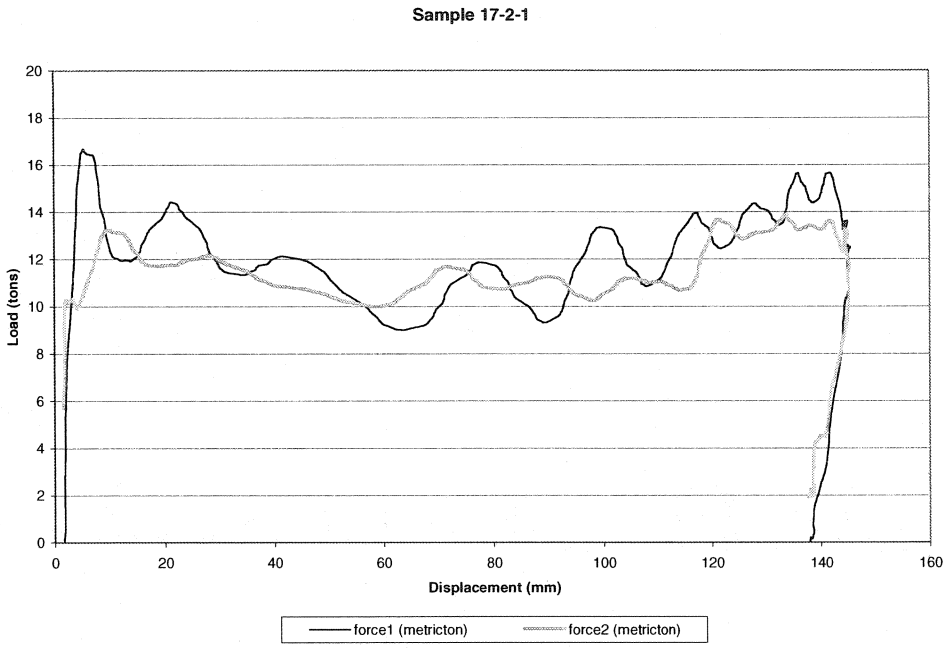

Figure 3.23– Processed impact data for sample 17-2-1.

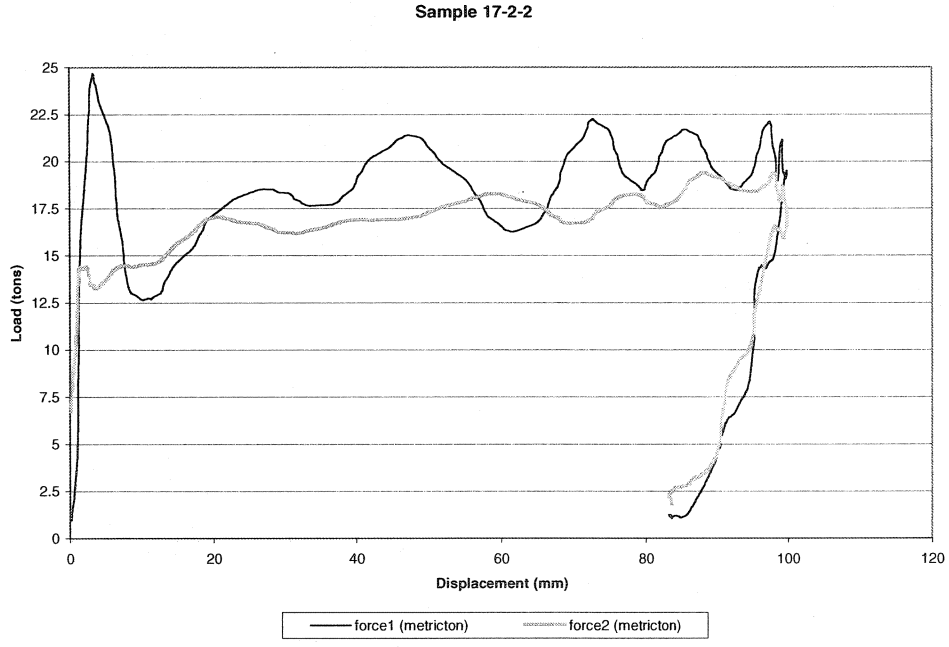

Figure 3.24– Processed impact data for sample 17-2-2.

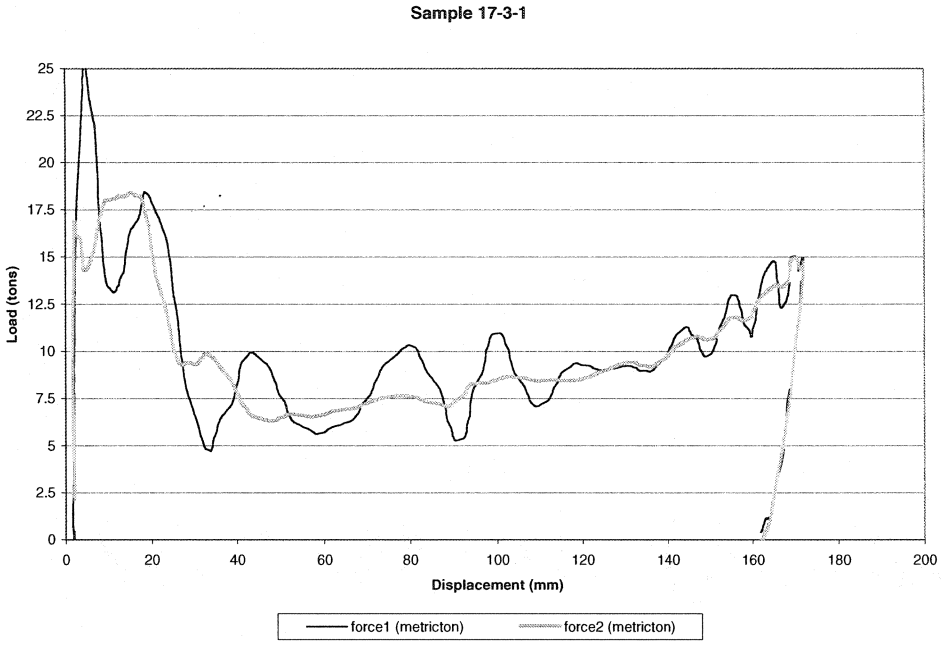

Figure 3.25– Processed impact data for sample 17-3-1.

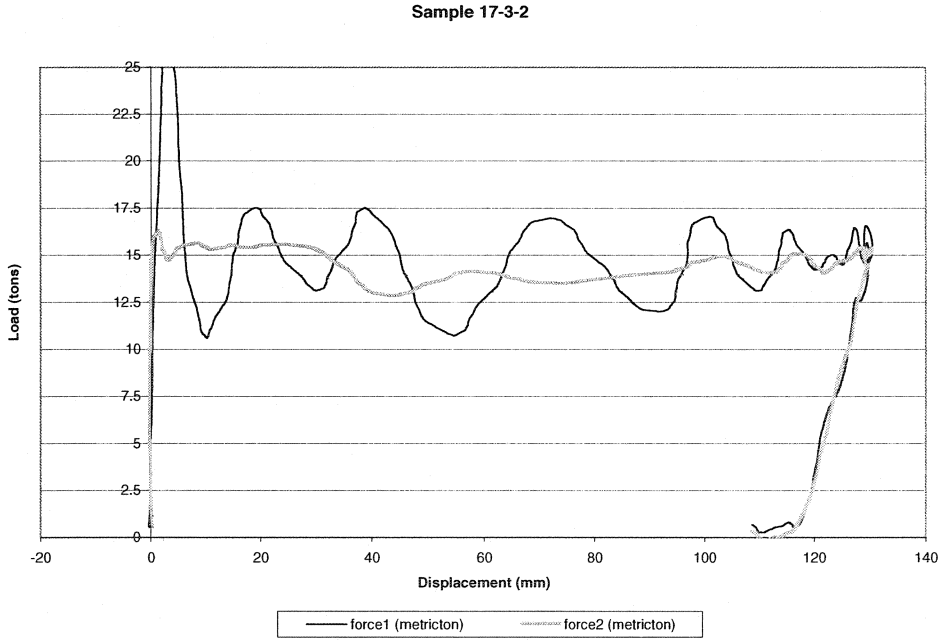

Figure 3.26– Processed impact data for sample 17-3-2.

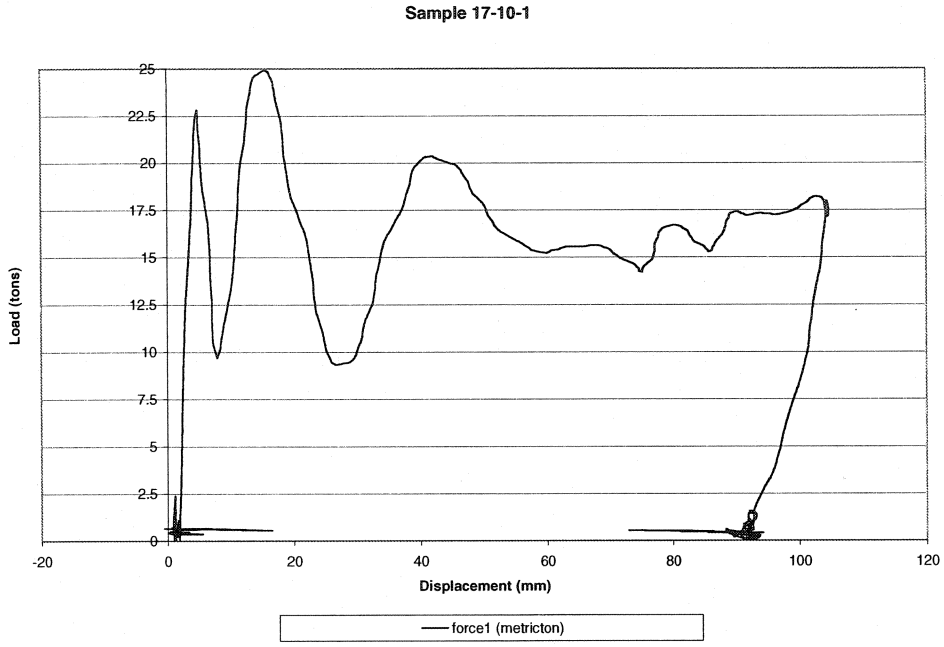

Figure 3.27– Processed impact data for sample 17-10-1.

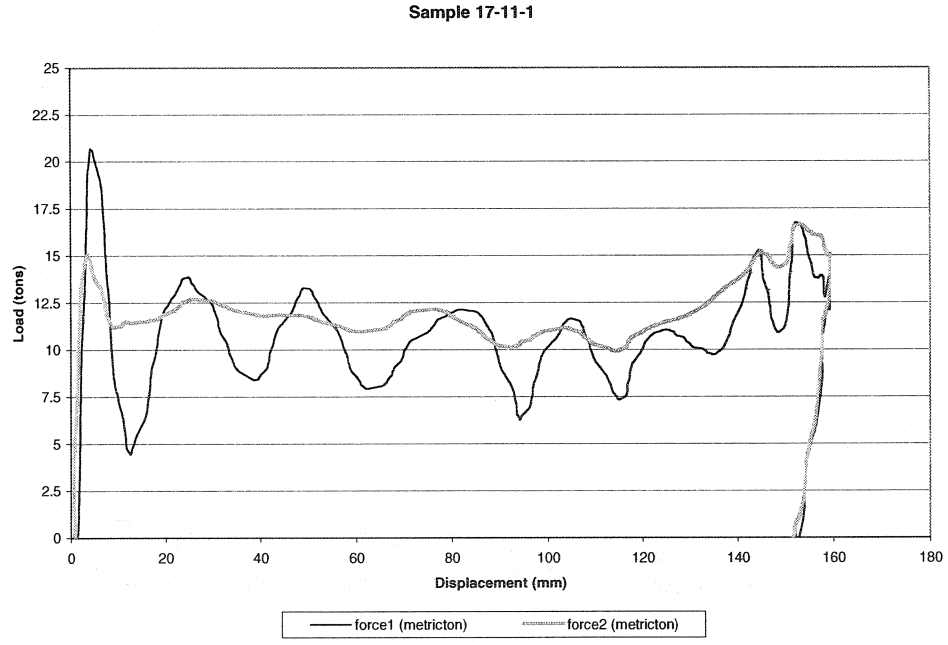

Figure 3.28– Processed impact data for sample 17-11-1.

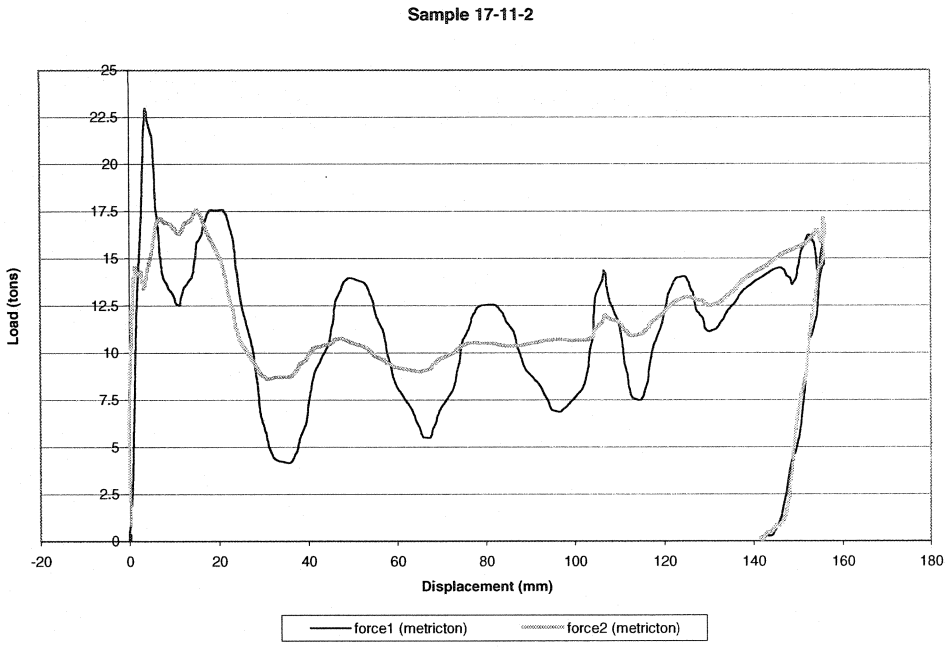

Figure 3.29– Processed impact data for sample 17-11-2.

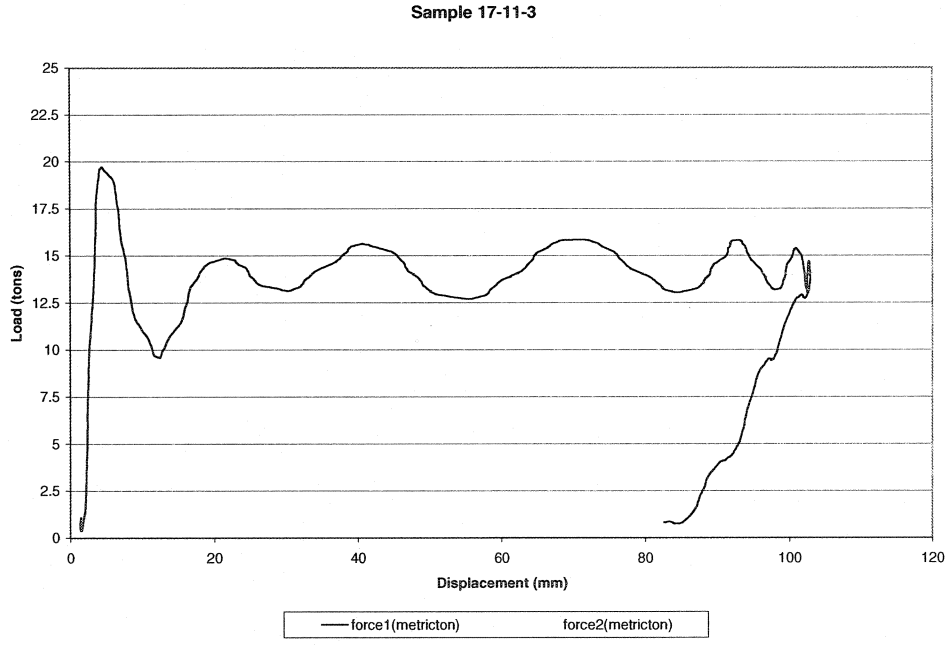

Figure 3.30– Processed impact data for sample 17-11-3.

Note that no graph is available for 4th cycle but loads LC1 and LC2 available.

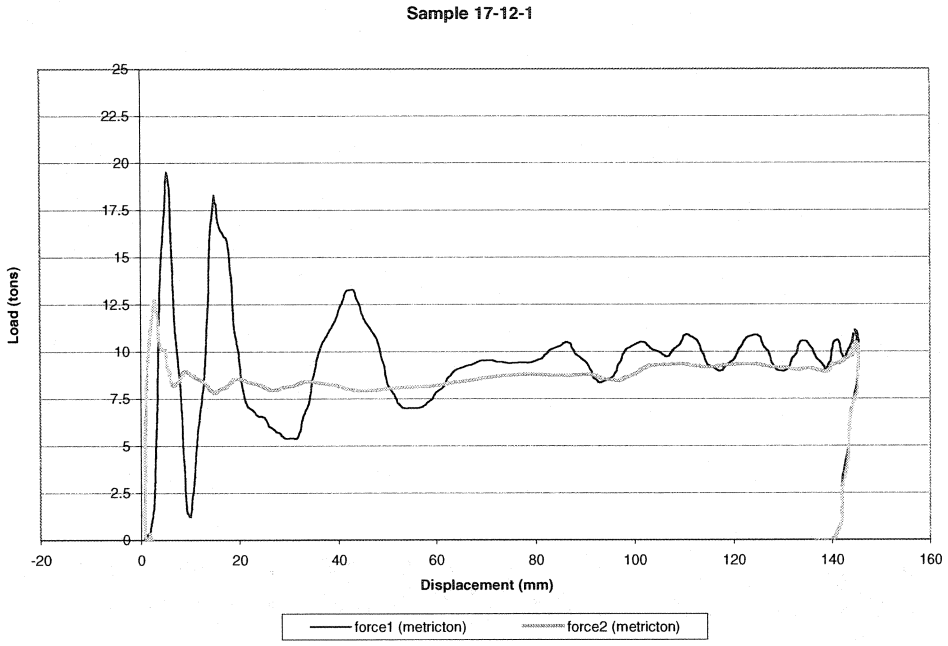

Figure 3.31– Processed impact data for sample 17-12-1.

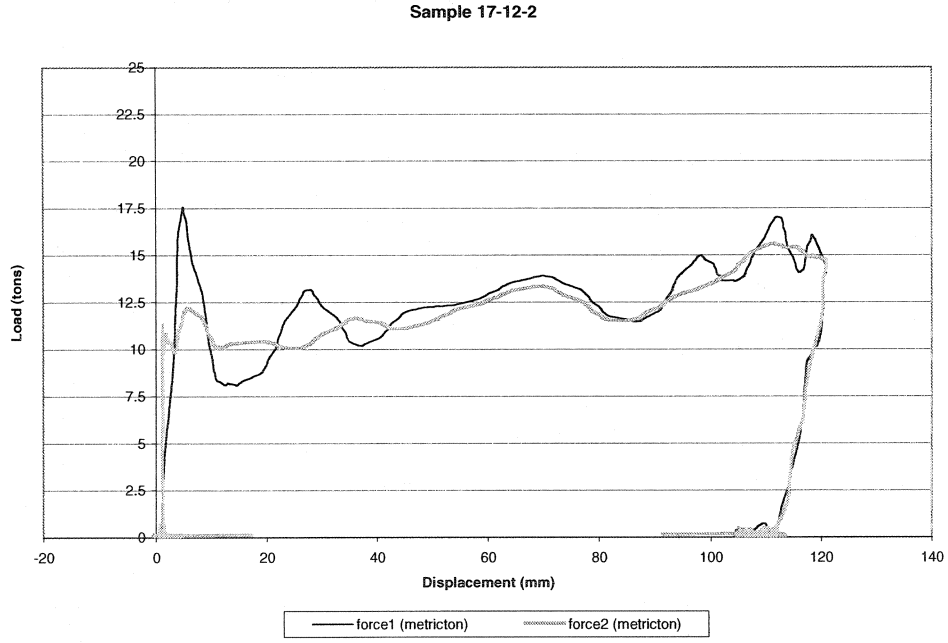

Figure 3.32– Processed impact data for sample 17-12-2.

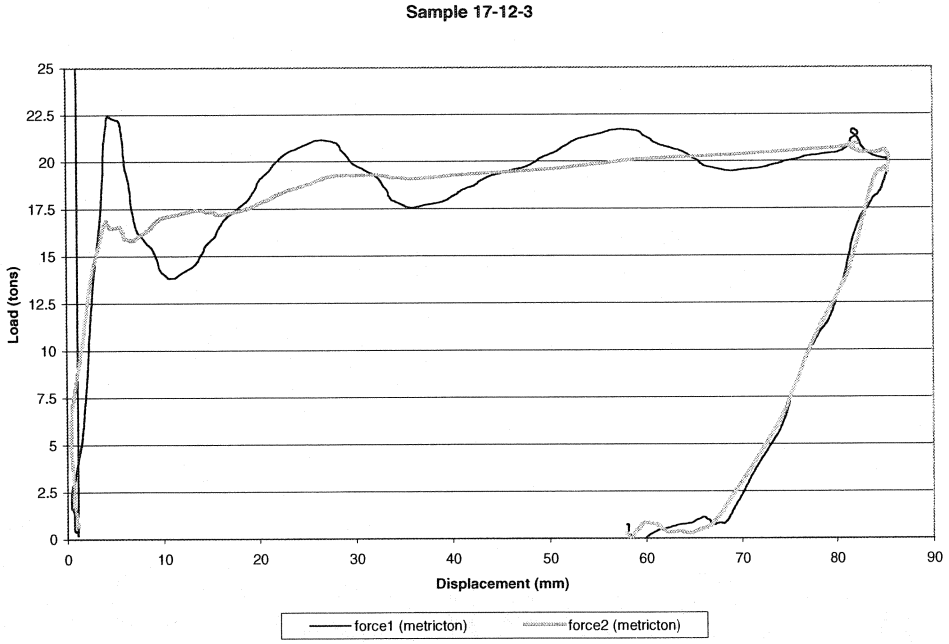

Figure 3.33– Processed impact data for sample 17-12-3.

No graph for cycle 4 is available, but the load LC1 is available.

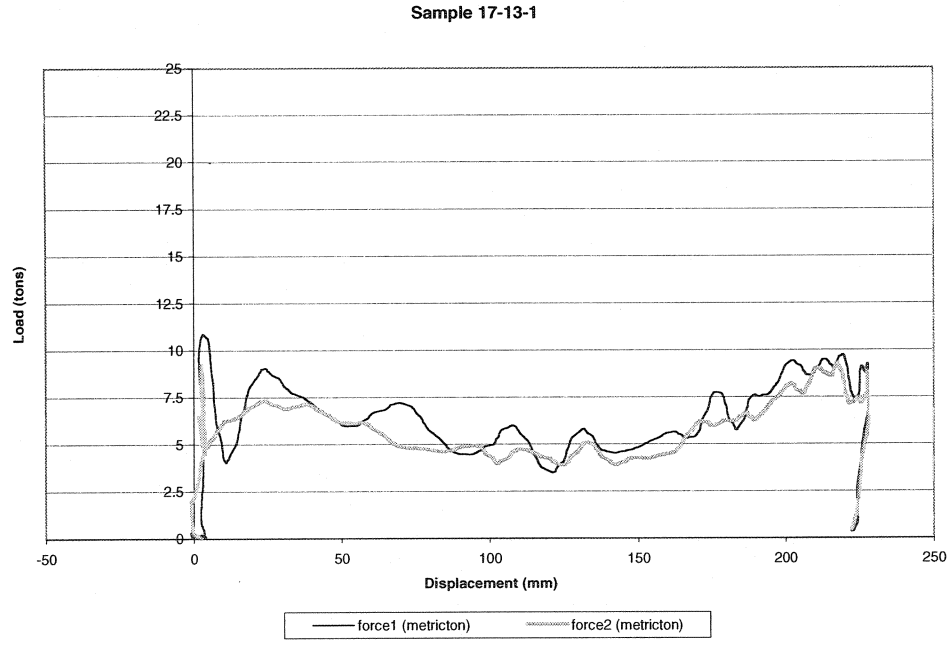

Figure 3.34– Processed impact data for sample 17-13-1.

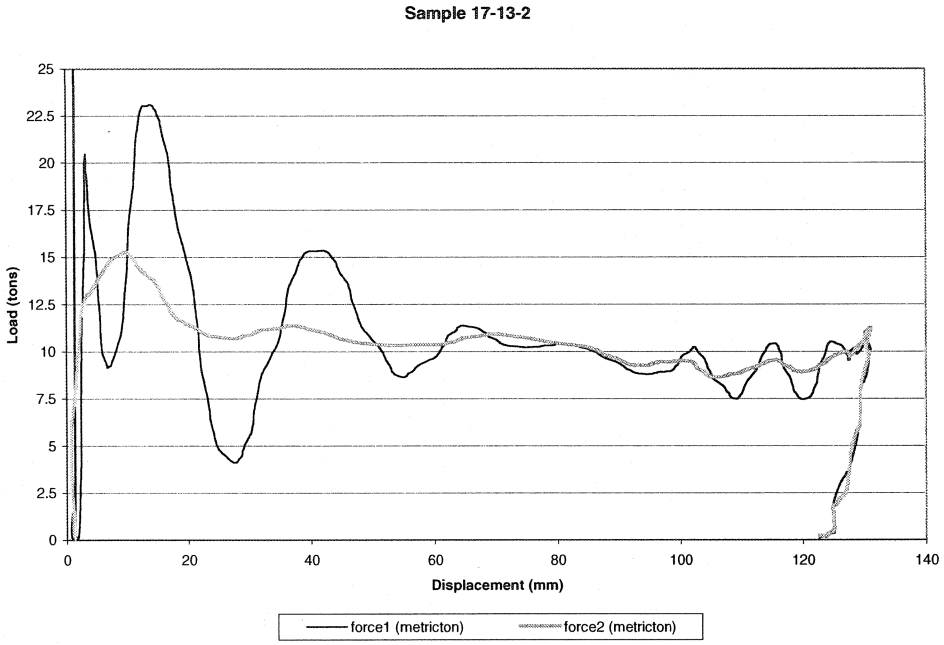

Figure 3.35– Processed impact data for sample 17-13-2.

No graph available for cycle 3, but loads are available. The same applies for cycle 4.

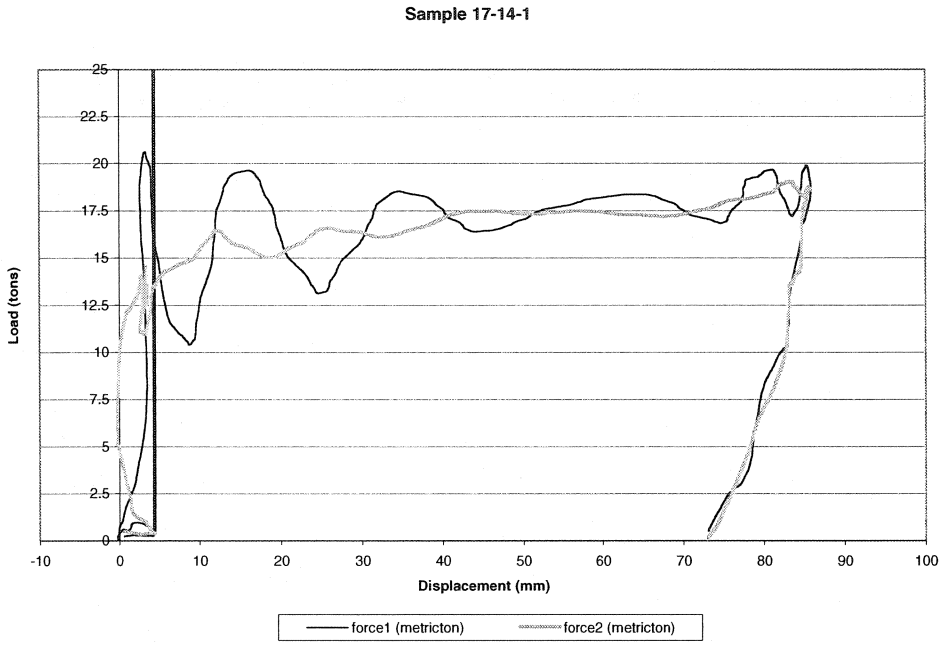

Figure 3.36– Processed impact data for sample 17-14-1. No graph available for cycle 2. Loads available for cycle 3. Load at failure at cycle 5 and total bar displacement available.

CHAPTER 4
RESULTS ANALYSIS AND PROPOSED DISPLACEMENT EVALUATION METHOD FOR TENDONS SUBMITTED TO IMPACT LOADING

4.0 Introduction

The quasi-static pull testing performance of the MCB is dependent of the tendon steel properties, the resin mix quality and its strength. In Section 4.1, the characteristic curve for the MCB is analyzed and compared to the performance of tendons introduced in Chapter 2. In Section 4.2, impact testing results are presented by relative work. In Section 4.3, a relatively simple displacement evaluation method for tendons submitted to dynamic loading is introduced.

4.1 In situ pull testing results

Figure 4.1 illustrates a summary of pullout testing results and Table 4.1 contains a compilation of parameters that can be extracted from them. As indicated in Figure 4.1, none of the tendons were tested to failure. Most of the elastic elongation occurred in the first 5 mm or so of displacement. The onset of plastic elongation averages 112 kN which fits the steel yield load for the prototype MCB bolt. The following plastic deformation consisted of a mix of steel permanent elongation and the cone retracting in its resin matrix. Data from all five pull tests was compiled in Table 4.1. Considering that it is a relatively small sample size, data spread was assumed to follow a "Student-t" probability distribution. The probable value of the mean of each parameter given a confidence interval of 95% can be expressed as (e.g. Hines and Montgomery, 1990):

$$(LowerLimit - UpperLimit) = \bar{x} \pm t_{\alpha/2,n-1} s/\sqrt{n} \qquad (4.1)$$

where *LowerLimit* and *UpperLimit* are respectively the smallest and highest probable value of the sample mean, $\bar{x}$ is the sample mean, s is the standard deviation, n is the number of samples and $t_{\alpha/2,n-1}$ is the t-distribution value. The intervals for the yield point of the bolting system, the elastic and plastic stiffness, the displacement at 145 kN and work were calculated using equation 4.1.

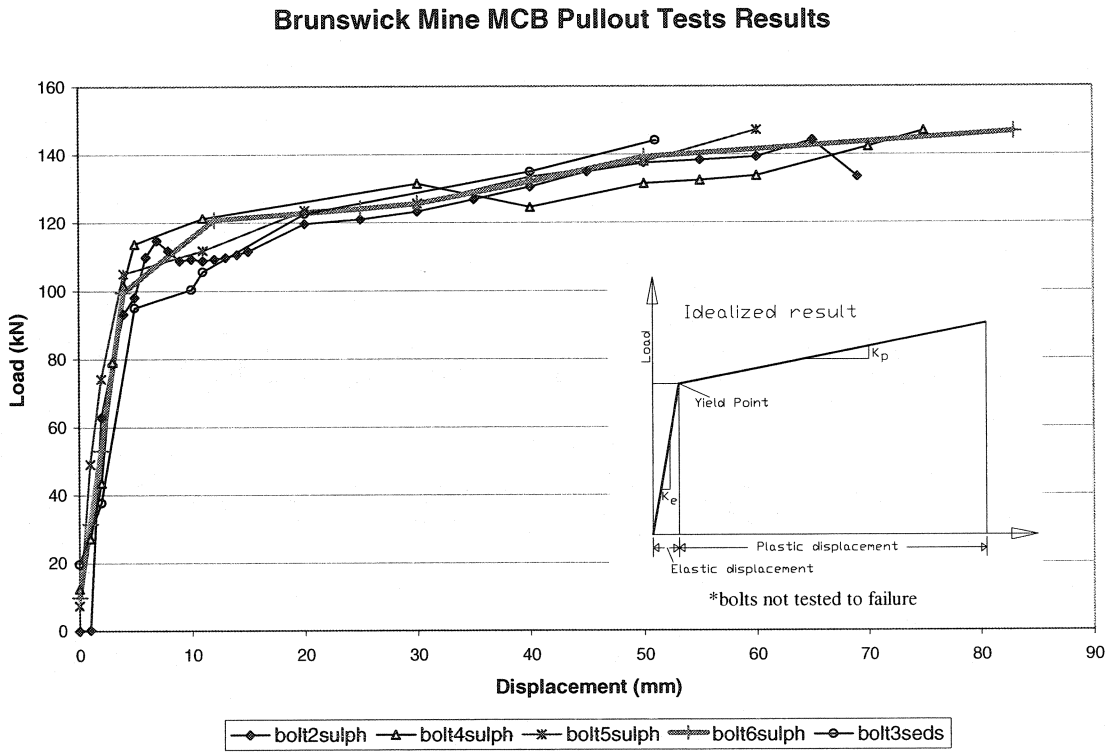

Figure 4.1 – Summary of quasi-static pullout test results performed at Brunswick mine.

The yield point is a point on the stress-strain curve at which there is a sudden increase in strain without a corresponding increase in stress (Oberg et al., 1996). It appears that the yield point for 1060 steel, as given in Table 4.1, falls into the range provided by the pull testing on the bolting system. It is assumed for the calculation of the maximum displacement and work that the bolting system yields at a load value equal to that of the steel yield point. The elastic stiffness K_e and plastic stiffness K_p of each sample was evaluated as the gradient of the curve defined by a linear regression based on the bolt's

measured response through its elastic and plastic ranges. The displacement forecasted at the ultimate strength is derived from the maximum tensile strength and yield point given by the 1060 steel specification, and by varying the stiffness within the range found using equation 4.1:

$$\mathrm{Disp}_{(\max,\min)} = \mathrm{ElasticDisp}_{(\max,\min)} + \mathrm{PlasticDisp}_{(\max,\min)} \tag{4.2}$$

or

$$\mathrm{Disp}_{(\max,\min)} = \frac{\mathrm{YieldPoint}}{\mathrm{K}_{e(\min,\max)}} + \frac{(\mathrm{TensileStrength} - \mathrm{YieldPoint})}{\mathrm{K}_{p(\min,\max)}} \tag{4.3}$$

where $\mathrm{Disp}_{(\max,\min)}$ are the maximum and minimum displacement forecasted, $\mathrm{ElasticDisp}_{(\max,\min)}$ and $\mathrm{PlasticDisp}_{(\max,\min)}$ the maximum and minimum elastic and plastic displacements respectively, YieldPoint is the yield point of the tendon material, TensileStrength the ultimate tensile strength of the tendon material, $\mathrm{K}_{e(\min,\max)}$ and $\mathrm{K}_{p(\min,\max)}$ the minimum and maximum elastic and plastic stiffness of the tendon's characteristic response.

The quasi-static elastic work:

$$\mathrm{We} = \int \mathrm{F}dx \tag{4.4}$$

where F is the force measured up to the yield point of the bolt sample and dx is the displacement, can be evaluated assuming:

$$\mathrm{We}_{(\max,\min)} = \frac{\mathrm{ElasticDisp}_{(\max,\min)} * \mathrm{YieldPoint}}{2} + \mathrm{PlasticDisp}_{(\max,\min)} * \mathrm{YieldPoint} + \frac{(\mathrm{TensileStrength} - \mathrm{YieldPoint}) * \mathrm{PlasticDisp}_{(\max,\min)}}{2} \tag{4.5}$$

Results from equations 4.1 to 4.5 are shown in Table 4.1. A simplified quasi-static loading tendon performance comparison is provided in Figure 4.2 where the performance of the MCB in quasi-static loading is compared to the data supplied by Kaiser et al. (1996) in Table 2.11. Each tendon support system has a niche of applications, depending on the expected loading mechanism, installation methods, etc. Cable bolts have the highest tendon load capacity, but also tolerate the least amount of displacement, along with rebars.

Table 4.1 – 2.1 m MCB pullout test performance parameters

	Mean	Std. Dev.	Value calculated with eq. (4.1) or *specs.*
Measured Yield Point (kN)	113	4.4	108-119
Measured Yield Point displacement (mm)	4.1	1.1	3-6
Measured elastic bolting system stiffness (kN/m)	21564	5705	14500-28600
Measured plastic deformation system stiffness (kN/m)	641	193	630-775
Measured displacement at 145 kN (mm)	59	10	46-72
Steel yield point (kN) according to specifications (1060 steel, Oberg et al., 1996)			*112*
Steel ultimate strength (kN) according to specifications (1060 steel, Oberg et al., 1996)			*189*
Displacement forecasted at ultimate strength (mm) using eq. (4.3)			105-132
Necessary work to break tendon in quasi-static loading (kJ) using eq. (4.5)			15-19

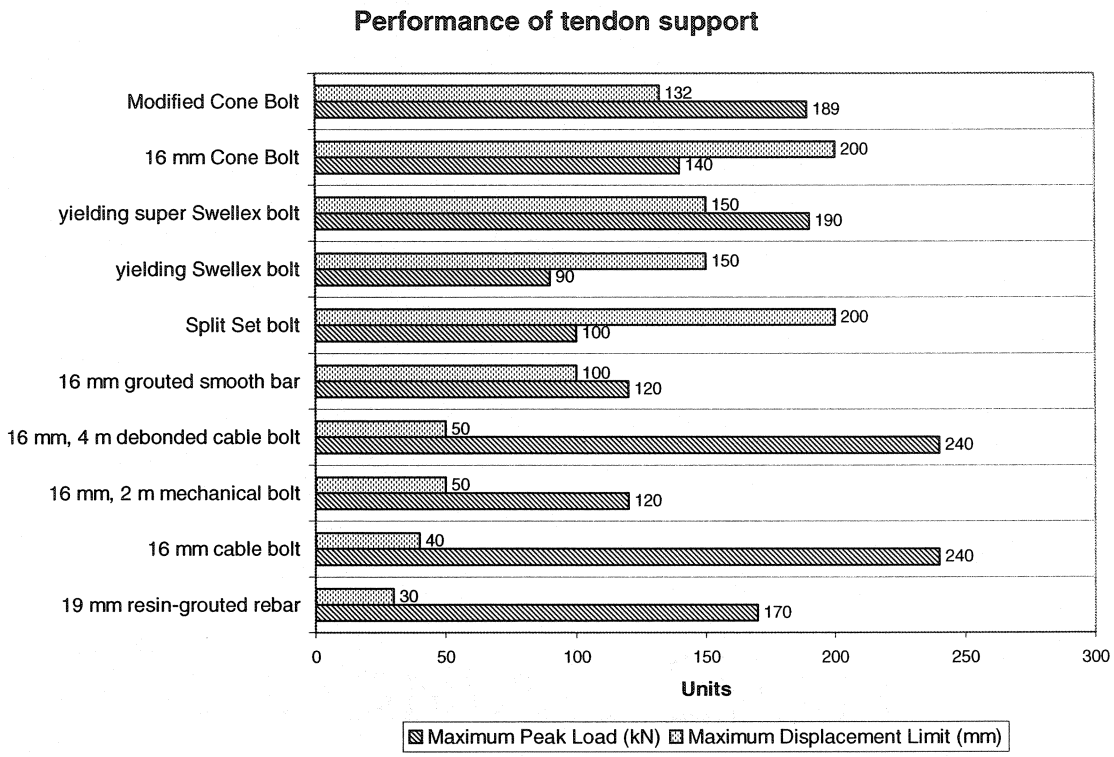

Figure 4.2 – Quasi-static tendon performance comparison (data from Table 2.11 and 4.1) including the prototype Modified Cone Bolt.

The field pull test results can be further compared with data from Langille et al. (1996) for resin rebar and Tannant et al. (1994) for the 16 mm resin anchored Cone Bolt. Figure 4.3 illustrates the field pull test results as compared to that information. The graph contains two curves for rebar pull testing (Langille et al., 1996), one for a resin anchored 16 mm South African Cone Bolt (Tannant et al., 1994) and some of the prototype MCB pull test results. Rebar reinforcement is meant to act as stiff support and consequently did not yield to high loads. The resin anchored Cone Bolt systems have yielded under high loads. Issues regarding the 16 mm Cone Bolt pertained to the resin mix quality which was different from one installation to the next.

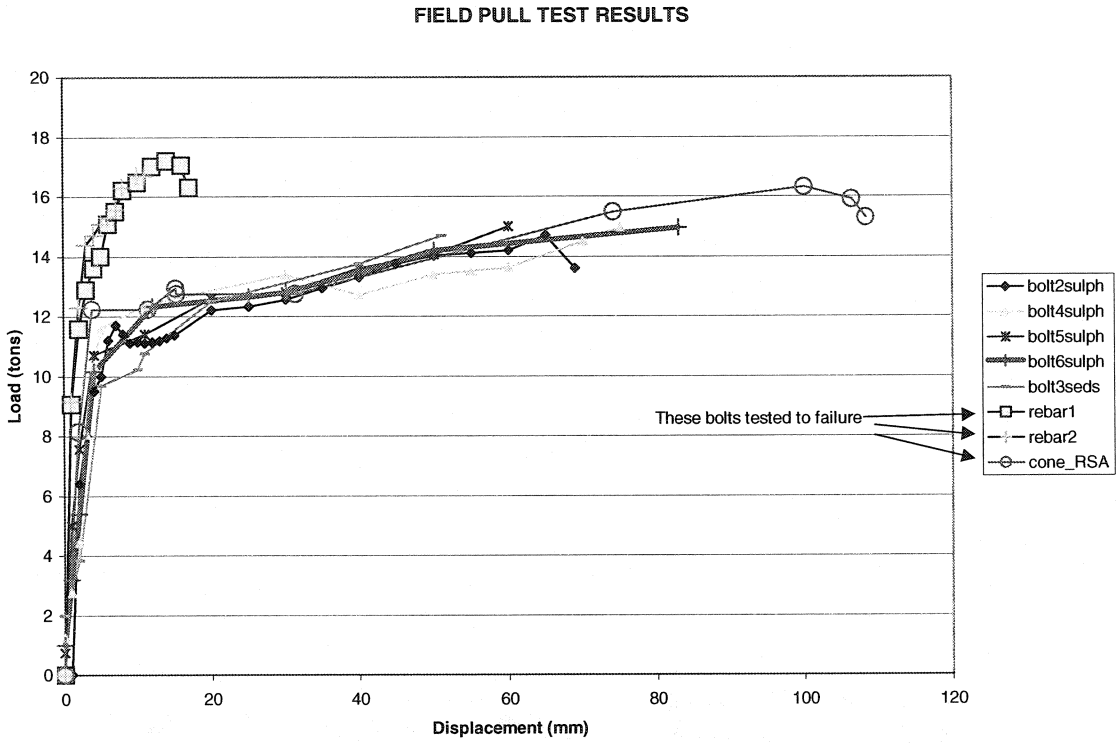

Figure 4.3 – Tendon pull test performance comparison (from Gaudreau, 2000c).

The resin quality variability is one of the factors that could affect a tendon such as the MCB. If the resin mixing quality is variable from one installation to the next, the resin strength may be influenced, and this will produce variability in the pull test performance. Additional pull tests on the MCB could narrow the parameters mean range. This process could affect the maximum and minimum performance parameters. Impact testing results provided additional confidence for the performance of the MCB system under efforts comparable in work. These results are analyzed in the next section.

4.2 Impact testing results

Figure 4.4 illustrates a schematic of parameters that can be extracted from impact testing results, presented in Chapter 3. Discrepancies between the proposed schematic and a typical impact testing curve are highlighted in Figure 4.5, as well as comments relative to the graph. The energy absorption during each impact test can be calculated by the work given by eq. (4.4):

$$We = \int F dx$$

where F is the load as measured by the bottom load cell when available and dx is the displacement increment measured by the transducer. The total additive energy from cyclic impact testing consists in the addition of each energy absorption evaluation up to the sample failure. Whenever testing logs contain tendon displacement readings before and after the impact test, as well as the impact load and the drop height, the energy absorption capacity can be evaluated as the potential energy:

$$\text{Energy Absorption} = m * g * h \qquad (4.6)$$

where m is the impact weight, g the gravitational constant and h the drop height plus the displacement increment measured after the test. The duration of the impact is taken to be the time at the onset of elastic recovery.

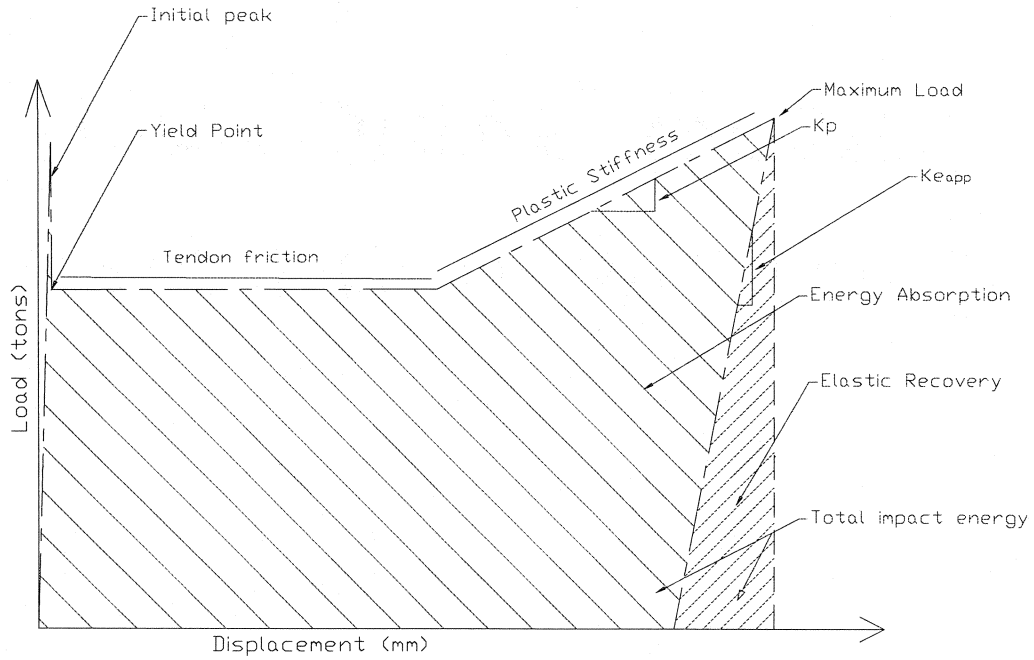

Figure 4.4 – Parameters extraction from impact testing. Compare with Figure 4.5.

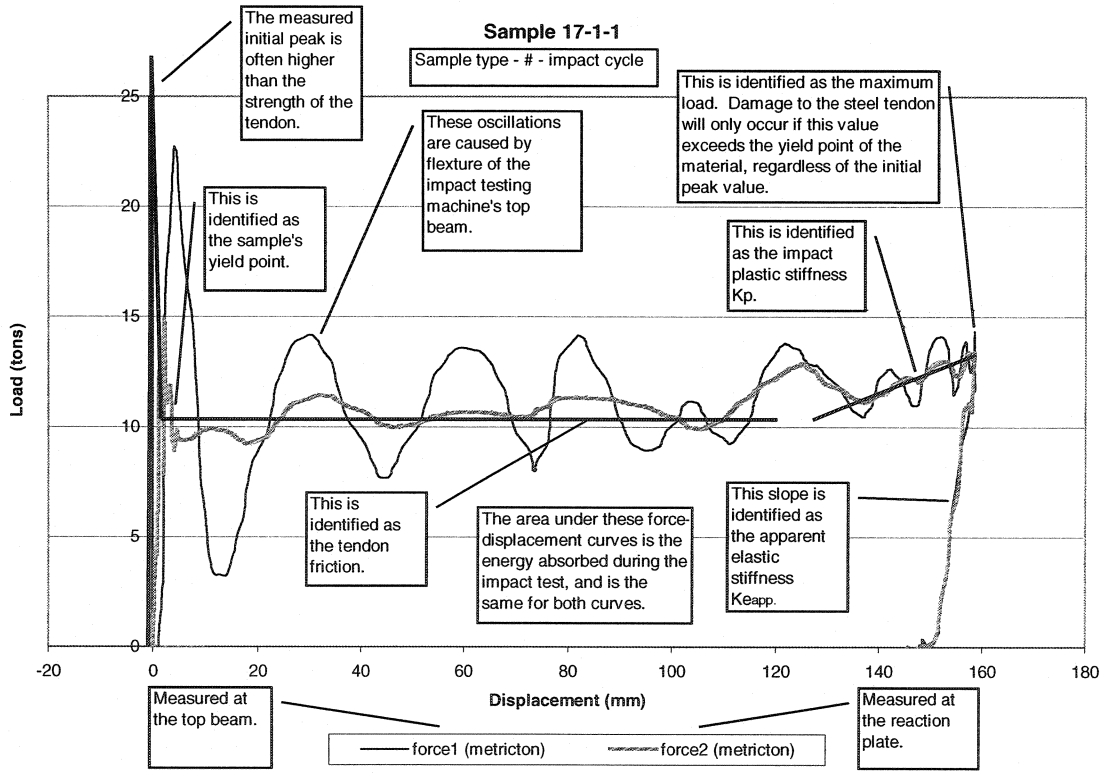

Figure 4.5 - Parameters extraction and comments superimposed on sample 17-1-1 test.

Four samples were tested to failure. Table 4.2 and 4.3 disclose the cyclic impact testing results on 1.7 m MCB samples. A summary of results for tendons tested to failure (or with multiple impacts) is presented in Table 4.2. All testing results are presented in Table 4.3.

For tendon 17-11, the absorption energy was calculated from load-displacement graphs presented in Chapter 3 (Figures 3.28 to 3.30). The work load between parenthesis in Table 4.2 is the energy absorbed during the last cycle of loading and was calculated according to a fixed work load of 20 tons and the tendon displacement measured after the breaking of the bar. This energy absorption evaluation method was used when displacement transducer data was unavailable. No displacement transducer was installed for the last cycle of loading because of the potential damage to the sensor. The lower limit load value of 20 tons was selected for energy absorption calculations, being the maximum load value read at the previous cycle of loading. For tendons 17-3, 17-12, 17-13 and 17-14, the energy absorption was calculated from the potential energy dissipated through the tendon according to the final displacement manually measured after the elastic recovery. For these tests, the work for the last cycle is again shown between parenthesis and this work is calculated as the energy from the fixed 20 tons load and the displacement as measured directly from sample before and after the test. The load at failure is the maximum load measured by the top load cell at the moment of failure. This load is not available for sample 17-3 because no instrument was installed for this test. The minimal load at failure is of 191 kN which matches well the specification of 1060 steel, having a tensile strength of 189 kN. This increases confidence in results shown in quasi-static loading.

Note that elastic energy recovered after each cycle is inherently removed from total testing energy quantities and energy summations. The MCB has a minimum of 46 kJ cyclic energy absorption capacity according to Table 4.2. Calculation of maximum static

pullout testing energy absorption gives 23.5 kJ according to Table 4.1, which is roughly half of the impact testing energy absorption calculation.

Table 4.2 – Tendons tested to failure and tendon load measured during last cycle of loading

Sample	Cycles to failure	Energy absorption by cycle (kJ)	Total additive energy (kJ)	Load at failure (tons)
17-3	4 at 1000 kg	16.4+17.5+18.3+(7.4)	59.6	Not available
17-11	4 at 1000 kg	17.3+17.0+12.7+(3.2)	50.3	19.6 thread failed
17-12	4 at 750 kg	11.0+12.0+12.3+(10.6)	45.9	23.7 nut slipped
17-13	4 at 750 kg (no failure)	11.6+12.1+12.9+14.2	50.8	Not applicable
17-14	5 at 750 kg	10.6+11.4+12.3+13.0+(12.4)	59.6	23.0 thread failed

In Table 4.3, the potential energy should be approximately equal to the absorbed energy. The first is calculated from tape measurements, the second from the instrument curves as previously stated. Total energy in Table 4.3 is the energy *including* the elastic deformation. In general, the potential energy measurements are in good agreement with the instrumented energy absorption calculation. The discrepancy between the measured potential energy calculation and the instrumented energy absorption calculation can probably be attributed to the displacement transducer wire, which can be slightly off-axis during the tendon movement. This would cause higher energy absorption than reality. Furthermore, if the recall spring of the displacement transducer potentiometer wire is too soft, the displacement measured during the impact will be shorter than reality.

Table 4.3 – Yield points and impact plastic deformation stiffness for each test.

Sample number #	Max. Load (kN)	Yield Point (kN)	Impact			Energy (kJ)		
			Tendon friction (kN)	Plastic stiffness Kp (kN/m)	Impact duration (ms)	Absorp-tion	Total	Potential at equil.
17-1-1	131.0	92.2	103	713	61.5	16.6	17.1	16.2
17-1-2	192.2	144.2	157	940	41.0	17.1	18.6	17.2
17-2-1	127.8	99.5	108	835	57.4	16.4	16.6	16.2
17-2-2	187.5	140.0	147	829	45.1	16.0	17.3	16.9
17-3-1	143.2	91.2	170, 073	858	66.2	16.2	16.6	16.4
17-3-2	144.2	155.0	147	801	53.3	17.6	18.7	17.5
17-3-3	-	-	-	-	-	-	-	18.3
17-10-1	173.6	150.0	171	965	42.2	15.7	16.6	15.7
17-11-1	153.0	109.9	122	1339	62.2	17.3	17.8	16.2
17-11-2	162.8	139.3	171, 098	1300	61.2	17.0	17.8	17.6
17-11-3	145.2	137.9	137	-	41.0	12.7	13.9	18.5
17-11-4	192.2	-	-	-	7.5	-	-	-
17-12-1	101.2	83.4	78	-	61.2	12.6	12.9	11.0
17-12-2	144.2	105.7	98	1043	50.0	13.9	14.4	12.0
17-12-3	197.2	161.5	162	-	35.0	14.1	15.7	12.3
17-12-4	232.5	-	-	-	18.1	-	-	-
17-13-1	83.8	86.9	69	595	85.8	13.3	13.5	11.6
17-13-2	106.1	128.4	147, 108	-	61.8	12.1	12.3	12.1
17-13-3	167.8	-	-	-	53.5	-	-	12.9
17-13-4	139.6	-	-	-	63.5	-	-	14.2
17-14-1	179.9	120.0	147	680	32.8	12.7	13.8	10.6
17-14-2	-	-	-	-	-	-	-	-
17-14-3	193.2	-	-	-	30.0	-	-	12.3
17-14-4	-	-	-	-	-	-	-	13.0
17-14-5	226.5	-	-	-	16.5	-	-	-

Note that sample 17-14 was not waxed. The latter showed a higher impact yield point than most samples on the first cycle of impact. It can be generally stated that the higher the adhesion between the tendon and the resin, the higher is the yield point of the tendon-resin-test tube system. The basis of this statement is the assumption that impact loads are distributed along the tendon length through waves (e.g. Engel, 1978; Collins, 1993). To illustrate this statement, lets hypothesise that oscillations present on load-displacement data such as that of Figure 4.5 relate to the event of a wave crest at the instrumented tendon head. The graph shows nine oscillations during the impact load. Assuming that the deflection of the tendon is directly proportional to the applied force and not a function of time, that the steel material remains in the elastic range and that no energy is lost in the impact, the theoretical impact load on a stiff system would be (Collins, 1993):

$$F = W\left(1+\sqrt{1+\frac{2hEA}{Wl}\left(\frac{1}{1+\frac{ql}{3W}}\right)}\right) \tag{4.7}$$

where W (N) is the drop weight, E (Pa) the elastic modulus of the bar and A (m^2) its cross-sectional area, h (m) the dropping height of the weight, l (m) the length of the bar and q (N/m) the unit weight of the bar (and the test sample holding tube).

Using equation 4.7, the impact load for a drop height of 1.5 m with an impact weight of 1000 kg, a tendon length of 1.7m, a Young's modulus of 220 GPa, a bar cross-sectional area based on a diameter of 17.2 mm and a unit weight of 10 kg/m is 950 kN. With a sufficiently soft tendon which can move steadily at a high enough load to retain the drop mass, and considering that it does not pass the steel yield point, the full impact load of 950 kN could have been dispersed in 9 load cycles travelling through the tendon, which gives a value of 105 kN maximum load. This is generally in good agreement with the experiments. Now, if the adhesion of the resin matrix to the bar is too high, the impact

wave cannot travel through the tendon without having to break the resin bond. The resin bond breakage requires time. As the passage of the oscillating front is back, the impact wave "turns back" to the reaction plate before the load can be spread through the entire tendon length, causing premature plastic elongation of the steel next to the reaction plate. This phenomena has been observed after cycle 1 for sample 17-14. The commercial MCB tendon is greased to prevent resin from bonding to the tendon. This ensures that the full tendon length is used to dissipate impact energy.

For all tests, the displacements travelled and energy dispersed are higher for the impact tests than for the quasi-static loading tests. The plastic stiffness was evaluated from impact testing for two reasons. First, to quantify the increased rate of plastic elongation that is observable at the end of the impact loading cycles. Second, to verify if it is at all comparable to that of the quasi-static pull tests. The plastic stiffness Kp measured at impact is in the range of 760 to 1050 kN/m as evaluated using equation 4.1 and results from Table 4.3. The quasi-static evaluation of Kp was in the range of 630 to 775 kN/m. It could be argued that the stiffest potential quasi-static Kp is within the range of the impact plastic stiffness. It is also possible that the impact plastic stiffness calculated values could have been altered by other controlling parameters relative to impact dynamics as compared to quasi-static loading. The maximum quasi-static plastic stiffness of 775 kN/m will therefore be chosen as the characteristic value for the support system in Section 4.3.

The impact tendon friction force is in the range of 80 to 154 kN. Its arithmetic mean value is 117 kN which is slightly higher than the steel yield point, but the bolting system has shown the capability of collapsing through the resin at loads lower than the steel yield point, e.g. tests 17-1-1, 17-2-1, 17-3-1, 17-11-1, 17-12-1, 17-12-2 and 17-13-1. This suggests that friction falls into a fairly broad range that is affected by other factors in the impact mechanism. Also note that samples were not all tested immediately after they were spun in the resin. The liquid wax used at the time of the prototype testing had time-

dependent debonding properties. Samples tested or cycled after a long setting time (days or weeks) showed higher friction loads than these tested just after the sample preparation. Hence, results should be interpreted with care.

4.3 Proposed displacement evaluation method for tendons submitted to impact loading

In this Section, a displacement evaluation method is proposed for tendons submitted to impact loading, given a tendon burden, impact velocity, the tendon's yield point and its plastic stiffness under quasi-static loading. The method can be used to estimate the tensile load within a tendon submitted to axial impact loading. The proposed calculation method could be used to interpret the maximum energy absorption capacity of the tendon for a single impact, and to evaluate the maximum load in the tendon for a given choice of ejection velocity and tendon burden. The ejection velocity could be derived from energetic considerations equations, given a plausible violent rock mass failure of a given depth and expected energy. The burden of the tendon, or impact mass, can be estimated from the depth of failure expected in the rock mass and the bolting pattern applied. One could evaluate if the tendon can withstand the given impact, by verifying if the axial load in the bolt exceeds its ultimate tensile strength. Furthermore, it should be possible to estimate the axial load applied by the tendon that could modify the depth of failure expected by clamping of the rock mass. The latter has the effect of strengthening rock materials so that they can sustain larger loads.

An adequate model for tendon displacement submitted to impact loading is required to analyze impact test results and could ultimately be used to predict the energy absorption capacity of support systems based on no failure cases for one impact using the NTC impact test rig. Cyclic impact testing was performed on the MCB bolting system. Although it would have been interesting to set the impact testing for higher impact energy, so to break the tendon on first impact and directly evaluate its maximum energy

absorption capacity, the available equipment could not be set for higher drop heights nor bigger drop weights. The relative effect of an increase of the impact velocity and/or the drop height in the testing protocol on the tendon's response must also be assessed. For the benefit of the MCB testing program, the velocity for all tests was higher than 5 m/s, and increasing at every cycle of loading for one sample since the tendon reaction plate was pushed further down with each blow. Drop loads were varied between 750 kg and 1000 kg. The impact tests on the MCB prototypes have provided valuable information useful for the selection of a calculation method for the displacement of tendon support submitted to impact loading.

The following phenomena were observed during the impact tests protocol:

-The impact load-displacement curves show an oscillatory behavior, possibly representing the exchange of load from the nut to the cone in a number of pulses through time. Ideally, the calculation method should reflect the oscillatory behavior.

-When the so-called maximum load reaches a value larger than the static yield point of the steel, the carbon coating on the steel bar flakes off, suggesting plastic deformation of the tendon. Ideally, the model should be applicable beyond the elastic range.

-There are no signs of plastic deformation on steel bars for which the initial impact peak load (see Figure 4.4) was larger than the static yield point of the steel.

-The bar can slide further into the test tube even at the last impact cycle on a sample, when the yield point of the steel is almost equal to the ultimate tensile strength.

-Discrepancies in yield load were observed between tests.

The discrepancy in yield load can be due to the adhesion of the tendon in the resin matrix. If the adhesion is strong, the load transfer from the reaction plate to the conical anchor is not completely achieved before the plastic deformation wave travels back to its origin, resulting in premature deformation near the collar of the test tube. This can momentarily create uneven steel properties over the tendon length.

The observed phenomena suggest that the tendon support system materials can be hardened due to plastic strain, and that the impact cycles have no apparent effect on Young's modulus or on the ultimate tensile strength of the steel.

The proposed calculation method for the displacement evaluation of tendon support submitted to impact loading is based on critically damped harmonic motion (Engel, 1978; Derrick and Grossman, 1987; Thomas and Finney, 1992; Van Sint Jan, 1994) and incorporates a so-called "friction factor" and a yield point offset. The critically damped harmonic motion model consists in a single spring and a dashpot attached to fixed points at each distant end and to a mass at the inner end. A spring and a dashpot in series constitutes a Maxwell model (Mase, 1970; Gibowicz, 1993). A Maxwell substance, or an elasticoviscous material, behaves differently under rapidly changing stress in contrast with slow loading. The MCB support system behavior displays this characteristic. The friction factor is a force referring to friction loss and heat dissipation during impact loading, it is not a yield point. Thus unlike a true Maxwell substance, the proposed model incorporates the combination of the so-called friction force of the tendon in the holding matrix and the action of the yield point when the tendon goes beyond the plastic range.

The proposed calculation method consists of two main steps. The first relies on a rheological model used to simulate the displacement of a tendon under impact loading. The second involves potential energy and work balanced with the friction factor imparted to the rheological model. The outcome is the approximation of the maximum tendon displacement under impact loading, or alternatively its maximum axial load for a given mass, impact velocity and characteristic plastic stiffness. The rheological model chosen to simulate the displacement of tendon support under impact loading consists of a mass attached to a slider, a spring, and a dashpot in series (Figure 4.6). The mass m is impacted at initial velocity and displacement v_0 and x_0. The spring has a plastic stiffness of k_p to which is added a constant yield force of F_y when displaced. The dashpot has a

damping factor c, proportional to the plastic stiffness of the spring and to the size of the impact mass. Positive displacement x is downwards. The overall constant yield force value F_y (N) consists of:

$$F_y = \text{YieldLoad} + F_f \tag{4.8}$$

where YieldLoad is the yield load (N) of the tendon material and F_f is the friction factor (N) representing all sources of friction losses.

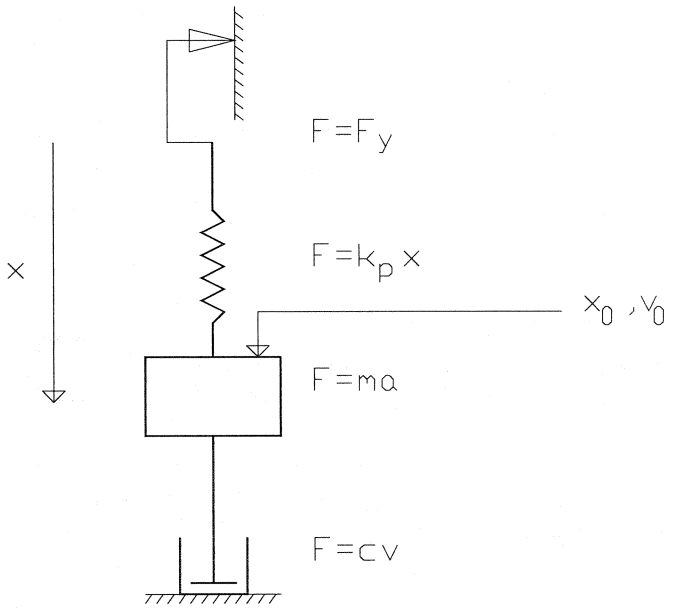

Figure 4.6– Rheological model.

The model should then require only input parameters that are known a priori from quasi-static pull testing results and specifics, such as the impact mass and initial velocity, the tendon support system plastic stiffness, and the yield load of the tendon material. Solving the equilibrium of this model (e.g. Figure 4.6) for forces, we have:

$$m\frac{d^2x}{dt^2} + c\frac{dx}{dt} + k_p x + F_y = 0 \tag{4.9}$$

where m is the mass (N), c the damping factor, k_p the plastic system stiffness (N/m) as evaluated from pull testing of the tendon, and F_y the overall constant yield force (N) for the displacement of the system, calculated as the addition of the tendon material's yield load and the friction factor (eq. 4.8).

Using substitutions (4.10) and (4.11) in (4.9), one gets the second order non-homogeneous differential equation (4.12).

$$2b = \frac{c}{\mathrm{m}} \tag{4.10}$$

$$w = \sqrt{\frac{\mathrm{k_p}}{\mathrm{m}}} \tag{4.11}$$

$$\frac{d^2x}{dt^2} + 2b\frac{dx}{dt} + w^2x + \frac{\mathrm{F_y}}{\mathrm{m}} = 0 \tag{4.12}$$

Assuming a critically damped system:

$$b = w \tag{4.13}$$

The solution to the homogeneous equation takes the form:

$$x_h = (C_1 \cdot t + C_2) \cdot e^{-wt} \tag{4.14}$$

The particular solution is expected to take the form (e.g. Derrick and Grossman, 1987):

$$x_p = R \tag{4.15}$$

And differentiating:

$$x_p^{'} = 0 \tag{4.16}$$

$$x_p^{''} = 0 \tag{4.17}$$

Replacing x in equation (4.12) by equations (4.15), (4.16), (4.17):

$$R = \frac{-\mathrm{F_y}}{\mathrm{k_p}} \tag{4.18}$$

Thus, using (4.15) and (4.18):

$$x_p = \frac{-\mathrm{F_y}}{\mathrm{k_p}} \tag{4.19}$$

The general solution to the differential equation, representing the position of the mass on the x axis (m) is thus:

$$x_g = x_h + x_p \tag{4.20}$$

$$x_g = (C_1 \cdot t + C_2) \cdot e^{-wt} - \frac{\mathrm{F_y}}{\mathrm{k_p}} \tag{4.21}$$

The mass velocity can be calculated using a derivation of displacement through time. Using the change of variables,

$$u = C_1 \cdot t \qquad ; \; du = C_1 dt \tag{4.22}$$

$$v = e^{-wt} \qquad ; \; dv = -we^{-wt} dt \tag{4.23}$$

$$v = C_1 \cdot e^{-wt} \cdot (1 - wt) - w \cdot C_2 \cdot e^{-wt} \tag{4.24}$$

Using the initial conditions for initial displacement (x_0) and speed (v_0):

$$x_0 = C_2 - \frac{F_y}{k_p} \tag{4.25}$$

$$v_0 = C_1 - w \cdot C_2 \tag{4.26}$$

Rearranging (4.25), one obtains the particular solution constant C_2:

$$C_2 = x_0 + \frac{F_y}{k_p} \tag{4.27}$$

And using (4.26) and (4.27), the particular solution constant C_1:

$$C_1 = v_0 + w \cdot (x_0 + \frac{F_y}{k_p}) \tag{4.28}$$

The variables for the rheological model equations (4.21), (4.24), (4.27) and (4.28) are parameters m (N), x_0 (m) and v_0 (m/s) which must be defined by the user. The yield load of the tendon material, consisting of part of the threshold value F_y (N), as well as the plastic stiffness of the system k_p (N/m), are factors specific to the tendon support system. They can be drawn preferably from quasi-static pull testing and materials specifications, or alternatively from impact tests results. In the latter case, the plastic impact stiffness can be calculated from the end of the load displacement curve at small impact weight velocity, where the peak may appear if the impact load was sufficiently strong to deform the tendon. The force (N) in the tendon can be estimated using:

$$F_{bar} = x_g \cdot k_p \tag{4.29}$$

where x_g (m) is the model's calculated tendon head displacement (4.21) and k_p (N/m) is the plastic stiffness of the tendon support system.

The calculated tendon head displacement will not provide accurate results without the introduction of the friction force and the balance of the potential energy and the work of the tendon as it moves under impact load. Equations (4.11), (4.21), (4.27) and (4.28) can be integrated in a spreadsheet in order to calculate a given tendon displacement submitted to impact loading. The spreadsheet is used to balance the potential energy and the work of the tendon under impact load using the friction factor F_f.

Potential energy absorption (J) can be calculated as:

$$E_{bar} = \frac{m \cdot v_0^2}{2} + m \cdot g \cdot \max x \qquad (4.30)$$

where g is the gravitational constant (m/s^2) and max x (m) the maximum displacement calculated. The work required to pull out the tendon in impact load (J) can be calculated from the load displacement graph (eq. 4.4):

$$We = \int F dx$$

Thus equations (4.30) and (4.4) can be balanced in the spreadsheet by changing the friction force F_f, which can be argued as the "equilibrium" force in the impact mechanism based on the discussion of Section 4.2:

$$E_{bar} = We \qquad (4.31)$$

For modeling of the MCB system in single impact, the factor k_p can be estimated at 775 kN/m, which corresponds to the possible stiffest response calculated from the quasi-static loading tests (Table 4.1). It falls within the calculated impact plastic stiffness measured at a range from 760 to 1050 kN/m (Table 4.3). Higher values of k_p are required to calculate the MCB system's reaction to multiple impacts.

The steel yield load has a value of 112 kN, according to reference specifications (Table 4.1). The average friction force for freshly spun debonded waxed tendon samples, according to first impact testing results in Table 4.3 falls in the range of 80 to 154 kN, and the nominal average value of 117 kN can be used as a start point for the energy balance exercise. Since the energy balance exercise is an iterative process, any value close to the tendon's yield load is considered satisfactory as a first trial.

Figures 4.7 to 4.9 show the tendon load evaluation result for a sample having a k_p value of 1050 kN/m, a yield load of 112 kN, and a friction force F_f of 93 kN, at an impact weight of 1000 kg and initial impact velocity of 5.7 m/s. This impact velocity corresponds to a drop height of 1.66 m and the k_p value to a tendon whose grout matrix could have stiffened under a first large impact. The maximum load evaluated in the bar is 169 kN (see Figures 4.7 and 4.9), and the simulated impact time to the onset of elastic recovery is 70 ms (see Figure 4.7). On a similar set up, 163 kN was measured for maximum tendon load on sample 17-11-2 and the impact duration was 61.2 ms to elactic recovery and 74 ms for the complete test. The friction force of 93 kN falls into the tested range of 80 to 154 kN. Note that this result is consistent with the experimental observations shown in Table 4.3.

One can compare the calculated tendon axial load through time of Figure 4.7 with the 17-11-2 impact test result shown in Figure 4.8. The Force 1 curve representing the load cell located on top of the test rig displays more oscillations than Force 2 for the load cell located at the reaction plate. These oscillations are less pronounced at the deceleration of movement. As the rate of displacement decreases, the load measured on both load cells increases. The graph contains the calculated axial load in the tendon through time to be compared with the shape of the instrumented load curves. Figure 4.9 can be compared to Figure 3.29.

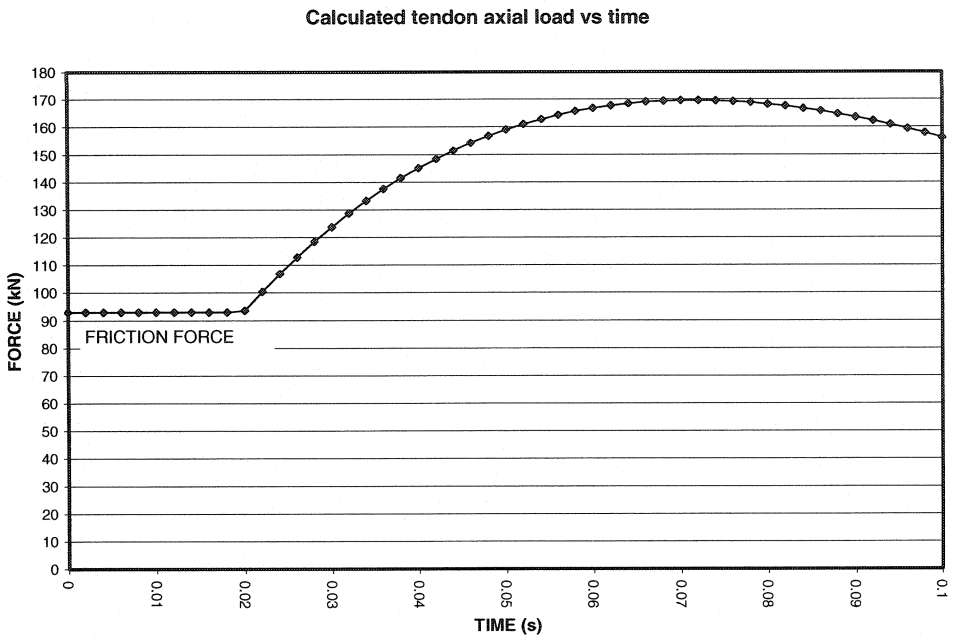

Figure 4.7 – Calculated tendon axial load graph.

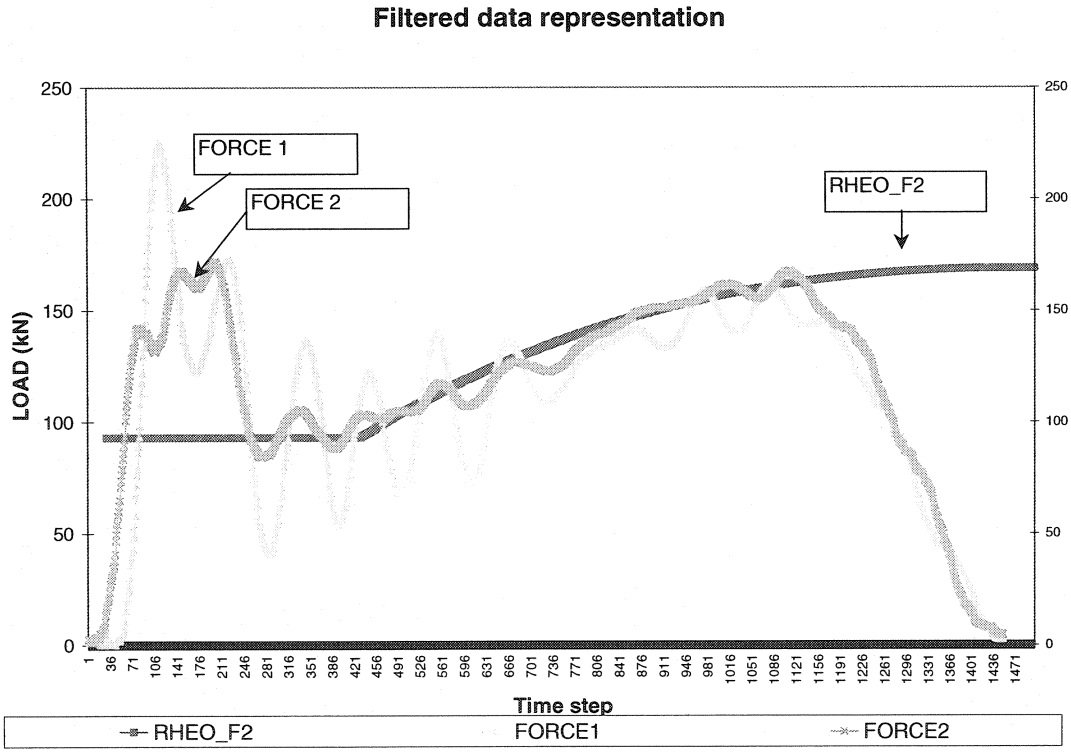

Figure 4.8 – Filtered data representation for instrument signals during test 17-11-2.

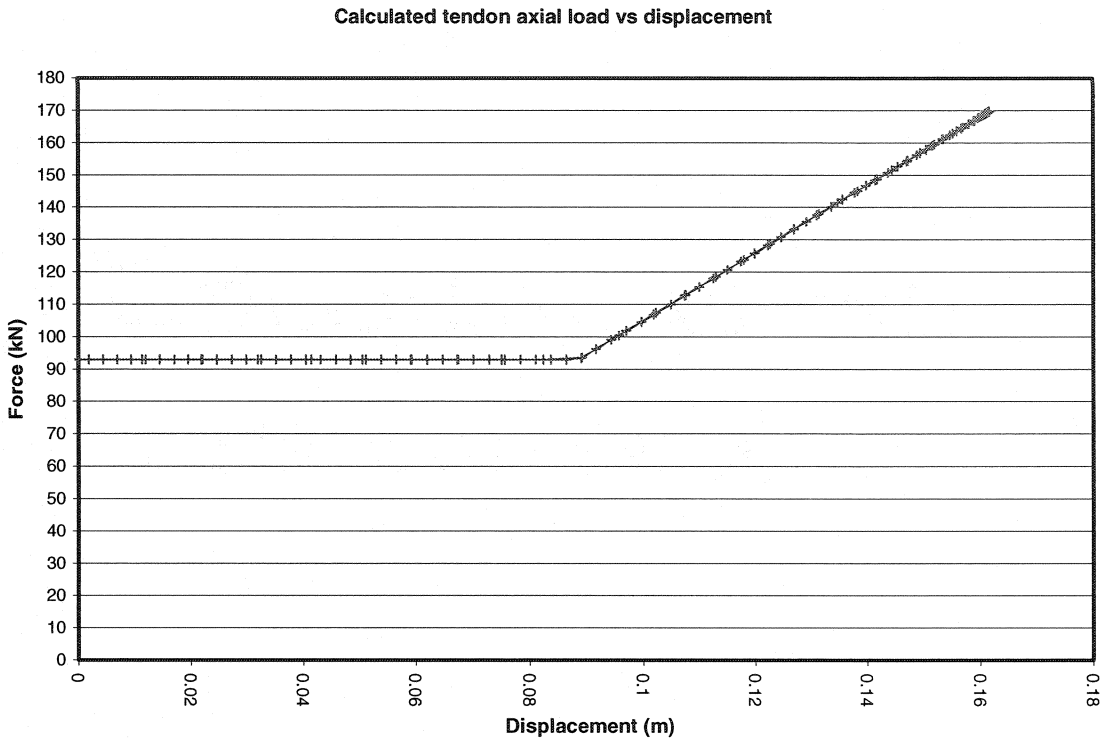

Figure 4.9-Calculated load-displacement graph.

The proposed displacement evaluation method for tendons submitted to impact loading can be used to estimate the maximum energy absorption capacity of a given tendon submitted to impact load. The potential energy absorption of a tendon can be estimated by matching the calculated maximum load to the known ultimate tensile capacity of the tendon. The latter can be measured from cyclic impact testing or simply taken from the tendon material's specifications.

For example, if the model is used for a plastic stiffness range corresponding to that of the quasi-static pull out testing results given in Table 4.1, the calculated single impact absorption capacity of the prototype MCB ranges from 32 to 40 kJ. This result was attained by fixing the impact mass velocity at 5.4 m/s and by increasing the impact weight only to match the ultimate tensile strength of the tendon. With the same range of plastic stiffness and drop weight of 1000 kg, one can calculate the capacity range of the

MCB tendon system by modifying the impact speed. The result of such an approach ranges from 29 to 35 kJ. It appears that there is no particular solution to the energy absorption capacity of a tendon. The latter depends on the combination of ejection speed and tendon burden. Further to this, one can consider that the choice of the potential ejection speed is critical to the evaluation of the level of energy absorption capacity of a tendon. For example, if an ejection velocity of 3.0 m/s is selected, comparable to that selected in the literature review as responsible for the onset of damage in headings, the minimum MCB system capacity becomes 45 kJ. By lowering the plastic stiffness of the bolting system within the range found in quasi-static testing, the bolt reacts entirely in "friction" energy dissipation and its capacity is 50 kJ. The friction energy dissipation in the proposed model equations could include energy losses due to other mechanisms than friction such as heat losses and noise.

After cyclic impact testing to the failure of the tendon, samples 17-11 and 17-14 were sawed apart to measure the amount of displacement of the cone inside the resin. These two samples were chosen because they had been tested using two different drop weights. Figure 4.10 and 4.11 illustrate the split test tube samples. Figure 4.10 shows the cone moved 127 mm into the resin matrix. The drop weight mass used for cyclic impact tests on this sample was 1000 kg. Figure 4.11 shows the cone moved 177 mm into the resin matrix. The mass used for these cyclic impact tests was 750 kg. The conical anchor displacement, the total measured bar and cone displacement are shown in Table 4.4. Figures 4.10, 4.11 and Table 4.4 demonstrate that the prototype MCB both plastically elongates and "plows" through the resin.

An application of the proposed displacement evaluation method on cyclic impact testing was considered in the context of this Thesis. However, once the first impact has proceeded, it becomes difficult to evaluate with certainty what the effect of each impact cycle is on the material properties imparted to the model, particularly for the plastic stiffness of the tendon support system. For example, one can refer to the estimated load

for the second impact test on sample 17-12 shown in Figures 4.7 to 4.9 where the plastic stiffness of the support reaction was chosen to be the maximum plastic impact stiffness measured for all tests through equation 4.1.

It is clear that the choice of tendon burden and impact velocity has the greatest influence on the overall calculated or estimated performance of tendon support under impact loading. The phenomenon is accentuated when using small impact velocities or small drop weights. According to the modeled response, more energy could be dispersed by other means than plastic elongation. Note that steel also exhibits non-linear plastic deformation characteristics under impact load (Ansell, 1999; Figure 4.8). This is not accounted for in the proposed calculation method.

Table 4.4 – Broken MCB analysis

Sample number (max. impact)	Total cone anchor displacement (mm)	Total bar and cone displacement (mm)	Impact displacement cycles (mm)
17-11 at 1000 kg impact and initial velocity > 5 m/s (19.6 tons)	127	400 in 4 cycles	Cycle 1: 150
			Cycle 2: 130
			Cycle 3: 110
			Cycle 4: 10
17-14 at 750 kg impact and initial velocity > 5 m/s (23.0 tons)	177	470 in 5 cycles	Cycle 1: 70
			Cycle 2,3: (230)
			Cycle 2,3: (230)
			Cycle 4: 100
			Cycle 5: 70

In essence, simple pull out testing of tendon support could be envisioned as a means of constructing a set of observations that can be used to approximate the reaction of tendon support in impact load given a simple calculation method such as that presented in this section. The impact testing rig at NTC premises was quite useful in understanding controlling parameters for the performance of tendon support submitted to impact loading. Although simplified, the displacement evaluation method for tendons submitted

to impact loading could be an asset to the engineer wishing to postulate on the best choice of a support system for a given failure mechanism.

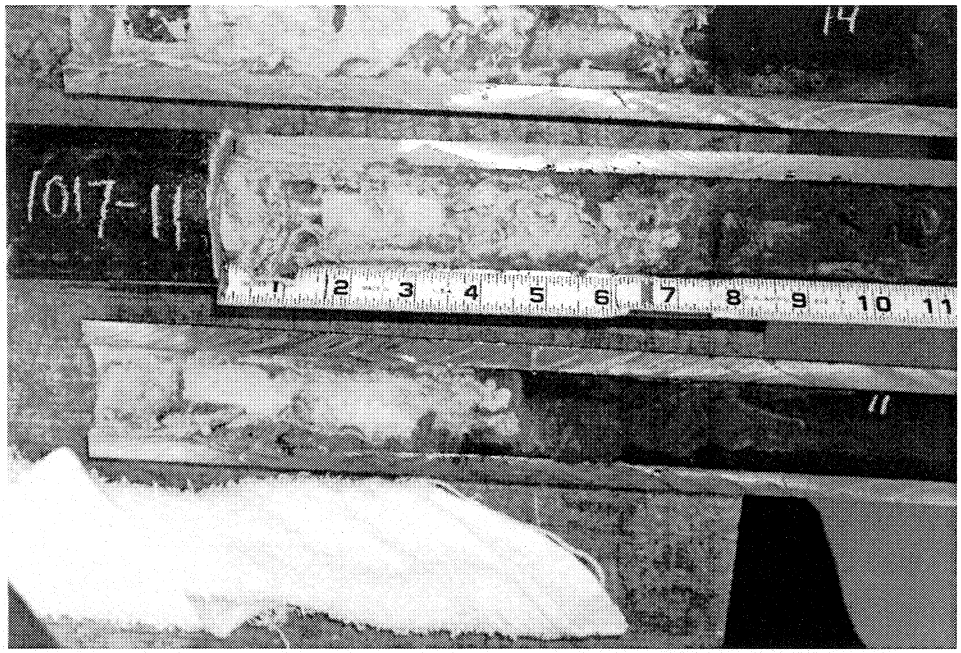

Figure 4.10 – Split test tube for sample 17-11.

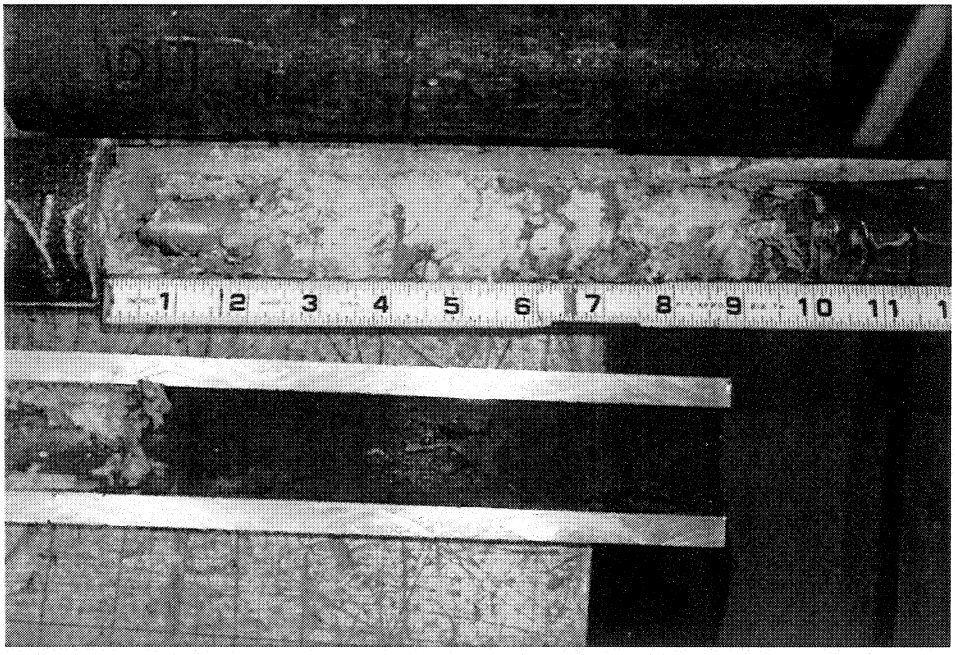

Figure 4.11 – Split test tube for sample 17-14.

There is no consideration in the calculation method for the adhesion of the tendon inside a holding matrix. The overall work required to debond the tendon from the holding matrix could be added to the work required to pull it in eq. (4.31). A greater adhesion would increase the energy absorption capacity of the tendon but could reduce its ability to slide. Thus, it was not incorporated into the proposed calculation method.

The proposed displacement evaluation method for tendons submitted to impact loading is summarized here for clarity. In order to obtain the axial load in the tendon as well as the energy quantity absorbed through the tendon's movement in impact load, one can follow the following steps (the use of a spreadsheet is recommended):

1. Define an arbitrary friction force F_f representing the friction losses and other energy dissipation sources. For the first iteration, it is suggested to use the tendon support system's yield load measured with pull tests, if not available the yield load of the tendon material.
2. Calculate the axial displacement x_g for different time increments, typically in the order of milliseconds, using equations (4.11), (4.21), (4.27) and (4.28).
3. Calculate the axial force in the tendon F_{bar} using equation (4.29).
4. Construct a load displacement graph for the reaction of the tendon. The graph must be set so that if the axial force in the tendon F_{bar} is not greater than the friction force F_f, then the force in the tendon F_{bar} equals the friction force F_f.
5. Calculate the potential energy dissipated through the tendon E_{bar} using equation (4.30).
6. Calculate the work done during the pull We using eq. (4.4).
7. Repeat steps 1 to 6 until the potential energy E_{bar} is approximately equal to the work We.

CHAPTER 5
DISCUSSION AND CONCLUSION

5.1 Discussion

Testing and calculation methods are proposed in this thesis for the performance assessment of tendon support systems submitted to dynamic loading.

Energy amounts pertaining to tendon support maximum capacity under impact loading are in some cases fairly high. One must realize that if a single tendon is required to contain expected rockburst energy in the tens of kilojoules, the engineer must be careful about personnel exposure. One should consider all alternatives for which some or all of the conditions responsible for the burst potential could be avoided or removed safely.

Of outmost importance in the design of rockburst support systems is the choice of the surface support materials such as strapping or screening to contain the rockburst. The surface covering material is responsible for the transfer of the dynamic load to the tendons. Further work is required to address the various interactions between failing rock and the reinforcement system as a whole, more specifically regarding the depth of failure expected in an area.

The commercial MCB tendon has the same geometry as the prototype MCB presented in this report, apart from the mixing blade length. The one used in the validation tests prior to commercial production had a length of 25 mm. The commercial MCB has a mixing blade length of about 45 mm. The modification was done to obtain better mixing properties and increased installation efficiency using mechanized bolting rigs. The steel properties, the manufacturing method, the tendon debonding agent and the resin type used for the commercial MCB units are different than during the validation phase.

Specifically, the conical anchors for the prototype bolts were machined; they are forged on the commercial unit. The steel type for the commercial unit is C1055 modified, the modification pertains to the addition of vanadium for easier machining of the rolled threads. The debonding agent is now heavy industrial grease, better suited for mass production than wax, and having properties that are less affected by time. The grease does not alter the resin performance according to the resin manufacturer.

Preliminary testing indicates a slightly higher energy absorption capacity for the commercial MCB. Note that a large proportion of tendons tested to failure broke at the cone rather than the threaded end.

Energy losses due to the friction of the drop weight onto the steel tube or heat generation are not accounted for in Table 4.3. Some of the discrepancies between the potential energy verification and the instrumented work energy calculation can be explained by the instrumentation method chosen for displacement of the tendon reaction plate. The wire potentiometer was sometimes pulled off-axis during the downward motion of the tendon, as was sometimes observed on the slow motion videos. The problem was corrected before the validation phase tests by modifying components of the impact test rig. The potentiometer problem would lead to the underestimation of the tendon displacement during the initial phase of the movement.

During the installation of the MCB tendons, it would have been interesting to note the rotation speed of the dolly and the penetration speed. This could have been useful for the record. Last, polyester resin gets stronger with time. The time lag between sample preparation and impact testing was not considered in the calculations. Sometimes, one sample could be tested at a few cycles of loading, stored, then tested to failure. It is unknown how this affected the results.

Impact tests of the MCB prototype support system have given insight on the mechanisms of movement of a tendon in axial loading. The proposed experimental data analysis methods in this thesis for field trials of tendons as well as laboratory impact testing all convey the notion of a measure of load and displacement history in various means and forms. An analysis on load only for tendons submitted to loads beyond the elastic range of the support system can only highlight the material properties of the tendon material.

The proposed calculation method for tendon axial load under impact loading has been inspired from observations done in the testing phase, particularly the load-displacement history and the observable damage on the steel tendon. The model is most useful for first impact analysis in the laboratory. This applies to an underground application as well. Once tunnel walls have been distorted by a large impact supported by rockburst support, entangled broken blocks can squeeze the bolts and prevent them from yielding to large loads. In theory it would be possible to use the initial displacement condition x_0 of the calculation model to simulate the tendon quasi-static displacement before the application of an impact load, but it could not be compared to laboratory or experimental field evidence.

5.2 Conclusion

This thesis covered notions of mine seismology, quasi-static and impact testing techniques as well as a proposed analysis method for the performance of tendon support submitted to dynamic loading. Efforts were done to decipher impact testing mechanisms and the data collection to verify the correctness and usefulness of the proposed analysis method.

A rockburst is a phenomenon resulting from the violent failure of a rock mass. It is characterized by the ejection of rock fragments from rock faces exposed to energy release from the violent failure. Rockburst mechanisms can be classified into categories. For

example, the source of damage can be attributed to stress-induced fractures, strain bursting, buckling, face crush/pillar burst, shear rupture and fault-slip (Fig. 2.4). Underground tunnels are commonly reinforced with tendon support elements and one or successive layers of liners such as mesh and/or shotcrete. The various available tendon support systems and liners commercially available react differently to imposed dynamic loads.

It is proposed to characterize the quasi-static performance of tendon support elements with a complete in-situ load-deformation curve. The latter can be evaluated using pull tests. The yield point of the tendon support system, its plastic stiffness k_p and the quantity of elastic displacement can be obtained from the load-deformation curves (Fig. 4.1). Since it can be hazardous to perform pull tests to the failure of the tendon, the ultimate tensile strength of the tendon is ordinarily derived from the tendon manufacturer's specifications or simply the material specifications. The amount of plastic displacement to the failure of the tendon can be extrapolated from these specifications. It is advisable to pull the tendon from the wall to such displacement lengths to reveal the plastic stiffness of the support system. This should be done whenever the expected support system's yield point is reasonably smaller than the ultimate capacity of the tendon, so that the pull test can be done safely.

Impact tests using the NTC rig have revealed interesting aspects of the reaction of tendon support under impact load. Test results on the prototype Modified Cone Bolt are presented in this thesis. It appears that load-displacement graphs are particularly useful to analyze the tendon's reaction under impact load. The maximum axial load in the tendon can be extracted from these and information can be deduced from the shape of the load-displacement graph. The NTC rig was equipped with high capacity load cells and a displacement transducer to track the reaction of the tendons (Fig. 3.17). Every test was at least instrumented for load and a record of the final displacement of the tendon at each impact. Whenever possible the rig was equipped with a load cell underneath the reaction

plate of the tendon and a tendon displacement transducer. An oscilloscope recorded the load and displacement transducer data.

Instrumented dynamic testing allows the evaluation of potential energy absorbed through the tendon support system during each test. Other impact test rigs have been used throughout the world to evaluate the dynamic capacity of tendon support. Different impact test rigs will most probably be set to use various impact mass and velocity values. The attribution of a large impact velocity on a given tendon support system can provoke a different reaction than a low velocity blow. It is recommended to clearly identify the impact mass and velocity values used for the impact test when reporting results for tendon support systems.

Complications can occur while proceeding to the evaluation of the maximum energy absorption capacity of tendon support under impact load using impact test rigs. Some tendon support systems cannot be broken in a single blow and one must perform multiple impact tests in order to drive the tendon to failure or at least past the tendon's yield point. Some difficulties can occur while calculating the maximum energy absorption capacity of tendon support systems from multiple impact testing. For example, the prototype MCB portrayed a total additive energy absorption capacity in the range of 45.9 to 59.6 kJ after multiple impact tests using different drop weight and height values. The cyclic impact test results could have been affected by the choice of the drop weight and height quantities as well as variability in the tendon installation parameters such as the quality of the resin mix. Inversely, a hazardous situation can occur if a tendon support system breaks at the first impact using large drop mass and impact velocity values and little potential energy has been consumed by the displacement of the tendon support system. Also, confusion could result while comparing plausible energy absorption values from different laboratories using different impact weights and impact velocity settings.

The author proposed a calculation method to evaluate the quantity of displacement, or the axial load, of tendon support under impact loading for given impact mass and velocity values, as well as the characteristic deformation behavior of the tendon support system. The calculation method is based on rheological equations describing critically damped harmonic motion.

The proposed displacement evaluation method for tendons submitted to dynamic loading could be useful to approximate the reaction of a tendon support system given details of its performance requirements. It could be applied at any mine site without much effort other than in situ pull testing of said tendon support systems. The model exhibits linearity for both plastic stiffness and velocity damping characteristics. Note however that steel exhibits a non-linear stress-strain characteristic envelope in impact loading.

Improvements could be done to the model by integrating the non-linear behavior of the tendon system deformation and velocity damping. Otherwise, and maybe more importantly, improvements could be done in formulating a method to calculate the influence of confinement stress increase in the rock mass provided by the rockburst support system to the depth of failure during the impact load. Observations in the field by the author at Brunswick Mine have so far indicated that the depth of failure may be affected by the support system in impact loading.

5.3 Recommendation for future work

The author suggests the application of the proposed displacement evaluation method for tendons submitted to dynamic loading to other support elements. Ideally, the method would be applied to such smooth surface tendons as Split Sets, Swellex, and cable bolts. The successive pull testing of the tendons in a mining environment and impact testing on an appropriate rig could further validate the calculation approach, especially regarding

the application of the calculation method to various tendon burden and block ejection velocity values.

Furthermore, it may be appropriate to apply the calculation method to the reaction of tendon support under dynamic loading in the rock mass. For example, it is possible to evaluate the extent and shape of an unstable zone through observations and calculations (see Figure 2.5). Thus, for the strain bursting, face crush or buckling mechanisms, one could consider evaluating the amount of excess energy available in the event of violent failure. Given the:

-tendon support system characteristic k_p,

-tendon material's yield point,

-tendon support installation spacing,

-initial depth of failure,

-excess energy in the event of a violent failure,

one could calculate the tendon burden and the plausible ejection velocity through kinetic energy, and thus the plausible maximum axial load. To add on the previous considerations, one could further elaborate by calculating the effect of the confining pressure exerted by the instantaneous axial load in the tendon during the rockburst and its consequence on the final depth of failure of the rock mass.

REFERENCES

ANON. (1982). Rockburst terminology. Circular No. 28/82, Chamber of Mines of South Africa Research Organization, Johannesburg.

ANSELL, A. (1999). Dynamically Loaded Rock Reinforcement. Doctoral Thesis, Royal Institute of Technology, Sweden, Bulletin 52, 185 p.

CHARETTE, F. (1991). Guide condensé du boulonnage. Centre de Recherches Minérales, Gouvernement du Québec, 97 p.

CHARETTE, F. and HADJIGEORGIOU, J. (1999). Guide pratique du soutènement minier. Association Minière du Québec Inc., Ste-Foy, 142 p.

CHOQUET, P. (1987). Guide d'utilisation du boulonnage. Centre de Recherches Minérales, Gouvernement du Québec, 269 p.

COLLINS COBUILD English Language Dictionary (1987). John Sinclair (ed.), London, p.445, p.1310.

COLLINS, J.A. (1993). Failure of Materials in Mechanical Design, 2nd edition. John Wiley & Sons.

COOK, N.G.W. (1965). A note on rockbursts considered as a problem of stability. J. S. Afr. Inst. Min. Metall., pp. 437-446.

COOK, N.G.W. and ORTLEPP, W.D. (1968). A yielding rockbolt. Chamber of Mines of South Africa Research Organization Bulletin, No. 14.

COOK, N.G.W., HOEK, E., PRETORIUS, J.P.G., ORTLEPP, W.D., SALAMON, M.D.G. (1966). Rock mechanics applied to the study of rockbursts. Journal of the South African Institute of Mining and Metallurgy, Vol. 66, pp. 435-528.

DERRICK, W.R. and GROSSMAN, S.I. (1987). A first course in differential equations with applications, 3rd edition. West Publishing Company.

DYSKIN, A.V. and GERMANOVICH, L.N. (1993). Model of rockburst caused by cracks growing near free surface. Rockbursts and Seismicity in Mines, Young (ed.). Balkema, Rotterdam. pp. 169-174.

ENGEL, P.A. (1978). Impact Wear of Materials. Elsevier Scientific Publishing Company, 339 p.

FAY, A.H. (1947). A glossary of the mining and mineral industry. United States Bureau of Mines Bulletin 95 (reprinted from 1920 edition without changes).

GAUDREAU, D. (2000a). Yieldable Tendon Support, report on Q4-2000 MCB impact testing. Noranda Inc. Technology Centre internal report, project R2-9684.

GAUDREAU, D. (2000b). Modified Cone Bolt installation procedure. Noranda Technology Centre, 2 p.

GAUDREAU, D. (2000c). Noranda Inc. Chief Engineer's Meeting presentation. Noranda Technology Centre.

GAUDREAU, D. (2001). Internal memorandum to Bell Allard mine. Noranda Technology Centre.

GIBOWICZ, S.J. (1988). The mechanism of seismic events induced by mining : a review. Rockbursts and Seismicity in Mines, Keynote presentations.

GIBOWICZ, S.J. (1993). An introduction to mining seismology. Academic Press. 399p.

GILLERSTEDT, P. (1999). Full scale pull- and shear laboratory tests of conebolts (unpublished). Boliden Ltd.

GILL, D.E. and AUBERTIN, M. (1988). Évaluation du potentiel de coups de terrain dans les mines d'Abitibi. Rapport de recherche de l'URSTM présenté à l'Institut de Recherche en Santé et Sécurité du Travail (IRSST).

GILL, D.E., AUBERTIN, M., SIMON, R. (1993). A practical engineering approach to the evaluation of rockburst potential. Proc. 3rd Int. Symp. on Rockbursts and Seismicity in Mines. P.Young (ed.) Balkema, pp. 63-68.

HAILE, A.T., JAGER, A.J., WOJNO, L. (1995). Strata control in tunnels and an evaluation of support units and systems currently used with a view to improving the effectiveness of support stability and safety of tunnels. Simrac report GAP026. CSIR Division of Mining Technology.

HEDLEY, D.F.G. and WHITTON, N. (1987). Performance of bolting systems subject to rockbursts. Underground Support Systems, Special Volume 35, The Canadian Institute of Mining and Metallurgy, pp. 73-77.

HEDLEY, D.F.G. (1992). Rockburst handbook for Ontario hardrock mines. CANMET Special Report SP92-1E, CANMET, Energy, Mines and Ressources Canada.

HINES, W.W. and MONTGOMERY, D.C. (1990). Probability and Statistics in Engineering and Management Science, 3rd edition. John Wiley & Sons, 732p.

HOEK, E. (2000). Rock engineering. Course notes by Evert Hoek. p. 264.

HOEK, E. and BROWN, E.T. (1980). Underground excavations in rock. The Institution of Mining and Metallurgy. London, pp. 236-240.

HOEK, E. and WOOD, D. (1987). Support in underground hard rock mines. Underground Support Systems, Special Volume 35, The Canadian Institute of Mining and Metallurgy, pp. 1-6.

HOEK, E., KAISER, P.K., BAWDEN, W.F. (1995). Support of Underground Excavations in Hard Rock. Balkema, Rotterdam, 215 p.

ISS INTERNATIONAL (2002). Moment tensor inversions. In ISS International web site. [On-line]. http://www.issi.co.za. (Page consulted in October 2002).

JAGER, A.J., WOJNO, L.S., DAWE, S.G. (1990). Rock Support Tendons which May be Caused to Yield. South African patent application 90/4879.

JAGER, A.J. (1992). Two new support units for the control of rockburst damage. Proc. Rock Support in Mining and Underground Construction, Balkema, Rotterdam, pp. 621-631.

JOUGHIN, N.C. and JAGER, A.J. (1983). Fracture of rock at stope faces in South African gold mines. Rockbursts prediction and control, Institution of Mining and Metallurgy, London, pp. 53-66.

KAISER, P.K., TANNANT, D.D., MCCREATH, D.R., JESENAK, P. (1992). Rockburst damage assessment procedure. Rock Support in Mining and Underground Contstruction, Kaiser & McCreath (eds). Balkema, Rotterdam. pp. 639-647.

KAISER, P. (1993). Keynote address: support of tunnels in burst-prone ground - towards a rational design methodology. Rockbursts and Seismicity in Mines, Young (ed.). Balkema, Rotterdam, pp. 13-27.

KAISER, P., MCCREATH, D.R., TANNANT, D.D. (1996). Canadian Rockburst Support Handbook. Geomechanics Research Centre.

KAISER, P. (2000). Personal communication in the context of the verification of the procedures used for the MCB prototype validation.

KRISTOF, B. (1988). Brunswick Mining - #12 Mine Rock Properties. Brunswick Mining and Smelting.

LABRIE, D. (1998). Resultats essais de laboratoire. CANMET.

LANGILLE, C.C., TANNANT, D.D., GALBRAITH, J. (1995). Investigation of One-pass Grouted Support Systems for use in a High Stress Mining Environment. 97th Annual General Meeting of C.I.M. Rock Mechanics and Strata Control Session, Halifax, Nova Scotia, pp. 162-171.

MALONEY, S., KAISER, P.K. (1996). Evaluation of the Support Characteristics of Resin Grouted Conebolts at Brunswick Mine, a research proposal. Geomechanics Research Centre, Laurentian University. Submitted to Don Peterson, Ground Control Engineer, Noranda Mining and Exploration Limited, Brunswick Mining Division, 7 p.

MASE, G.E. (1970). Continuum mechanics. Schaum's outline series, McGraw-Hill, pp. 196-216.

MAXWELL, S.C. and YOUNG, R.P. (1997). Assessing induced fracturing around underground excavations using velocity imaging and induced seismicity. Rockbursts and Seismicity in Mines, Gibowicz and Lasocki (eds). Balkema, Rotterdam, pp. 179-183.

MENDECKI, A.J. (1997). Seismic Monitoring in Mines. A.J. Mendecki (ed.), Chapman & Hall, 262 p.

MÜHLHAUS, H.-B. (1990). Exfoliation phenomena in pre-stressed rock. Rockbursts and Seismicity in Mines, Fairhurst (editor). Balkema, Rotterdam, pp. 101-107.

OBERG, E., JONES, F.D, HORTON, H.L., RYFFEL, H.H. (1996). Machinery's Handbook, 25th edition. Robert E. Green, editor. Industrial Press Inc.

OBERT, L., AND DUVALL, W.I. (1967). Rock mechanics and the design of underground structures in rock. John Wiley and Sons.

ORTLEPP, W.D., (1992a). Invited lecture: The design of support for the containment of rockburst damage in tunnels – An engineering approach. Rock Support in Mining and Underground Construction, Kaiser and McCreath (eds). Balkema, Rotterdam.

ORTLEPP, W.D. (1992b). Implosive-load testing of tunnel support. Rock Support in Mining and Underground Construction, Balkema, Rotterdam, pp. 675-682.

ORTLEPP, W.D. (1993). High ground displacement velocities associated with rockburst damage. Rockbursts and Seismicity in Mines, Young ed., Balkema, pp. 101-106.

ORTLEPP, W.D. (1994). Grouted rock-studs as rockburst support: A simple design approach and an effective test procedure. The Journal of the South African Institute of Mining and Metallurgy, February 94, pp. 47-63.

ORTLEPP, W.D. and STACEY, T.R. (1998). Performance of Tunnel Support under Large Deformation Static and Dynamic Loading. Tunnelling and Underground Space Technology, Vol. 13, No. 1, pp. 15-21.

SALAMON, M.D.G. (1983). Rockburst hazard and the fight for its alleviation in South African gold mines. Rockbursts prediction and control, Institution of Mining and Metallurgy, London, pp. 11-36.

SALAMON, M.D.G. (1974). Rock mechanics of underground excavations. Advances in Rock Mechanics, Proc. 3rd Cong. Int. Soc. Rock Mech., Vol 1-B, pp. 951-1099.

SIMON, R. and GAUDET, N. (1998). Rapport essais de laboratoire. URSTM.

SIMON, R., AUBERTIN, M., GILL, D.E. (1998). Guide d'évaluation du potentiel de coups de terrain dans les mines à l'aide de la méthode ERP. IRSST, research report R-182.

SIMON, R. (1999). Analysis of fault-slip mechanisms in hard rock mining. Doctoral Thesis, McGill University.

SIMON, R., AUBERTIN, M., MITRI, H.S. (1995). Evaluation of rockburst potential in hard rock mines. 97th Annual General Meeting of C.I.M., Rock Mechanics and Strata Control Session. Halifax, pp. 257-266.

SIMSER, B., JOUGHIN, W.C., ORTLEPP, W.D. (2001). The performance of Brunswick Mines rockburst support system during a severe seismic episode and its implications for future strategic planning. Proc. 5th Int. Symp. Rockbursts and Seismicity in Mines, Johannesburg, September 2001.

STACEY, T.R. AND ORTLEPP, W.D. (1994). Rockburst mechanisms and tunnel support in rockburst conditions. Geomechanics 93, Rakowski (ed.). Balkema, Rotterdam.

STACEY, T.R., ORTLEPP, W.D. (1999). Retainment support for dynamic events in mines. Rock Support and Reinforcement Practice in Mining, Balkema, Rotterdam, pp.329-333.

STACEY, T.R., ORTLEPP, W.D. (2000). Support appropriate for Dynamic loading and large static loading in block cave mining openings. MassMin 2000, Brisbane, Qld., pp. 783-789.

STILLBORG, B. (1986). Professional users handbook for rock bolting. Series on Rock and Soil Mechanics, Vol. 15. Trans Tech Publications, pp. 48-51.

TALEBI, S., MOTTAHED, P., PRITCHARD, C.J. (1997). Monitoring seismicity in some mining camps of Ontario and Quebec. Rockbursts and seismicity in mines, Gibowicz and Lasocki (eds), Balkema, pp. 117-120.

TANNANT, D.D., KAISER, P.K., MCDOWELL, G.M. (1992). Dynamic support monitoring. Rock Support in Mining and Underground Construction, Kaiser & McCreath (eds). Balkema, Rotterdam, pp. 657-664.

TANNANT, D.D., BRUMMER, R.K., KAISER, P.K. (1994). Response of rockbolts to nearby blasts. International Workshop on Applied Rockburst Research, May 12, 1994, Santiago, pp. 257-264.

TANNANT, D.D. and BUSS, B.W. (1994). Yielding rockbolt anchors for high convergence or rockburst conditions. Proc. 47th Canadian Geotechnical Conference, Halifax.

TANNANT, D.D., BRUMMER, R.K., YI, X. (1995). Rockbolt behavior under dynamic loading: Field tests and modeling. Int. J. of Rock Mech. Min. Sci. & Geo Abstracts, 32, pp. 537-550.

THOMAS, G.B. and FINNEY, R.L. (1992). Calculus and Analytic Geometry, 8th edition. Addison-Wesley Publishing Company.

VAN SINT JAN F., M. (1994). A Procedure to Design Tunnel Support for Rockburst Conditions. International Workshop on Applied Rockburst Research, Santiago, Chile, pp. 277-286.

WAGNER, H. (1984). Support requirements for rockburst conditions. Proceedings of the 1st International Congress on Rockbursts and Seismicity in Mines, Johannesburg, 1982. SAIMM, Johannesburg.

WOLFRAM RESEARCH (1996). Mathematica Wavelet Explorer. Software reference manual.

WOYNO, L., JAGER, A.J., ROBERTS, M.K.C. (1987). Recommended performance requirements for yielding rock tendons. SANGORM Symposium – Design of Rock Reinforcing: Components and Systems, Johannesburg, pp. 71-74.

YU, T.R. (1980). Ground Control at Kidd Creek Mine. Underground Rock Engineering, CIM Special Volume 22, The Canadian Institute for Mining and Metallurgy, pp. 73-79.

APPENDIX 1

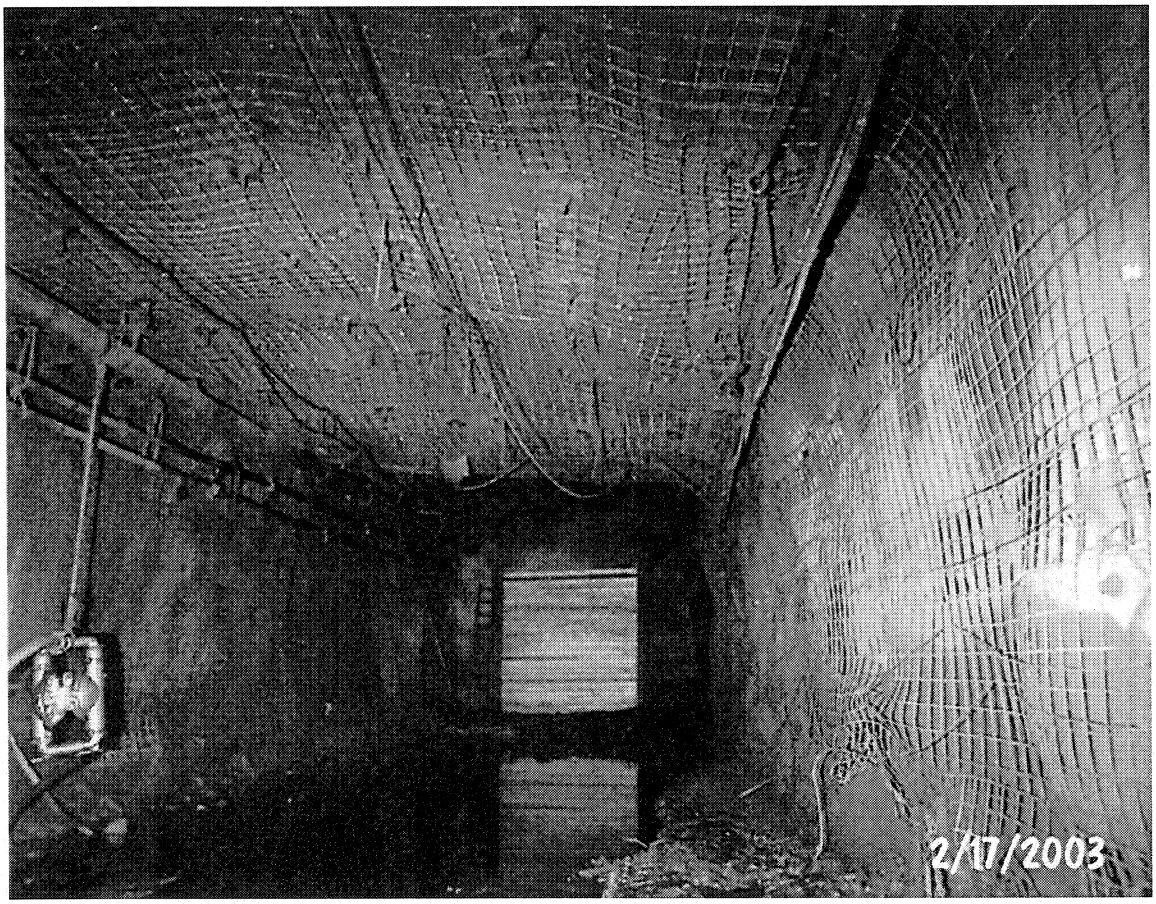

Figure A1 - Access to North Regional Pillar on 1000-3 Sub level North (Brunswick Mine). This access is lined with Brunswick's B-916 Rockburst Support Standard consisting of MCB tendons, 3/8" nominal thickness 6X6" domed reaction plates, 00 gage strapping and 6 gage flat welded galvanised screen panels.

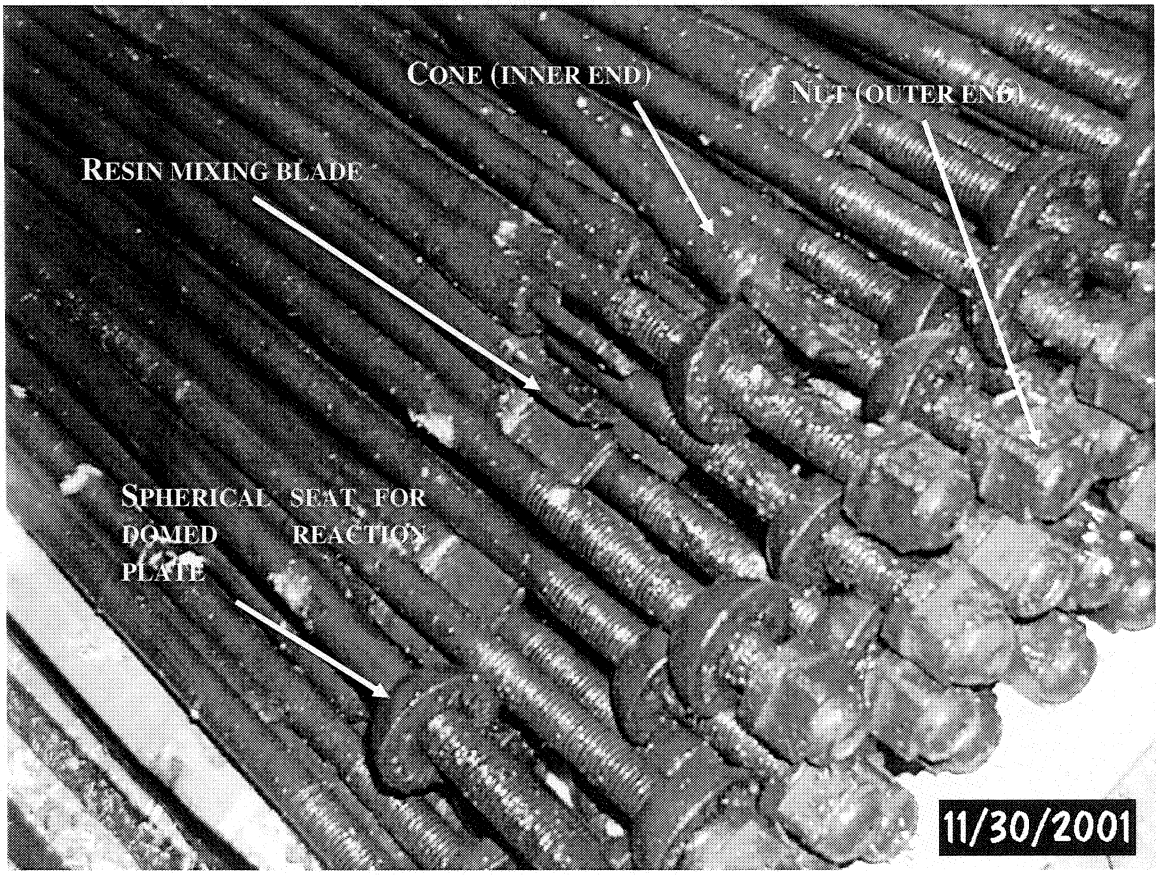

Figure A2 - A pile of MCB tendons as commercialised by Mansour Mining Inc. in Sudbury, ON under license from Noranda Inc. The view shows either distal or inner end of each tendon. The tendons are greased to prevent adhesion of the polyester resin to the anchor. Notice the 45 mm long resin mixing blade. The resin currently used at Brunswick mine along with MCB anchors has the trademark Coneloc and is manufactured by Dupont. Coneloc is an offspring of their Fasloc product.

Figure A3 - A specimen of Dupont's Coneloc (Fasloc) resin cartridges. The holding tube contains both adhesive and catalyst, separated by the packaging plastic membrane. These cartridges are inserted in the hole then the MCB tendon is pushed and spun through them. This mixes the adhesive and catalyst and the resin starts setting within 30 seconds. The reaction plate of the tendon is then adjusted to the rock surface.

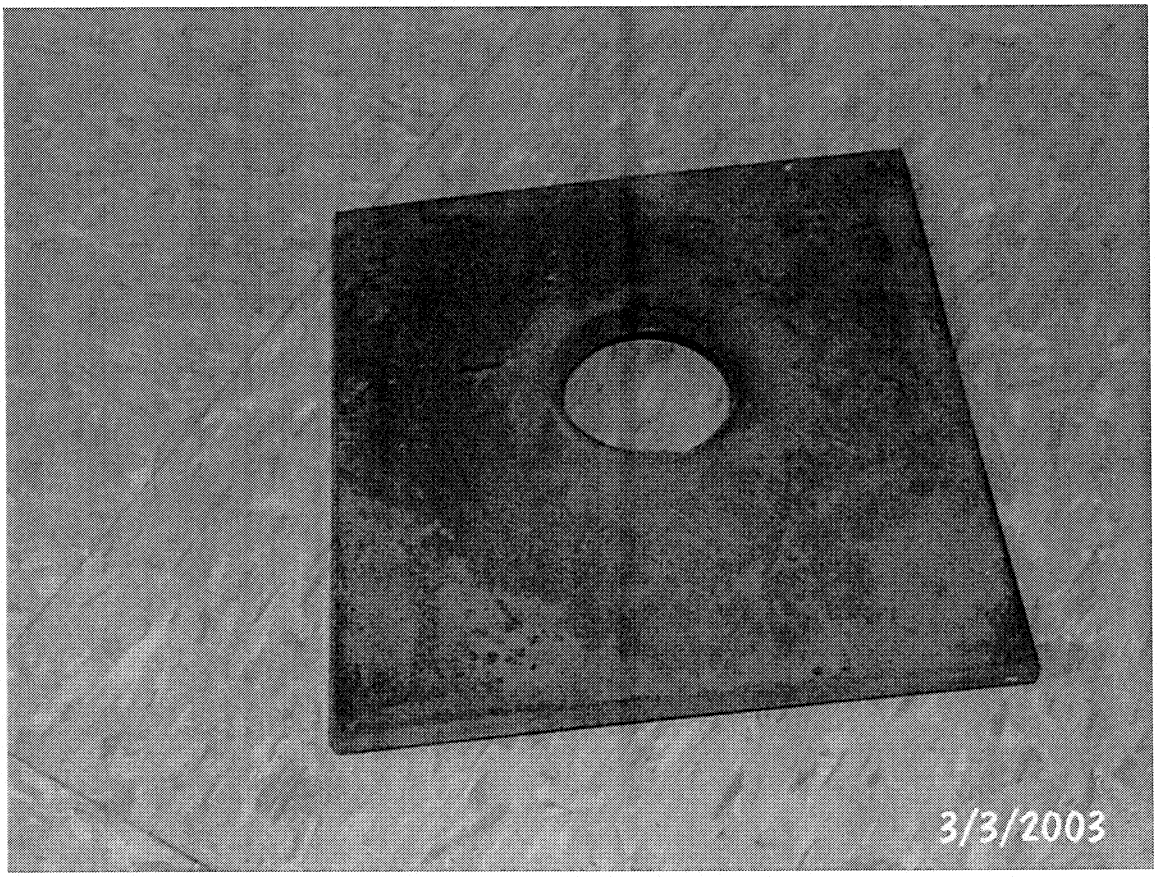

Figure A4 - A view of a reaction plate used in the rockburst support system at Brunswick. Its nominal dimensions are 6" X 6" width X 3/8" thickness (150 X 150 X 9.5 mm). The dome is approximately ½" deep (12 mm). The large hole accommodates the spherical seat that fits under the nut of the tendon.

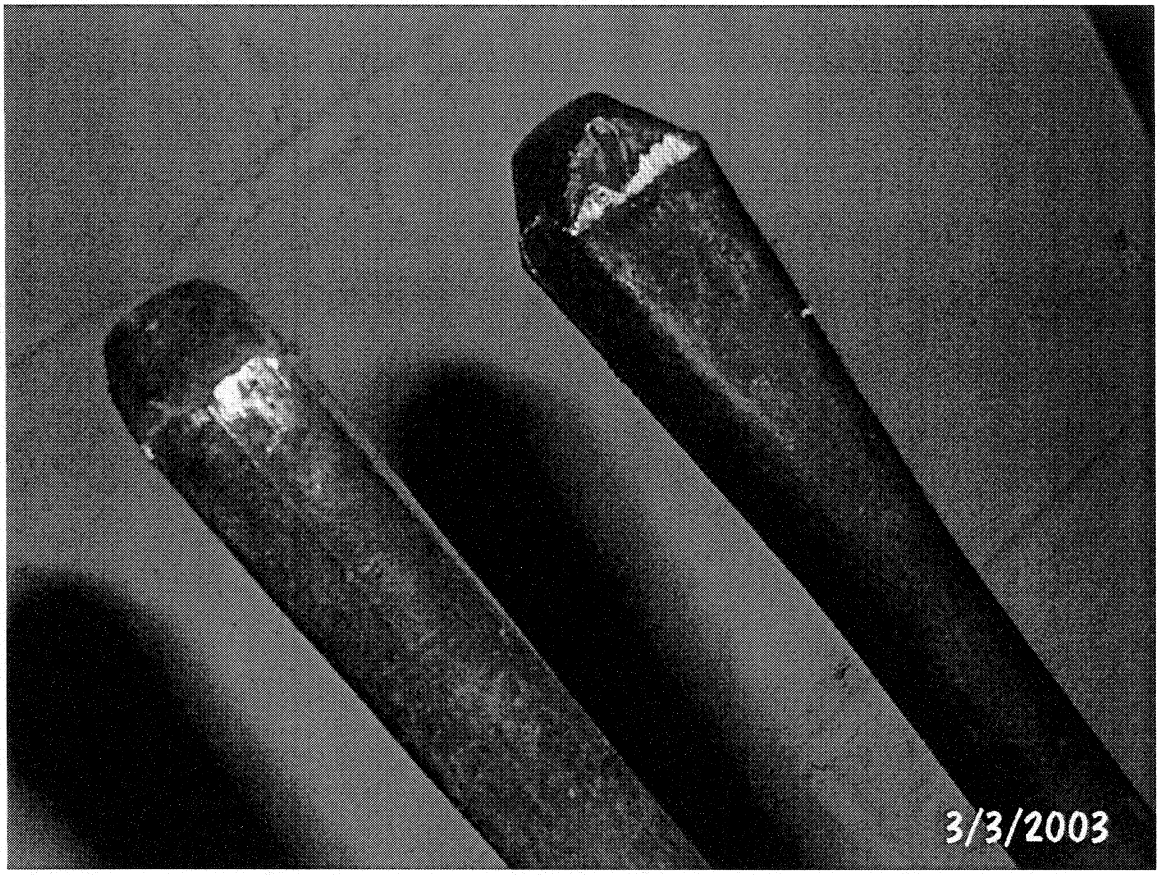

Figure A5 - The 16 mm South African Cone Bolt. The picture shows a front and side view of the anchor head. The flat conical shape arrangement does not provide consistent resin mixing quality from one installation to another. The 16 mm Cone Bolt is normally coated with wax to prevent adhesion of the grouting agent to the steel.

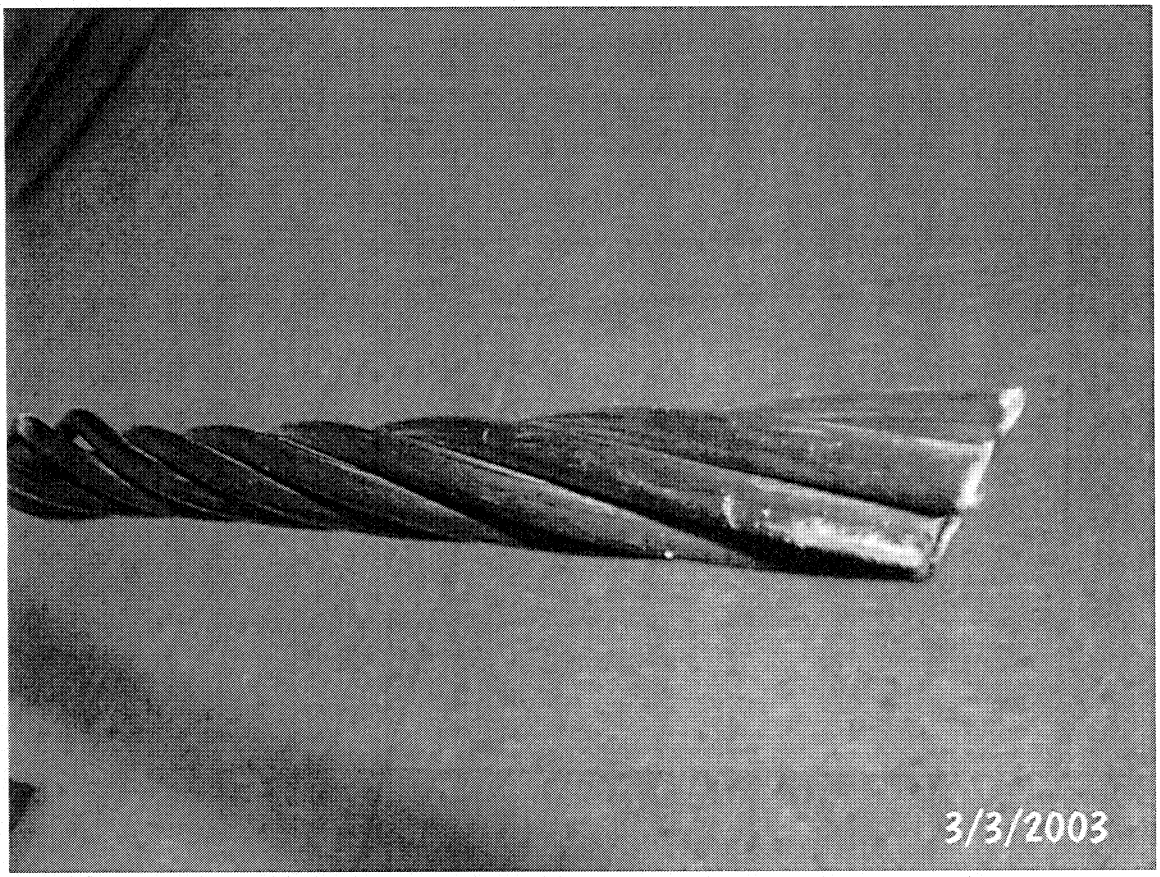

Figure A6 - Cable bolt strand. These stiff cables come in rolls. Their material properties are such that they elongate almost exclusively elastically, they don't allow much plastic deformation before failure. They are most generally grouted for mining use. They can be plated using a large reaction plate and a holding mechanism labelled "barrel and wedge" and can be tensioned.

Figure A7 - Close view to 20 M corrugated rebar. These are used for many tunnelling applications in Canada. They usually are grouted in a polyester resin matrix. Tendons are pushed into the hole and then spun to mix the resin components. Once the resin is set, the reaction plate is adjusted to the tunnel surface.

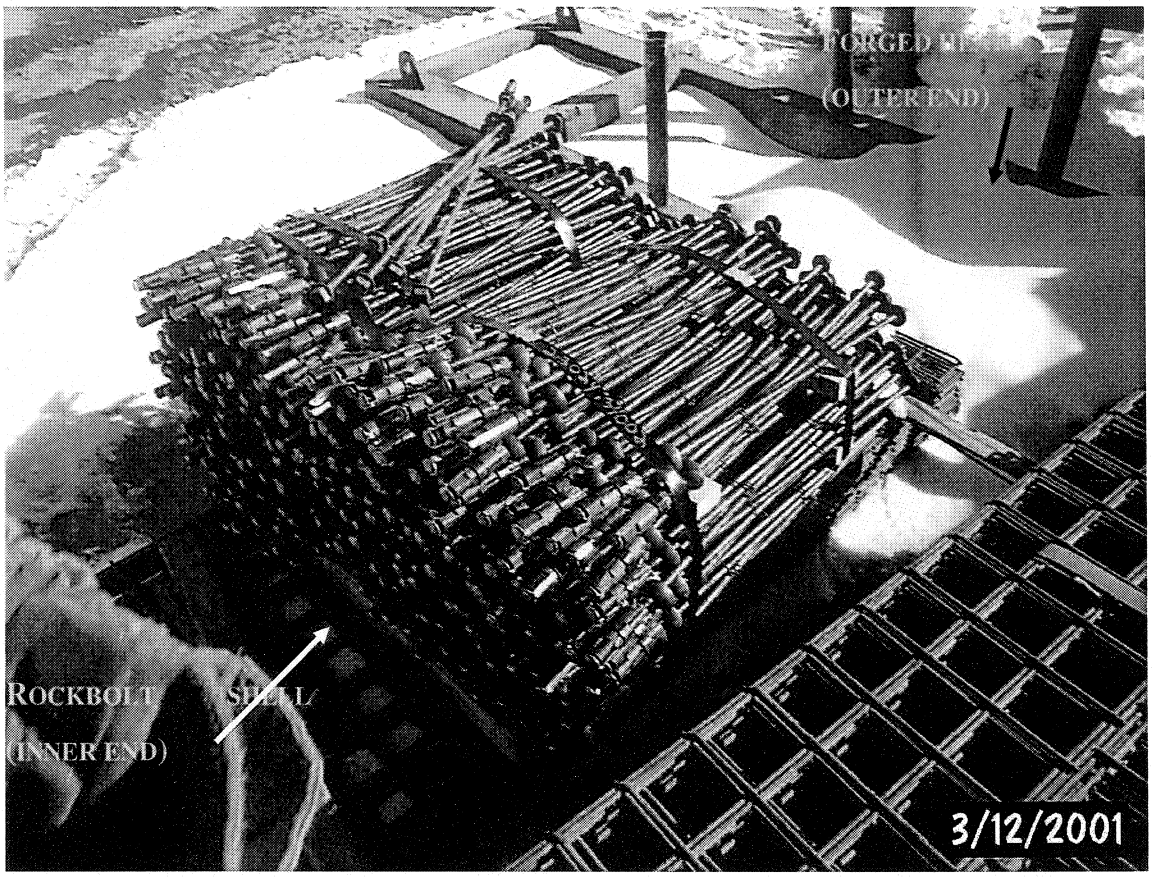

Figure A8 - A bundle of 0.9m long mechanical anchor bolts. In this case, one side has a forged head that fits standard dollies. The forged head usually bears a mark of the tendon length in feet. On the inner end, the tendon is threaded and accepts a mechanical shell. The latter consists of a wedge-like nut and two steel flaps. When torquing the tendon in the hole, the nut is pulled down and jams into the metal flaps resting on the bore hole wall. For it to work properly, the mechanical anchor bolt must be torqued and tensioned in the hole.

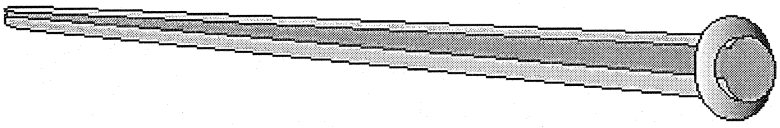

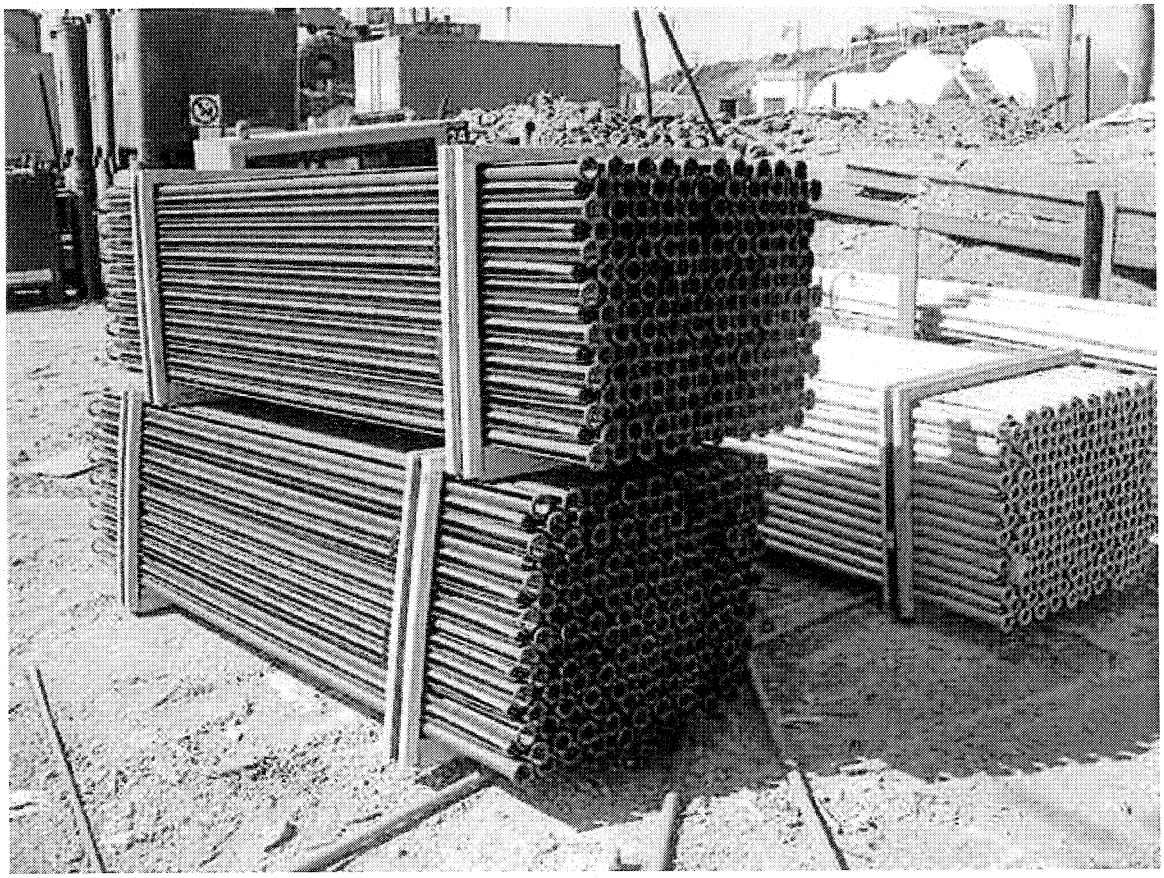

Figure A9 - Bundles of Standard and Galvanised Roc-Set bolts, manufactured by Brockhouse. These friction support tendons are conceptually similar to Split Sets tendons. Ingersoll-Rand's patent for the Split Set expired and a number of conceptually similar products have been commercialised since.

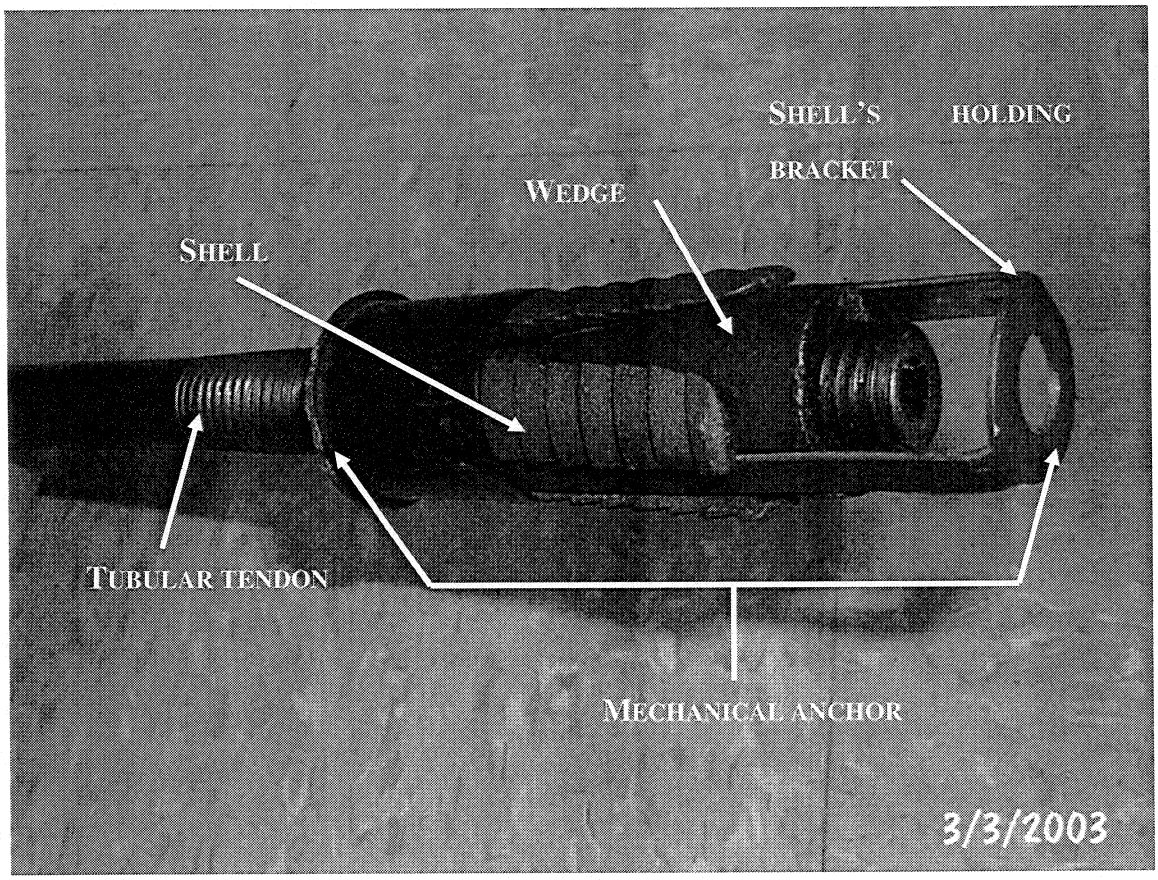

Figure A10 - Tubular bolt. These devices are similar in design to standard rock bolts but can be grouted in the hole through the use of the tendon's cavity.